Low Dielectric Constant Insulators and Gold Metallization for GHz Multi-Chip Modules
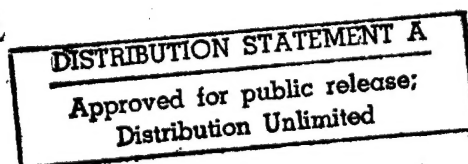
Principal Investigators:

Paul Kohl and Sue Ann Bidstrup
School of Chemical Engineering
404-894-2893 (PK), 404-894-2872 (SAB)

David Hertling
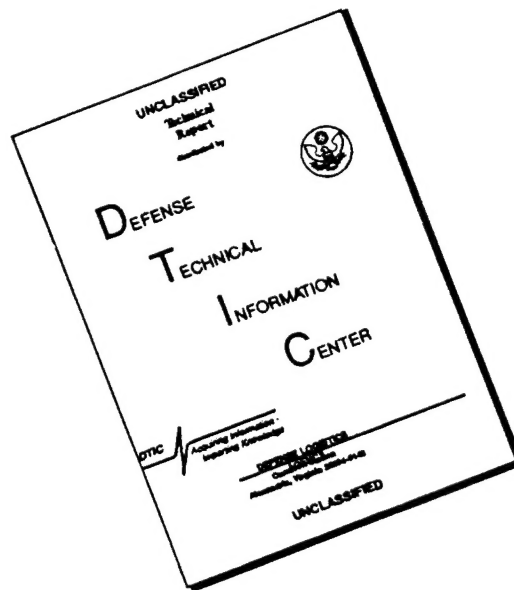School of Electrical Engineering
404-894-2932

Georgia Institute of Technology
Atlanta, GA 30332-0100

19960422 038

DISCLAIMER NOTICE

UNCLASSIFIED
Technical
Report

D_{EFENSE}

$T_{ECHNICAL}$

$I_{NFORMATION}$

C_{ENTER}

DTIC Acquiring Information
Imparting Knowledge

DEFENSE LOGISTICS
AGENCY
Cameron Station
Alexandria, Virginia 22304-6145

UNCLASSIFIED

THIS DOCUMENT IS BEST
QUALITY AVAILABLE. THE COPY
FURNISHED TO DTIC CONTAINED
A SIGNIFICANT NUMBER OF
PAGES WHICH DO NOT
REPRODUCE LEGIBLY.

Table of Contents

CHAPTER 1

SUMMARY

The goal of this program is to investigate new dielectrics, metals and processes for the fabrication of multi-chip modules which hold the promise of exceptional electrical performance in the GHz region in addition to high yield and high reliability. The low dielectric constant insulators are being evaluated through the fabrication of in-situ test structures using noble metals. In the course of doing this evaluation, a simple process for gold or silver MCMs has been investigated.

A processing scheme using noble metals (gold and silver) as the interconnection metallization in the module has been developed and is being characterized. The noble metal process has fewer process steps than the equivalent copper process and is potentially lower cost, particularly when high reliability is important. It has been observed that silver has an advantage in that it maintains its bulk conductivity during high temperature processing and has low residual stress. In addition, a unique adhesion material has been investigated and is currently being applied by n-Chip. This adhesion material would result in a significant cost reduction in the manufacture of copper or gold MCMs. The silver metallization technology and SiO_2 characterization is also being conducted with n-Chip. Silver has the highest room temperature conductivity of any material, however, it has reliability problems. The reliability studies suggest that at voltages (i.e. < 4 V) the failure mechanism is not operative, and modern dielectrics are significantly different than those used for in the studies. As a result, significant conductivity improvements may be realized with silver interconnections.

A second generation test module has been fabricated to provide test structures to evaluate new polymers and metals for multi-chip module applications. About half of the real estate is devoted to microwave structures designed at the Mayo clinic called "The High Frequency Passive Structure Coupon". The process has two

3

ground layers and two signal layers, and incorporates both microstrip and stripline waveguides, with characteristic impedance of 50 ohms, facilitating measurement with standard test equipment well up into the gigahertz regime. The emphasis for these structures is on evaluating high frequency electrical performance of actual MCM devices (waveguides).

A short list of organic and inorganic materials have been selected for evaluation as interlevel dielectrics with the noble metal interconnects. In-situ test structures are being fabricated to determine the electrical, mechanical and chemical properties of the dielectrics. Novel approaches to low dielectric constant insulators are being investigated in addition to the evaluation of existing materials. New techniques have been evaluated for rapid curing of polymer dielectrics.

Selection of thin film dielectrics is a key element in the performance and long-term reliability of GHz multichip modules. The overall performance depends on the ease of processing, chemical structure, electrical behavior and mechanical properties. Crucial characteristics which must be considered in the selection of materials to be used as interlevel dielectrics include: dielectric properties; moisture absorption; coefficient of thermal expansion; modulus; residual stress; adhesion; processing temperature; thermal stability; and thermal conductivity. The short list of polymers currently being investigated for use in GHz frequency MCMs include:

DuPont PI2545 (PMDA-ODA)
DuPont PI2566 (Fluorinated)
DuPont PI2611 (Low Stress)
Amoco Ultadel 7501 (Photosensitive)
Ciba-Geigy 400 Series (Pre-imidized and Photosensitive)
Allied-Maxdem polyquinolines
Dow Chemical benzocyclobutenes
BFGoodrich Polynorbornene

4

A number of inorganic materials have also been explored for interlevel dielectric applications, including:

Plasma Enhanced CVD Silicon Dioxide
Spin-on Glasses
Porous Silica

We have investigated the improvement in silicon dioxide performance through variation of deposition conditions. The effect of the measurement frequency on the dielectric properties of silicon dioxide has also been explored. We conclude that only vary modest improvements in dielectric constant can be achieved through changes in plasma temperature and frequency. The use of spin-on glasses and porous silica as interlevel dielectrics has been explored; it was determined that processing problems resulted in this application. Introducing porosity or fluorination into inorganic films have significant processing and reliability problems which make them unusable without new technical advances.

In order to compare the performance properties of the various dielectric materials, in-situ characterization techniques are required. Thermal cure history, fabrication environment and type of substrate upon which the pre-polymer is cast all can have a significant effect on the final film properties. Therefore, a polymer film cured on a particular surface may have significantly different properties than a film of the same material cured free of the substrate. In order that the characterization test results actually reflect the behavior of the polymer in a performance environment, it is necessary to measure the critical film properties directly on the substrate.

A number of methods have been used or developed for characterizing film properties directly on a silicon or metallized substrate. The in-plane modulus, residual stress, and in-plane coefficient of thermal expansion are measured using a Flexus Wafer Curvature Apparatus. The film thickness, refractive indices and degree of orientation are obtained using a Metricon Prism Coupler.

In applications requiring multilayer coatings, polymer properties normal to the plane are as crucial to the performance of the coating as polymer properties in the plane. Each of the characterization techniques mentioned above are restricted to the characterization of in-plane properties. The spin coat processing of polymer films may lead to molecules which are oriented in the plane of the film; this orientation will cause the electrical, mechanical and thermal properties in the plane of the film to be different from those properties through the plane of the film. In the industry, there is no test method for measuring mechanical and thermal properties normal to the plane of the film. In this study the microfabricated electrodes have been used to determine small changes in film thickness that result when the temperature in the film is varied. From these measurements, we have directly determine the coefficient of thermal expansion normal to the plane of the film.

In summary, a series of promising organic dielectrics have been selected for evaluation for use in GHz multi-chip modules. A series of in-situ characterization techniques have been developed for measuring electrical, mechanical and thermal properties of the interlevel dielectrics. The effect of the chemical system and processing variations on the performance properties of thin film dielectrics have been explored. Processing variations include the spin speed, film thickness, reaction temperature and degree of molecular orientation.

CHAPTER 2

STRESSES OF SPIN-CAST POLYMER FILMS ON SILICON SUBSTRATES

Abstract

Mechanical stress in multichip modules (MCM) is an important reliability and fabrication issue. The emergence of new electronic applications that operate at temperatures significantly higher or lower than room temperature place new demands on the stress behavior of polymer dielectric films. This work examines the stress as a function of temperature for a variety of dielectric polymers. Stresses above and below room temperature were examined using a wafer curvature measurement. The polymers with the lowest stresses were found to be the most rigid polymers.

Introduction

Knowledge of mechanical stresses in multichip modules is an important reliability and fabrication issue. High stresses at interfaces can be problematic during fabrications and can result in mechanical failure of devices. Stress induced wafer curvature cases difficulty in handling and in specific processes, such as photolithography. [1,2] The stresses generated in polymer films are, in general, due to the mismatch in the coefficient of thermal expansion (CTE) between the high CTE polymer and the lower CTE substrate material. [3] The thermal stress in the polymer arises from molecular orientation that is created during cure and the subsequent contraction of the polymer chains upon cooling from the cure temperature. [4] Measurement of the stress behavior of polymer films with temperature allows proper selection of materials to minimize the interfacial stresses.

Polymer insulators for use in electronic applications as interlevel dielectrics or for packaging purposes have been extensively studied and documented. [5-10] However, most of the previous work has been performed at or around room temperature. The stress developed between high CTE polymer insulators (e.g. >20 ppm/°C) and low CTE substrate materials varies as the temperature changes. [11,12]

7

The emergence of new electronic applications that operate at temperatures significantly higher or lower than room temperature place new demands on the stress behavior of polymer dielectric films. This work intends to investigate the stress-temperature behavior of a wide range of polymer films cast on silicon substrates and highlight likely candidates for both high temperature and subambient packaging dielectrics.

Stresses in solvent based polymer films arise from differences between the in-plane thermal expansion or contraction of the polymer film and the substrate on which it is cast. The factors that control these stresses include: the in-plane coefficient of thermal expansion (CTE) of the polymer film, the in-plane Young's modulus of the polymer, the Poisson's ratio of the polymer, polymer film morphology such as crystallinity and chain rigidity, and exposure to absorbants, such as moisture.[13,14] The in-plane CTE of a polymer film is primarily determined by the extent of in-plane orientation created during processing. Internal stress developed as a result of film shrinkage lead to a more highly oriented film. The increase in the in-plane orientation during processing is partially countered by molecular relaxation effects. The extent to which relaxation can occur is affected by the processing conditions and the polymer chain morphology. The degree of in-plane orientation in the final film is a function of the curing profile as well as the chemical make-up of the polymer. More rigid polymers will exhibit a higher in-plane orientation since the molecules do not have enough flexibility to orient more isotropically between the in-plane and through-plane directions. Birefringence, the difference between the in-plane and through-plane refractive indices of the film, corresponds to the degree of optical anisotropy, which reflects the molecular orientation. Using the birefringence of the film in conjunction with the stress as a function of temperature, some indication regarding the stiffness of a polymer film may be extracted.

Achieving low stress dielectric polymer films above room temperature is relatively easy because of the nature of the stresses in the films. The thermal stress developed between the high CTE film and the low CTE substrate decreases as the temperature rises above room temperature. In fact, the stress in the film usually goes to zero upon reaching either the glass transition temperature or the cure

temperature, whichever is lower. [3] A number of different commercial polymer systems has been examined by various researchers [1,2,3,15]; however, a comprehensive study of the stress-temperature behavior examining a variety of materials has not been undertaken. In this work, four polyamic acid based polyimides, PMDA/ODA, BTDA/ODA, 6FDA/ODA, and BPDA/PPD (DuPont PI-2540, PI-2555, PI-2566 and PI-2611, respectively); two acetylene terminated polyisoimides, National Starch EL-5010 and EL-5512; one preimidized polyimide, BTDA/DAPI (OCG Probimide 293); an amide modified polyamic acid based polyimide (Hitachi PIQ-L100); and a non-polyimide benzocyclobutene polymer (Dow Chemical Cyclotene 3022) were tested for their stress behavior as a function of temperature above room temperature.

Usage of polymer thin film dielectrics at subambient temperatures is a more difficult challenge. The polymer dielectric films can be required to survive the temperature cycling from room temperature to ~77 K, for low temperature electronic systems or high temperature superconductors (HTS). Previous work by Arora et al. examining the usage of DuPont Pyralin 2703D, a photodefinable polyimide with properties similar to PI-2555, as an encapsulant for HTSs resulted in severe cracking of the superconductor and degradation of the polymer in high humidity environments. [16] Stresses caused by the shrinkage of the polyimide were attributed as the cause of the cracking of the HTS and the delamination of the polyimide coating. Arora's work emphasizes the need for proper polymer selection for integration with HTS conductors. Minimizing the stress at subambient temperatures as well as moderating the changes observed in the stress with temperature are both important technical goals for integrating polymer dielectrics into low temperature devices. A variety of commercially available polymers have been tested as part of this work to determine their stress level at subambient conditions. The ideal polymer for HTS insulation in order to minimize degradation of the superconductor, would cure at a low temperature (<200°C), should not evolve moisture during cure, will be a good moisture barrier when fully cured, and will have a low CTE and modulus to minimize the stresses between the film and the HTS conductors. The polymers chosen for measurement of subambient stress include three polyamic acid based polyimides, PMDA/ODA, 6FDA/ODA and

BPDA/PPD, as well as a preimidized polyimide, BTDA/DAPI, an amide functionalized polyimide, PIQ, and a non-polyimide dielectric polymer, benzocyclobutene. The polyamic acid based polyimides, both amide functionalized and not, generate moisture during cure and must be cured at 350°C, however, the low cost of PMDA/ODA, the moisture barrier properties of 6FDA/ODA, and the low stresses in the rigid BPDA/PPD and PIQ materials make each of them likely candidates for low temperature microelectronic applications that do not include HTSs. BTDA/DAPI can be cured at a low temperature and generates no moisture during cure, due to its preimidization, but has a rather high CTE. BCB can be cured at a low temperature, generates no moisture during cure, and is a good moisture barrier.

Experimental

The stress in the polymer films were measured in-situ on silicon wafers using a Flexus F2320 Thin Film Stress Measurement System. The principle of this technique is the comparison of the curvature of the substrate before and after film deposition and calculating the film stress that is required to generate the observed curvature. The quantitative usage of the radius of curvature of a multilayer structure to extract the stress in the layers of the structure was first developed by Stoney in 1909.[17] Stoney's equation for stress in two dimensions is given by :

$$\sigma = -\frac{E}{(1-v)}\frac{h^2}{6Rt}$$

(1)

where s is the average film stress, $E/(1-n)$ is the biaxial modulus of the substrate (1.805×10^{11} Pa for <100> silicon wafers[18]), h is the substrate thickness, t is the film thickness, and R is the substrate radius of curvature. The Stoney equation for biaxially strained films obtained in equation 1 has been verified by numerous independent sources that use it to measure the stress of a thin film on a thick substrate.[19-28]

For stress testing, bare silicon substrates were scanned in the Flexus F2320 to determine the uncoated wafer curvature prior to polymer deposition. Each of the

polymers tested was spin-coated onto a silicon substrate to achieve a thickness of approximately 3 to 5 mm thickness after cure. The films were cured according to the recommended cure schedules of the manufacturers. All of the polymer films were cured in a nitrogen purged tube furnace. The typical cure cycle for the polymides was a 2°C/min from room temperature to 200°C, hold for 30 minutes, ramp at 2oC/min to 350°C, hold at 350°C for 1 hour and a cool down at approximately 2°C/min. The benzocyclobutene films in this work were cured at 275°C for 1 hour with heating and cooling ramps at 2°C/min. The curvature of the coated wafers was measured after cure as a function of temperature. Two temperature profiles were used in the Flexus measurements. The first has temperature holds at 50°C intervals, and the second was a slow (1°C/min or slower) continuous ramp from room temperature to the maximum temperature was utilized. Both temperature profiles allow the wafer to reach a thermal equilibrium with the stage in the Flexus unit. Faster ramp rates or shorter hold times cause the temperature of the wafer to lag the stage temperature. Stresses were calculated using Equation 1. The silicon properties were obtained from the CINDAS Database. [29] Temperature calibration, relating the Flexus thermocouple temperature to the actual wafer temperature, was performed by using an independent thermocouple which had been calibrated using liquid nitrogen (-196°C or 77 K) and ice water (0° C).[30]

The thickness of the films were measured using a commercially available prism coupler (Metricon Model 2010 Prism Coupler). The prism coupler technique utilizes the ability of thin films to act as an optical waveguide and provides an *in-situ* and non-destructive means to obtain both the refractive index and the film thickness accurately. [31][32] For the polymer films examined in this work, accurate simultaneous refractive index and film thickness data from prism coupler measurements can be expected for films less than 10 μm. Measurements of the refractive index of the film in both the in-plane and through-plane directions may be obtained by polarizing the laser source.

The Flexus stage was modified in order to achieve subambient temperatures and temperature calibration down to -170°C. Water condensation and subsequent

icing of the substrate at subambient temperatures were significant operational difficulties in initial work. [30] The condensed moisture distorted or blocked the laser beam used to measure the radius of curvature. To avoid this problem, the Flexus was double sealed (two barriers) and nitrogen gas flowed into the chamber. The pressure inside the glove bag was maintained slightly higher than atmospheric (approximately 0.2 psig). The Flexus was purged for at least two hours prior to cooling to subambient temperatures.

Measurements were made by holding the temperature at 20°C intervals for 20 minutes from 25°C to -170°C. This procedure allowed the wafer and film to come to a thermal equilibrium with their surroundings insuring stable stress measurements. Insufficient purging becomes apparent by an erroneous decrease (more compressive) in the measured stress as frost forms on the film and distorts the reflected laser beam. The sudden frosting of the film invalidates any further measurements at lower temperatures. Measurements above room temperature were used for comparison with the subambient measurements.

Results

Polyamic Acid Based Polyimides

PMDA/ODA (DuPont PI-2540) was spin-coated to a thickness of 3.92 μm onto a 4 inch diameter silicon substrate. The refractive indices of the PMDA/ODA film are 1.719 in-the-plane and 1.639 through-the-plane of the film. Stress as a function of temperature for PMDA/ODA is shown in Figure 1. The standard deviation of the stress calculated at each temperature is shown as error bars on Figure 1. The stress measurements were taken at 20°C intervals to 200°C and the slope of the stress as a function of temperature was found to be -0.05 MPa/°C.

Two films of BTDA/ODA (DuPont PI-2555) were cast onto silicon substrates at thicknesses of 3.66 μm and 3.74 μm. The refractive indices of the BTDA/ODA films were 1.686 and 1.667, in the in-plane and through-plane directions, respectively. The stress as a function of temperature for the thinner BTDA/ODA film, as well as the standard deviation of the stress measurements, are shown in

12

Figure 2. The measurements were taken at 50°C intervals with approximately 40 measurements at each temperature hold. The stress is generally linearly decreasing with increasing temperature, except between room temperature and 50°C. This slight increase in stress near room temperature was attributed to residual moisture which outgassed at higher temperature. The linear regression results for the two BTDA/ODA wafers are shown in Table 1. The slope of the stress measurements as a function of temperature for the two BTDA/ODA wafers is -0.15 MPa/°C. The stress reaches zero at approximately 275°C indicating the temperature at which the molecular orientation was locked in during curing.
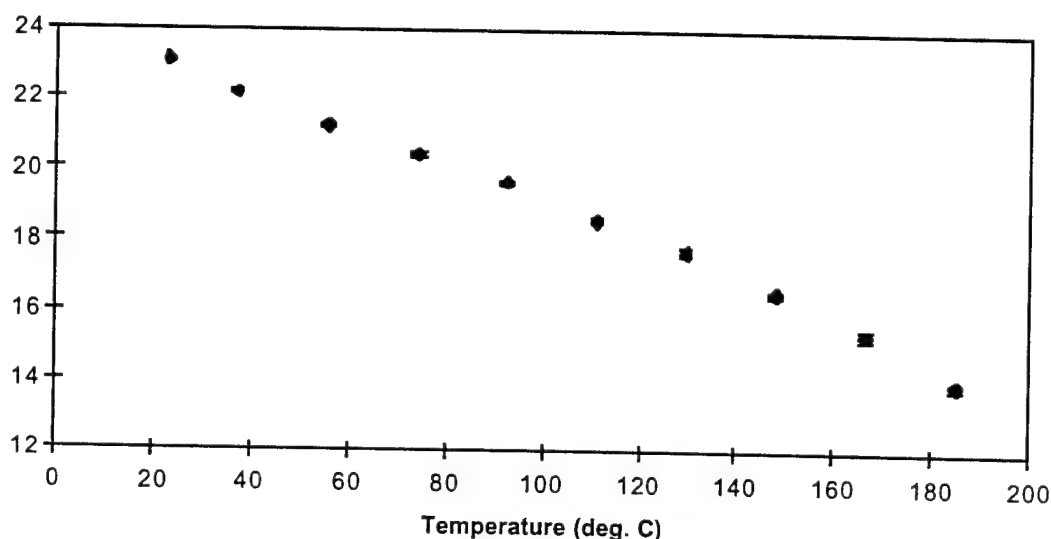

Figure 1 Stress as a Function of Temperature for PMDA/ODA

6FDA/ODA (DuPont PI-2566) was spin-cast onto two silicon substrates at thicknesses of 4.80 μm and 4.79 μm, respectively. The in-plane and through-plane refractive indices are 1.587 and 1.578, respectively. Stress as a function of temperature for the thicker film is shown in Figure 3. The standard deviation at each hold is shown in Figure 3 as error bars. The stress is linearly decreasing throughout the entire temperature range, reaching zero at approximately 280°C. The thinner film was measured four times to examine the reproducibility of the measurements as well as the comparison against the measurements from the first

film; the results of the five measurements are shown in Figure 4. The linear regression results for the 6FDA/ODA stress-temperature measurements are shown in Table 2. The average slope of the stress-temperature measurement is -0.15 MPa/°C. This result shows that the slope obtained is very reproducible because the standard deviation is less than 5% of the measured value.
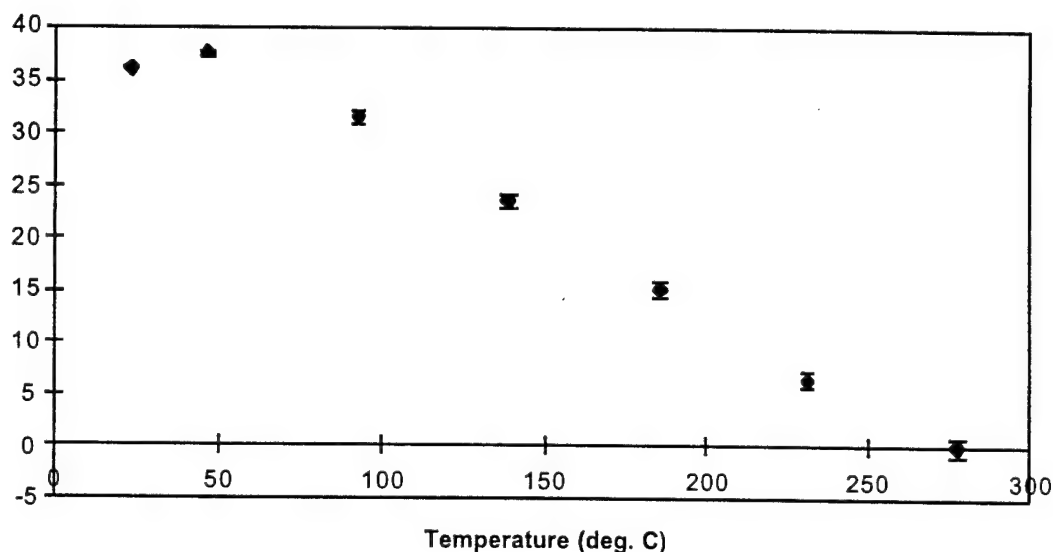

Figure 2 Stress as a Function of Temperature for BTDA/ODA

Table 1 Linear Regression Results for BTDA/ODA

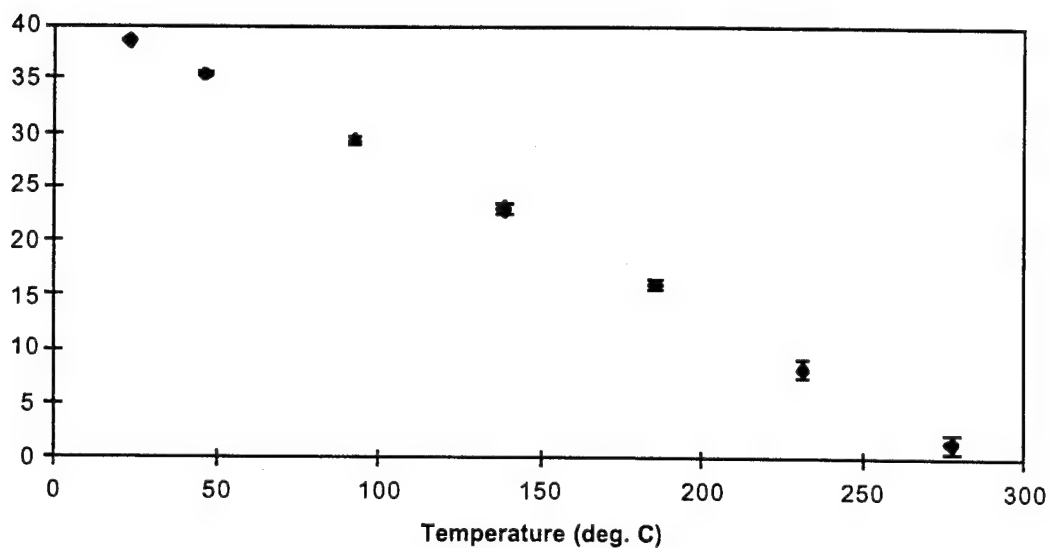| Film Thickness (μm)	Slope (MPa/°C)	Intercept (MPa)	R^2
3.74	-0.15	40.48	0.9610
3.66	-0.14	43.33	0.9806
Average	-0.15	41.90	---
St. Dev.	0.01	2.01	---

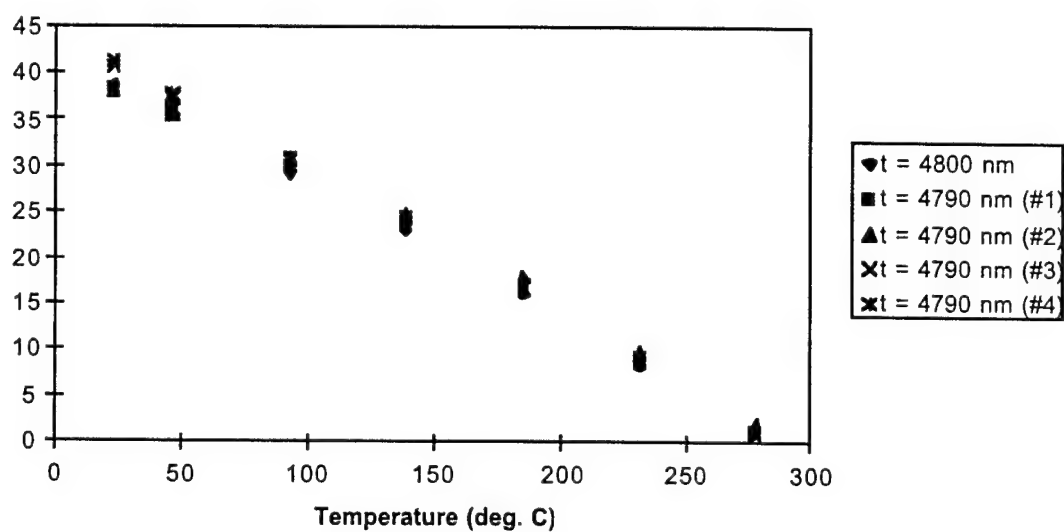Figure 3 Stress as a Function of Temperature for 6FDA/ODA

Figure 4 Five Stress-Temperature Measurements of 6FDA/ODA

15

Table 2 Linear Regression Results for 6FDA/ODA

Film Thickness (μm)	Slope (MPa/°C)	Intercept (MPa)	R^2
4.79	-0.16	45.21	0.9986
4.79	-0.16	44.75	0.9985
4.79	-0.14	42.73	0.9903
4.79	-0.15	42.82	0.9959
4.80	-0.15	42.52	0.9982
Average	-0.15	43.61	---
St. Dev.	0.01	1.27	---

Three films of BPDA/PPD (DuPont PI-2611) were spin-cast onto silicon substrates. The film thicknesses were 3.78 μm, 3.08 μm, and 4.19 mm respectively. The refractive indices for the BPDA/PPD films were 1.836 in-the-plane of the film and 1.619 through-the-plane of the film. The stress as a function of temperature for the thicker BPDA/PPD film is shown in Figure 5. The stress shows a decreasing trend with increasing temperature; however, the stress does not change linearly. A slight curvature in the stress-temperature curve may result from variations in the modulus and CTE of the polymer as a function of temperature. The stresses measured for the BPDA/PPD are approximately one order of magnitude lower than that seen in PMDA/ODA, BTDA/ODA, and 6FDA/ODA. This lower stress results from the higher rigidity of the polymer backbone of the BPDA/PPD polyimide chain. The standard deviation of the stress measurements is significantly higher than that observed in the other polyamic acid polyimides due to the much smaller changes in curvature observed with the BPDA/PPD films. The linear regression results from the three wafers are shown in Table 3. The average slope of the stress as a function of temperature is -0.01 MPa/°C. The slope in all three cases is

significantly smaller than those observed in the PMDA/ODA, BTDA/ODA, and 6FDA/ODA films. The lower slope (similar to the lower stress) indicates a lower in-plane coefficient of thermal expansion for the more rigid BPDA/PPD polyimide.
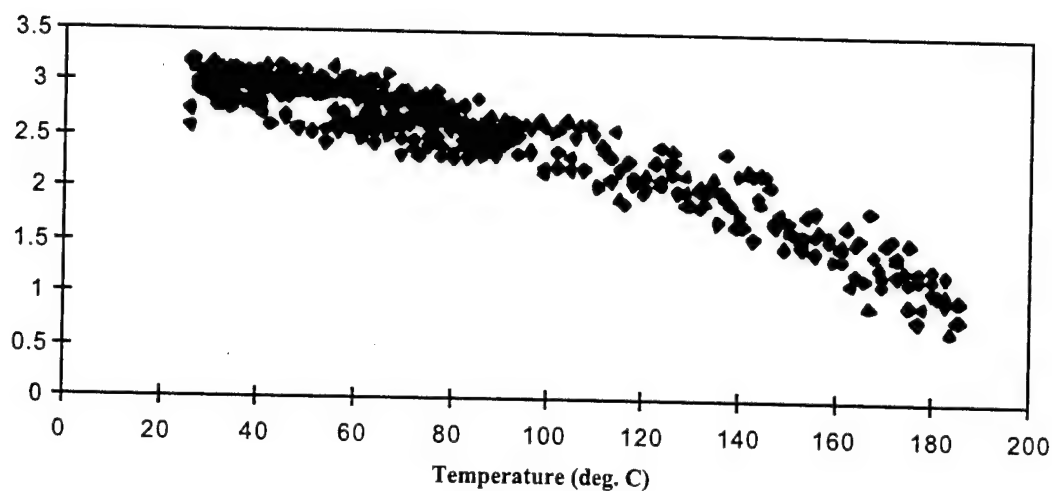

Figure 5 Stress as a Function of Temperature for 4.194 mm BPDA/PPD film.

Table 3 Linear Regression Results for BPDA/PPD measurements

Film Thickness (mm)	Slope (MPa/°C)	Intercept (MPa)	R^2	Temperature Range (°C)
3.08	-0.01	5.41	0.3129	25-300
3.78	-0.02	7.42	0.7498	25-300
4.19	-0.01	3.47	0.8775	25-200
4.19	-0.01	3.38	0.9230	25-200
Average	-0.01	4.92	----	----
St. Deviation	0.01	1.91	----	----

Acetylene-Terminated Polyimides

A 6.95 µm film of nonfluorinated acetylene-terminated isoimide (National Starch EL-5010) was cast onto a silicon substrate. The refractive indices of the EL-5010 film were 1.683 and 1.676, in the in-plane and through-plane directions, respectively. The stress as a function of temperature for EL-5010 is shown in Figure 6. The stress linearly decreases from room temperature to approximately 180°C above which the stress remains zero. The zero stress state above 180°C indicates that the film is above its glass transition temperature. The slope of the stress-temperature measurements below 180°C is -0.22 MPa/°C. This slope is somewhat higher than the slopes observed for the non-rigid rod polyamic acid polyimides which show a slope of approximately -0.15 MPa/°C. The higher slope indicates that the crosslinked EL-5010 has a higher CTE and/or modulus than that of the polyamic acid based polyimides.

A 6.80 µm fluorinated acetylene-terminated isoimide film (National Starch EL-5512) was cast onto a silicon substrate. The in-plane refractive index for the EL-5512 film is 1.610 and the through-plane refractive index is 1.605. The stress as a function of temperature for EL-5512 is shown in Figure 7. The stress linearly decreases from room temperature to approximately 230°C above which the stress remains approximately zero. Similar to the EL-5010 film, the stress measurements indicate a glass transition temperature below the 350°C cure temperature at approximately 230°C. The slope of the stress-temperature measurements below 230°C is -0.21 MPa/°C,
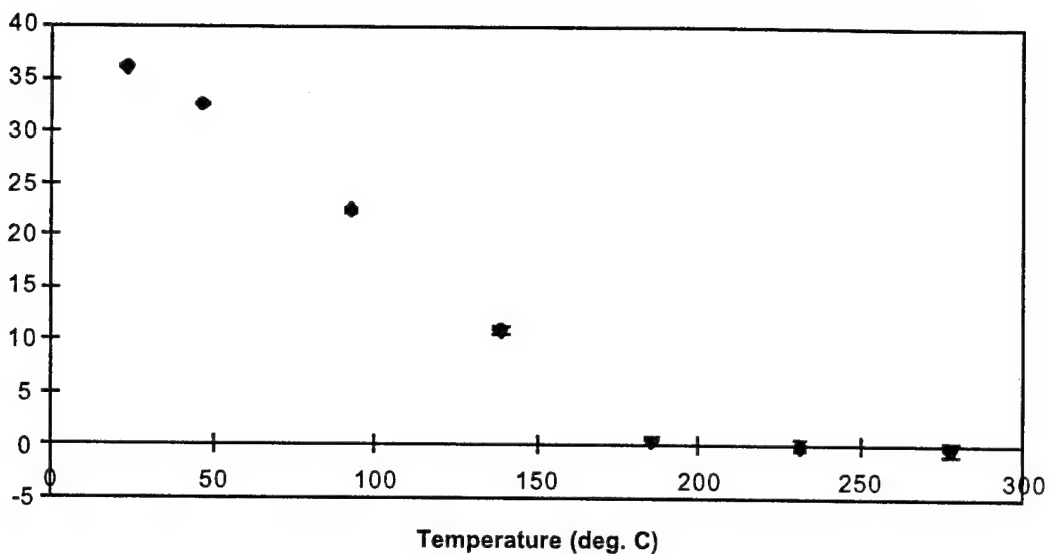
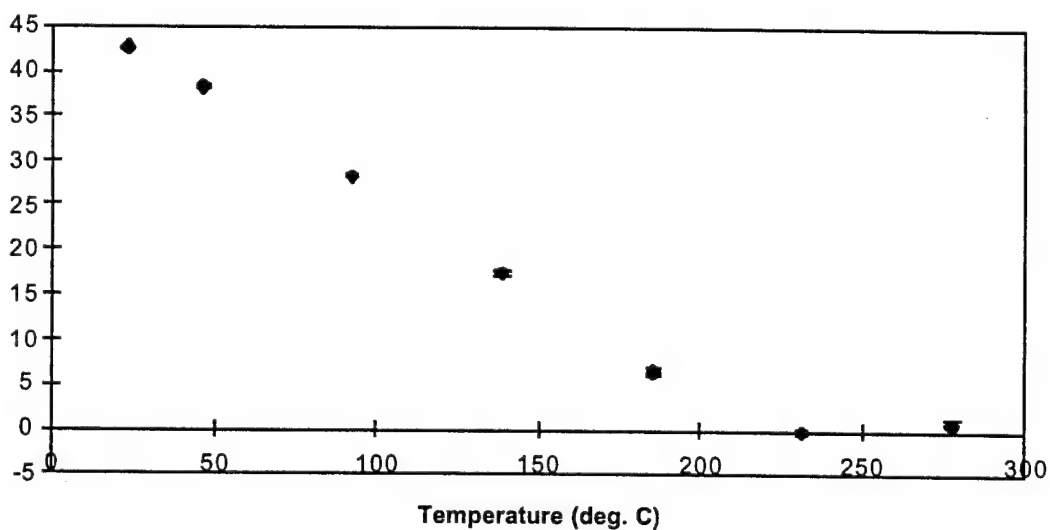Figure 6 Stress as a Function of Temperature for EL-5010

Figure 7 Stress as a Function of Temperature for EL-5512

similar to that found in EL-5010, again indicating a higher CTE and/or modulus than the polyamic acid based polyimides.

Polyisoindoloquinazolinedione

Four films of Hitachi PIQ-L100 were spin-cast on silicon substrates in thicknesses of 3.48 µm, 3.31 µm and two of 3.36 mm. The refractive indices determined by prism coupling are 1.838 in-the-plane of the film and 1.620 through-the plane of the film. The two 3.36 mm films were measured using two continuous ramps from 25°C to 200°C and back to 25°C at 1°C/minute and a third continuous ramp from 25°C to 100°C and back to room temperature at 0.2°C/minute. The other two films were measured using a ramp-and-hold program with holds every 50°C for 20 minutes from 25°C to 300°C. The continuous ramps were performed in a dry nitrogen environment to reduce the effect of moisture. The stress as a function of temperature for one of the continuous ramp experiments is shown in Figure 8. The results show a relatively flat stress on the first heating cycle followed by a linear change in the stress as a function of temperature for the subsequent heating and cooling cycles. The difference between the first heating and the subsequent cycles is most likely due to the presence of moisture in the film during the initial heating. Water molecules in the structure would plasticize the material reducing the stress. The observations in this experiment indicate that the polymer film is plasticized to some extent. The linear regression results for the continuous ramp measurements are shown in Table 4. The data in Table 4 for the
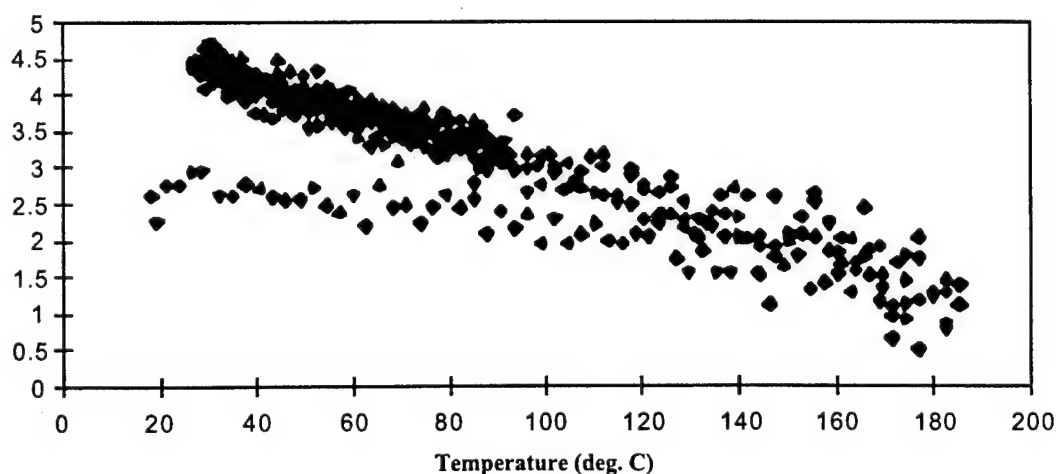

Figure 8 Stress as a Function of Temperature for PIQ-L100

Table 4 Linear Regression Results for PIQ-L100 Stress-Temperature Measurements

Film Thickness (mm)	Slope (MPa/°C)	Intercept (MPa)	R^2	Temperature Range (°C)
3.355	-0.02	4.94	0.9413	25-200
3.355	-0.02	5.24	0.9545	25-200
Average	-0.02	5.09	----	----
Standard Deviation	----	0.22	----	----
3.455	-0.003	2.57	0.1530	25-300
3.317	-0.006	1.99	0.1934	25-300
3.317	-0.003	2.68	0.0488	25-300
Average	-0.004	2.42	----	----
Standard Deviation	0.002	0.37	----	----
Overall Average	-0.01	3.25	----	----
Overall St. Dev.	0.01	1.91	----	----

continuous measurements exclude the data taken during the initial heating to 200°C. The average slope for these two measurements is -0.02 MPa/°C. The ramp-and-hold experiments were not performed under nitrogen and show a lower slope, similar to the initial heating cycle in the continuous ramp experiments, as shown in Table 4. Two measurements of the thinner film were taken in addition to the measurement of the thicker film using the ramp-and-hold program. The average slope of the three ramp-and-hold measurements is -0.004 MPa/°C with a standard deviation of 0.002 MPa/°C. These results indicate a very rigid polymer with an extremely low CTE, consistent with the chemical structure discussed in Section 1.2.

Preimidized Polyimides

Preimidized BTDA/DAPI (OCG Probimide 293) was coated onto a silicon substrate in a thickness of 4.53 μm. The refractive indices of the film are 1.633 in-the plane and 1.620 through-the-plane of the film. The stress as a function of temperature for BTDA/DAPI is shown in Figure 9. Measurements in Figure 9 were taken during a continuous temperature cycle, not at a series of holds, so standard deviations on the data are not available. The stress linearly decreases from room temperature to approximately 190°C with a slope of -0.13 MPa/°C. This slope is comparable to that found in the non-rigid rod polyamic acid based polyimides, indicating similar CTEs and moduli.

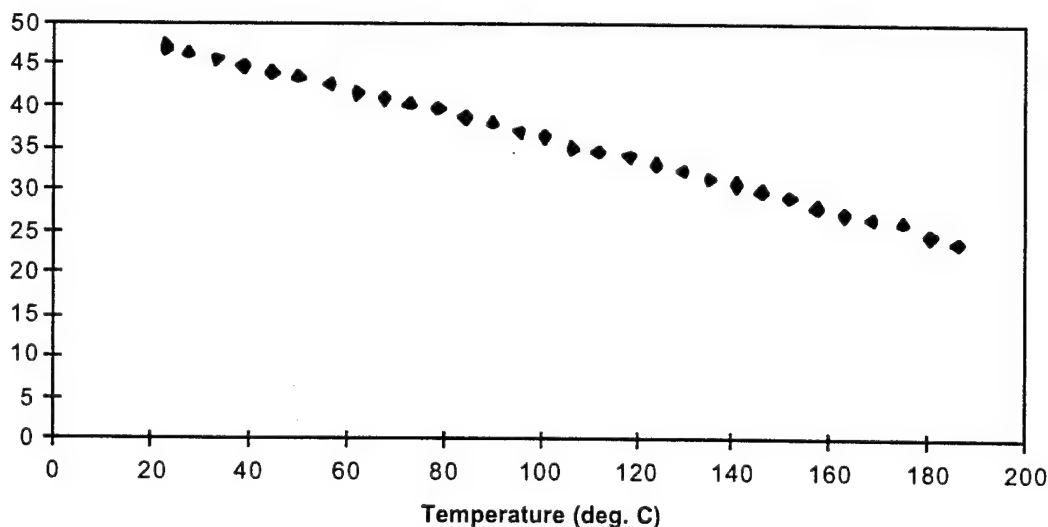**Figure 9   Stress as a Function of Temperature for OCG Probimide 293.**

Benzocyclobutene

Stress as a function of temperature was measured for a 6.97 mm BCB film on a 400 mm silicon substrate over the temperature range from 25°C to 175°C. The measurements above room temperature were performed using a continuous ramp. Two sets of measurements were performed and the linear regression results are

shown in Table 5. One set of stress-temperature data is shown in Figure 10. The measurements show a very linear relationship between the stress and temperature indicating the CTE and biaxial modulus are not functions of temperature.

Table 5 Linear regression results of BCB stress-temperature measurements.

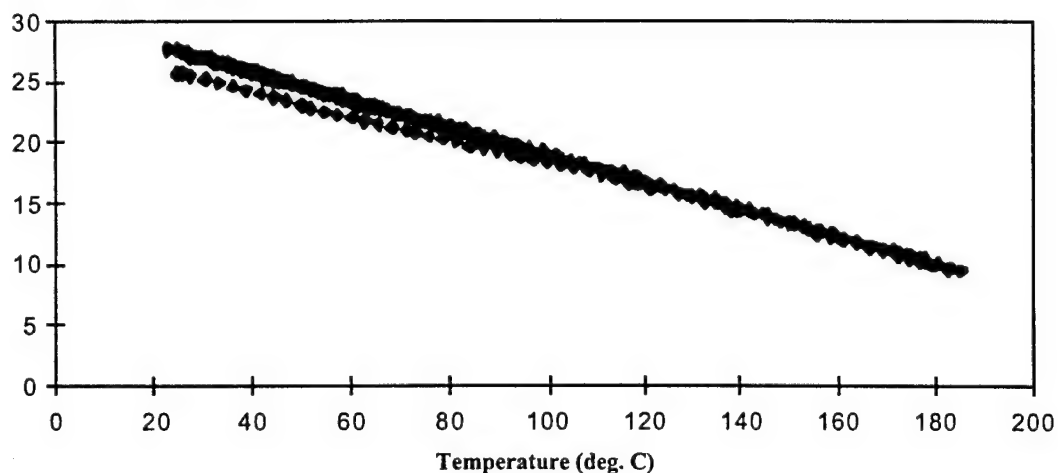| Run	Slope (MPa/°C)	Intercept (MPa)	R^2
1	-0.11	30.05	0.9947
2	-0.10	29.56	0.9970
Average	-0.11	29.81	----
St. Dev.	0.01	0.35	----

Figure 10 Stress as a function of temperature for BCB film on a silicon substrate using a continuous ramp profile.

Subambient Results

Polyamic Acid-Based Polyimides

PMDA/ODA was cast onto two 380 μm thick silicon wafers yielding film thickness of 4.37 μm and 3.92 μm, respectively. The first wafer was continuously temperature cycled over the range from -165°C to 175°C three times. Results from these temperature cycles are shown in Table 6. The second wafer was cycled only once using the ramp-and-hold procedure. The linear regression from this experiment is also shown in Table 6. A representative measurement of stress as a function of temperature for PMDA/ODA is shown in Figure 11; all four experiments show nonlinearity in the stress as a function of temperature. The stress at -165°C for the data shown in Figure 11 is 43.41±0.65 MPa.

6FDA/ODA was spin-coated onto two 380 μm thick silicon wafers. The average thickness of the films were measured and calculated to be 2.37 μm and 5.73 μm. The first wafer was scanned two times over the range of -165°C to 175°C and once from -110°C to 25°C with a hold at -105°C. The linear stress-temperature response of this film can be seen in Figure 12 where a continuous ramp from -165 to 175°C was used. Similar experiments were performed on the thicker polymer film: three measurements from -165 to 175°C and one from -95°C to 20°C. A typical result of the

thicker   film   from   -165   to   175°C   is   shown   in   Figure   13.

Figure 11 Typical Stress as a Function of Temperature Measurement for
PMDA/ODA Film

Table 6. Regression Results for PMDA/ODA in the Form of $y=ax^2+bx+c$

Film Thickness (µm)	a (MPa/°C^2)	b (MPa/°C)	c (MPa)	R^2
4.37	9x10^{-5}	-0.0905	25.588	0.9949
4.37	0.0002	-0.1138	26.025	0.9961
4.37	0.0002	-0.1181	28.185	0.9956
average	0.0002	-0.1075	26.599	
st. dev.	0.00006	0.0149	1.391	
3.92	0.0001	-0.0878	26.524	0.996

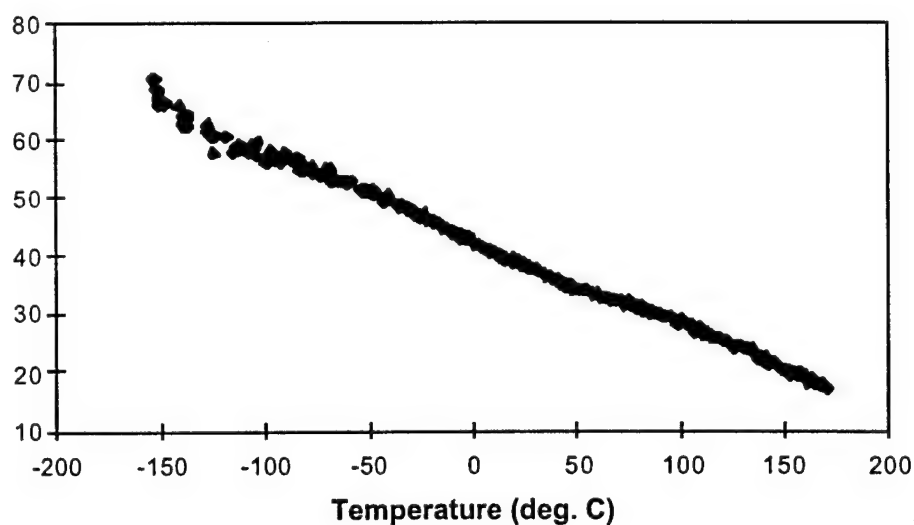

Figure 12. Stress as a Function of Temperature for 2.37 µm thick 6FDA/ODA film

Figure 13 Stress as a Function of Temperature for 5.73 μm thick 6FDA/ODA film

The regression results for the 6FDA/ODA measurements are shown in Table 7. The stress at -165°C was found to be 67.74±0.32 MPa for data shown in Figure 13.

Subambient measurements of BPDA/PPD film on a 400 mm silicon substrate were performed. The film thickness was 4.19±0.05 mm. The subambient measurements were performed using the ramp-and-hold temperature control while measurements above room temperature were performed using a slow (1°C/minute) ramp from 25°C to 200°C for two cycles followed by a very slow ramp (0.2°C/minute) from 25°C to 100°C. The stress-temperature results are shown in Figure 14. The stress-temperature plot shows some non-linearity in the subambient region with the stress increasing as the temperature decreases. The stress at -165°C is 9.35±0.85 MPa, considerably lower than the stress of PMDA/ODA or 6FDA/ODA at the same temperature. This result is due to the lower CTE of the BPDA/PPD film

27

than that of the other two polyimides. Regression of the stress-temperature data over the entire temperature range shown in Figure 14 yields

$$\sigma = 3.6941 - 0.0217 * T + 5.36x10^{-5} * T^2 \tag{2}$$

where s is the stress in MPa and T is the temperature in °C. The regression coefficient (R^2) for the quadratic relation is 0.9748.

Table 7. Linear Regression Results for 6FDA/ODA

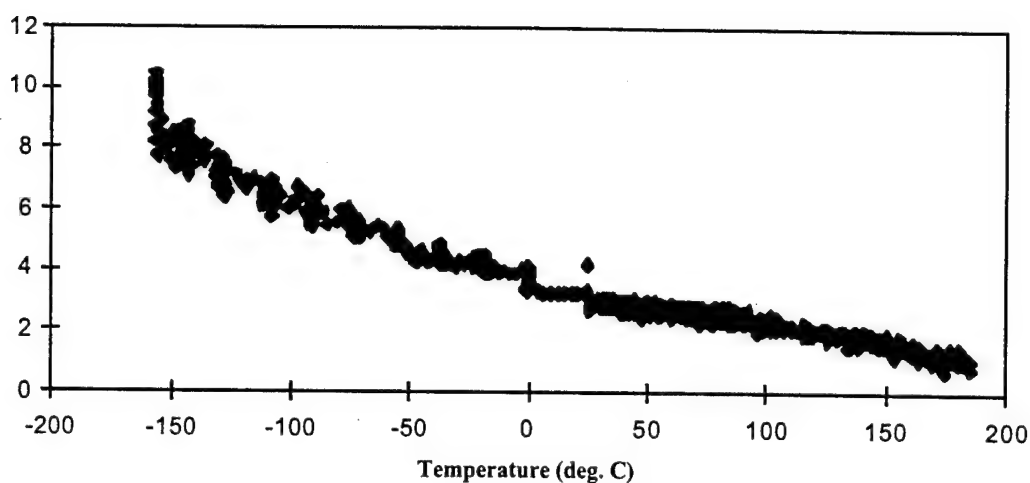| FilmThickness (μm)	Slope (MPa/°C)	Intercept (MPa)	R^2
2.37	-0.14	41.35	0.9949
2.37	-0.16	44.10	0.9831
2.37	-0.15	42.83	0.9956
average	-0.15	42.76	---
st. dev.	0.01	1.37	---
5.73	-0.18	44.18	0.9988
5.73	-0.16	44.38	0.9959
5.73	-0.16	45.33	0.9983
5.73	-0.15	41.74	0.9713
average	-0.16	43.91	---
st. dev.	0.01	1.53	---

Figure 14 Stress as a function of temperature for 4.19 mm BPDA/PPD film including subambient measurements.

Polyisoindoloquinazolinedione

Hitachi PIQ-L100 was tested on silicon substrates over the temperature range of -165°C to 175°C. Two films 3.36 mm thick were spin-coated onto 400 mm thick silicon substrates. Measurements above room temperature were performed using continuous ramps. Subambient measurements were performed using a ramp-and-hold procedure with holds every 20°C. The duration of the holds was 20 minutes. A typical result is shown in Figure 15. The subambient measurements show a generally increasing stress with decreasing temperature except for a level region below -100°C. This level region could result from either material changes in this region or from frosting on the wafer surface caused by insufficient purging. The level region was consistent between the two wafers tested. The film stress at -165°C is 8.29±0.76 MPa. Linear regression results for the two wafers tested are shown in Table 8. Regression was performed using all data from the measurements both above and below room temperatures. The slope is very small compared to the more flexible polyimides and is comparable to that of the rigid PI-2611 polyimide.

29

Figure 15 Stress as a function of temperature for PIQ-L100 from -165°C to 175°C.

Table 8 Linear regression results for subambient measurements of PIQ-L100.

Wafer	Data Used	Slope (MPa/°C)	Intercept (MPa)	R^2
1	All	-0.02	4.84	0.9141
2	All	-0.02	4.84	0.9086
Average	All	-0.02	4.84	----
St. Dev.	All	----	----	----
1	Linear Region	-0.02	5.09	0.9618
2	Linear Region	-0.02	5.18	0.9526
Average	Linear Region	-0.02	5.13	----
St. Dev.	Linear Region	----	0.06	----

Preimidized Polyimides

Probimide 293 preimidized polyimide was tested on silicon substrates over the temperature range of -165°C to 175°C using continuous ramps. The Probimide 293 film was 4.53±0.05 μm thick on a 380 μm thick silicon substrate. The stress as a function of temperature for one of the Probimide 293 temperature cycles is shown in Figure 16 and the linear regression results for all of the cycles are shown in

Table **9**. The stress at   -165°C for the data shown in Figure 16 is 75.48±0.65 MPa.

Figure 16. Stress as a Function of Temperature for Probimide 293

Table 9. Probimide 293 Subambient Linear Regression Results

Film Thickness (μm)	Slope (MPa/°C)	Intercept (MPa)	R^2
4.53	-0.16	46.45	0.9939
4.53	-0.16	47.81	0.9957
average	-0.16	47.13	---
st. dev.	----	0.96	---

Benzocyclobutene

Stress as a function of temperature was measured for a 6.97 mm BCB film on a 400 mm silicon substrate over the temperature range from -165°C to 175°C. The measurements above room temperature were performed using a continuous ramp profile. Below room temperature, a ramp-and-hold program was utilized with holds every 20°C for 20 minutes. Two runs were performed on the BCB film; one set of measurements is shown in Figure 17. The stress is highly linear from 175°C down to approximately -75°C where the slope changes and becomes more shallow. This change in slope may be due to either frosting of the wafer surface due to insufficient purging or the result of change in the mechanical properties of the polymer. Both runs showed a slope change at the same temperature. If the more shallow slope is due to polymer property variations with temperature, this would imply that the BCB film has either a lower CTE or lower biaxial modulus below -75°C. Linear regression calculations were performed on both runs using the data above -75°C. The linear regression results are shown in Table 10. Extrapolating the data below -75°C, the stress at -165°C is 48.69 MPa.
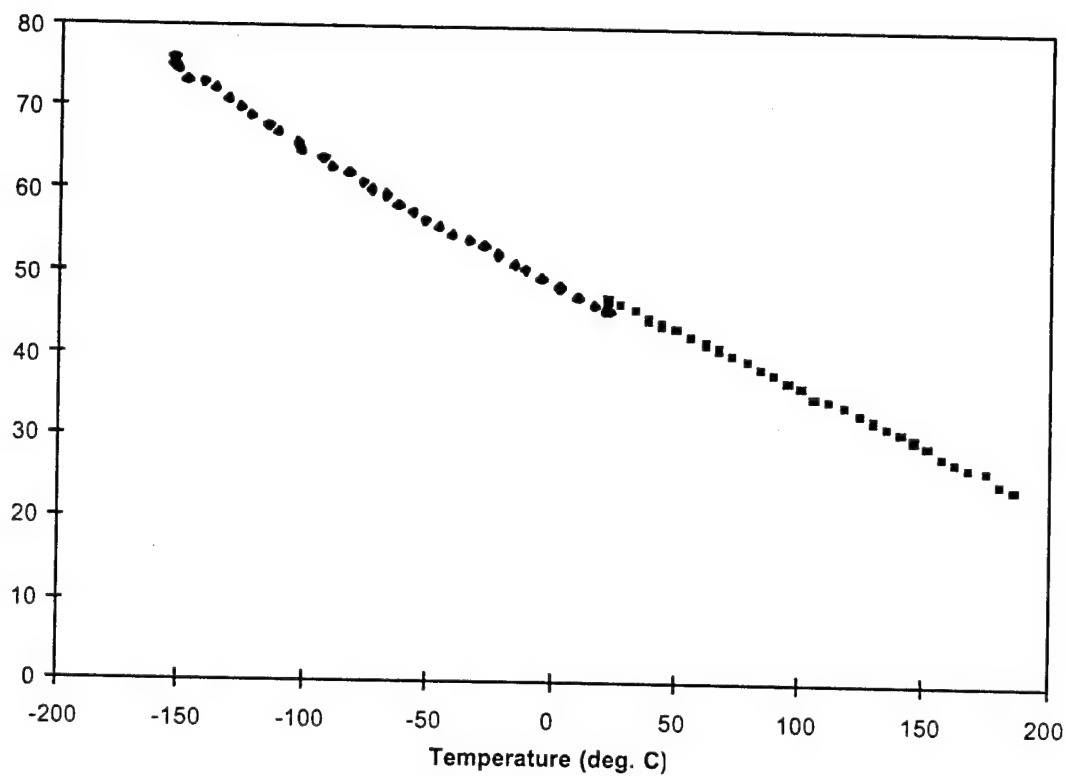
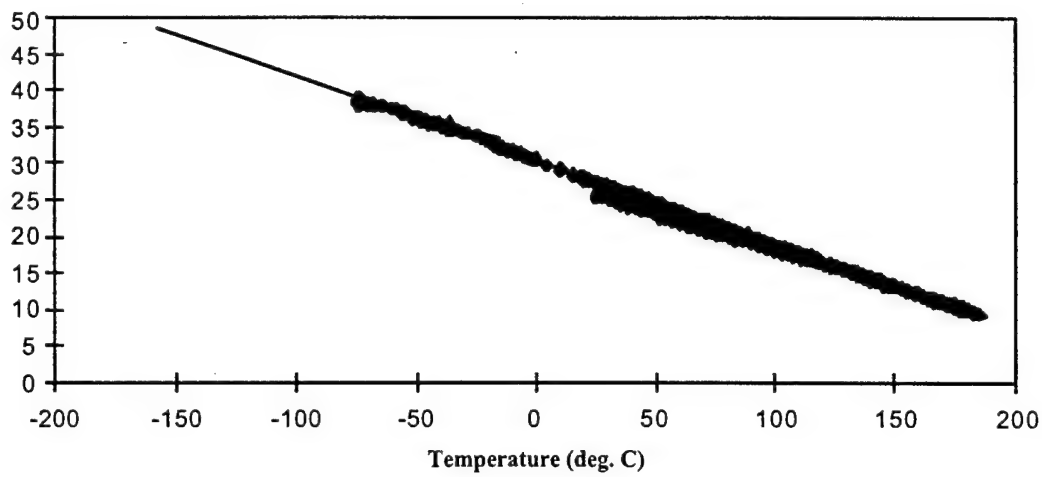**Figure 17** Stress as a function of temperature of BCB on silicon from -165°C to 175°C. Line represents the linear regression of data above -75°C.

Table 10 Linear regression results for 6.968 mm thick BCB on silicon.

Run	Slope (MPa/°C)	Intercept (MPa)	R^2
1	-0.12	30.42	0.9972
2	-0.11	30.21	0.9969
Average	-0.11	30.31	----
St. Dev.	0.01	0.15	----

Discussion

All of the polymers in this study show a decreasing stress with increasing temperature except for portions of the stress-temperature measurements of BTDA/ODA. The BTDA/ODA measurements show a slight increase in the stress from 25°C to 50°C. This increase may be due to a decrease in the moisture content of the film as the temperature increases, increasing the stiffness of the film.

Lin previously observed a relationship between the in-plane refractive index of a polymer film and the residual stress observed in the film. [33] In her work, Lin attributes decreases in film stress and increases in the in-plane refractive index to increasing backbone rigidity. A plot of room temperature stress versus in-plane refractive index for the polymers tested is shown in Figure 18. The residual stress decreases with increasing in-plane refractive index for the polymers examined, consistent with Lin's prior work. These results also agree with the observations of Numata et al. who showed that higher chain linearity resulted in polymers with lower in-plane CTEs and subsequently lower residual stresses. [34,35] Ree et al. also noted an increase in residual stress when a decrease in the orientation of a polymer occurred. [36] This effect was attributed to a change in the mechanical properties of the polymer film with changes in molecular orientation. The less oriented films exhibit a higher CTE that results in a higher residual stress, consistent with the results observed in this study. The relationship between the stress and the in-plane refractive index is approximately linear for the polyimides tested with BCB having a residual stress somewhat lower than would be expected for a polyimide of comparable refractive index. This difference in stress-orientation behavior between BCB and the polyimides is most likely due to the three-dimensional bonding in the thermoset BCB films relative to the linear chain structure in the polyimides. Even the acetylene-terminated crosslinking polyimides have relatively long chain segments between crosslinks relative to the short, monomeric distances found in the BCB structure.
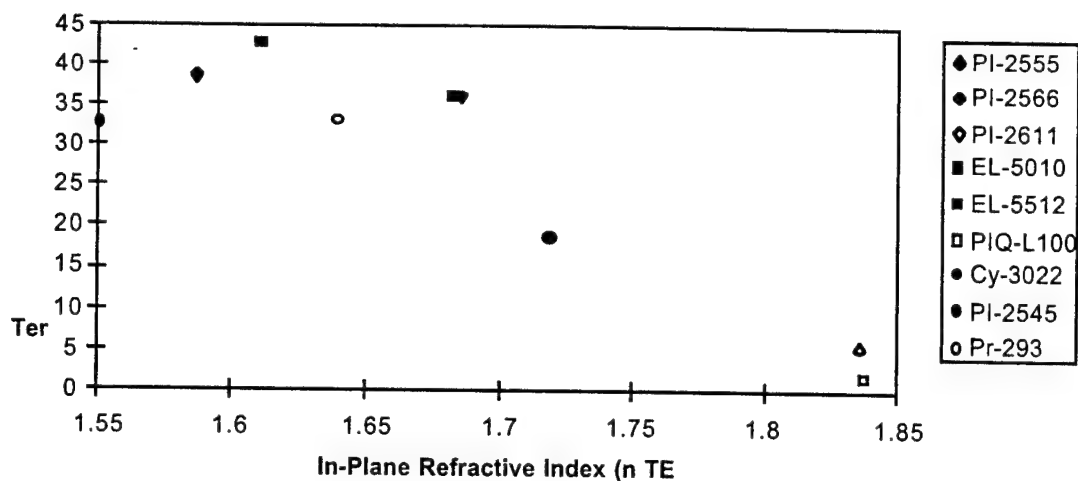
Figure 18. Film Stress vs. In-Plane Refractive Index

An interesting observation concerns the glass transition temperatures observed in the National Starch EL-5010 and EL-5512 films. The T_g is characterized by a leveling off of the stress at temperatures above the T_g. These materials have been reported by National Starch as having a T_g in the temperature range observed in this work. No other materials in this test series are reported to have a T_g in the measurement range, in fact, the DuPont polyimides are reported to have a T_g above the degradation temperature of the film.

From this study, DuPont PI-2611 and Hitachi PIQ-L100 both show very low stresses on silicon substrates. This result is due to the high rigidity of the polymer backbones. The polymer rigidity leads to high anisotropy as shown by the birefringence. The high anisotropy is a potential problem requiring study of the material properties in both the in-plane and through-plane directions in order to properly characterize the films for use in three-dimensional MCM-D applications. Benzocyclobutene has a low birefringence and a moderate stress due to its low modulus and low cure temperature. The National Starch polyimides, EL-5010 and EL-5512, show a glass transition temperature at approximately 180°C and 230°C respectively, making them unsuitable for high temperature applications because of flow of the dielectric and increased ion and dipole mobility above the T_g. The preimidized polyimide BTDA/DAPI is an interesting material due to its wide

36

processing temperature range and its moderate film stress. The remaining DuPont polyimides, PMDA/ODA, BTDA/ODA and 6FDA/ODA are unremarkable with moderate to high stresses and moderate anisotropy. 6FDA/ODA does have the advantage of lower moisture absorption than the other two materials making it a better candidate for non-hermetic applications.

PMDA/ODA has previously shown to have non-linear mechanical properties above room temperature and is to be expected to be non-linear at subambient temperatures. [37] 6FDA/ODA, BTDA/DAPI, and BPDA/PPD show a linear variation of the stress as a function of temperature from 25°C to -180°C. This result indicates that there are probably no change in the polymer properties in this temperature range.

The stress at -165°C for the six polymers tested are listed in Table 11. The highest stress was 75.48 MPa for the preimidized BTDA/DAPI polyimide. The high stress is most likely due to the relatively high biaxial modulus and high CTE of this material. Similarly, the 6FDA/ODA has a stress of 67.74 MPa resulting from the greater flexibility of the polymer backbone compared to all the materials besides the BTDA/DAPI which is more flexible. The PMDA/ODA and BCB films have comparable stresses at liquid nitrogen temperatures at a value of approximately 43 MPa. The lowest stresses at -165°C were found for the rigid BPDA/PPD and PIQ polyimides with values of 9.35 and 8.29 MPa respectively. These results indicate that while the BTDA/DAPI has a wider cure temperature available, it is unsuitable for subambient applications due to its extremely high stress at liquid nitrogen temperatures. 6FDA/ODA is also unsuitable for subambient devices in spite of its moisture barrier properties. The PMDA/ODA film has moderate stress at -165°C; however the relatively large moisture uptake and high cure temperature of the material make it inappropriate for subambient devices. The moderate stress at -165°C of BCB coupled with its low moisture uptake and low cure temperature makes BCB a suitable candidate for integration with HTS in subambient operation. The BPDA/PPD and PIQ stress at liquid nitrogen temperatures are very low, indicating usage of these materials is reasonable from a mechanical standpoint. However, both of these materials require curing at 350°C to ensure proper cure of the polymer and produce moisture as a byproduct of the cure. The BPDA/PPD

and PIQ materials may be useful for subambient applications that utilize conductors compatible with the high temperature, moist polyimide cure.

Table 11 Polymer stress on silicon substrate at -165°C.

Polymer	Stress at -165°C (MPa)	Standard Deviation (MPa)
PMDA/ODA	43.41	0.65
6FDA/ODA	67.74	0.32
BPDA/PPD	9.35	0.85
PIQ	8.29	0.76
BTDA/DAPI	75.48	0.65
BCB	43.17	0.51

Conclusions

Nine polymeric insulating materials were tested for their stress behavior as a function of temperature from room temperature to 175°C. All of the polymers coated on silicon wafers showed a decreasing stress with increasing temperature consistent with thermally generated stresses. The measurements also confirm a relationship between the in-plane refractive index and the room temperature residual stress in the film. A higher in-plane refractive index was seen to correspond to a material with a low residual stress at room temperature and a low refractive index corresponds to a higher residual stress. This relationship is the result of increased molecular orientation observed in both higher in-plane refractive indices and lower residual stresses. The lowest residual stresses were observed for the rigid-rod BPDA/PPD and PIQ polyimides.

Subambient stress measurements were made on six different polymer didlectric materials. Three materials tested, 6FDA/ODA, BTDA/DAPI, and BPDA/PPD, show linear relationships between stress and temperature from 175°C and -165°C. The other three materials, PMDA/ODA, PIQ, and BCB, show non-linear stress-temperature response below room temperature. The materials with linear

relationships between stress and temperature are expected to have a constant CTE and biaxial modulus over the temperature range, while those with non-linear relationships have temperature dependent material properties. The lowest stresses at liquid nitrogen temperatures were the rigid polyimides, BPDA/PPD and PIQ. For integration with HTSs, BCB is the material of choice due to its moderate film stress at liquid nitrogen temperatures and low temperature, moisture-free cure.

---

[1] J.T. Pan and S. Poon, "Film Stress in High Density Thin Film Interconnect", *MRS Proceedings Vol. 154*, pp. 27-37 (1989).

[2] M.A. Moske, J.E. Lewis, and P.S. Ho, "Stress Behavior During Thermal Cycling in Metal-Polyimide Layered Films", *Proceedings of the Annual Technical Conference of the Society of Plastics Engineers*, pp. 1731-1737 (1991).

[3] M.T. Pottiger and J. Coburn, "Internal Stress Development in Spin Coated Polyimide Films", *MRS Proceedings Vol. 227, Material Science of High Temperature Polymers for Microelectronics*, D.T. Grobb, I. Mita, and D.Y. Yoon, Eds., pp. 187-194 (1991).

[4] M. Ree, S. Swanson and W. Volksen, "Residual Stress and Its Relaxation Behavior of High Temperature Polyimides: Effect of Precursor Origin", *Proceedings of the Fourth International Conference on Polyimides*, C. Feger, M.M. Khojasteh, M.S. Htoo, Eds., Society of Plastics Engineers, pp. 601-617 (1991).

[5] P. Garrou, Proc. IEEE, **80**(12), pp 1942 (1992)

[6] T. G. Tessier, G. M. Adema, and I. Turlik, *Proc. Elec. Component Conf.*, IEEE, p127 (1989)

[7] B. T. Merriman, J. D. Craig, A. E. Nader, D. L. Goff, M. T. Pottiger, and W. J.Lautenberger, *Proc. Elec. Component Conf.*, IEEE, p 155 (1989)

[8] D. L. Goff, E. L. Yuan, H. Long, and H. J. Neuhaus, *Polymers for Electronics Packaging and Interconnection*, p 93 (1989)

[9] J.-H. Jou. and P.-T. Huang, Macromolecules **24**, p 3796 (1991)

[10] G. Elsner, J. Appl. Poly. Sci. **34**, p 815 (1987)

[11] M. Ree, T.L. Nunes and G. Czornyj, "Residual Stress Behaviour of Isomeric PMDA-ODA Polyimides", *Polymer*, **33**(6), pp. 1228-1236 (1992).

[12] J.-H. Jou and C.-S. Chung, "Curing Effect on the Relaxation Modulus and Thermal Expansion Coefficient of Rodlike Polyimide Films", *Macromolecules*, **25**, pp. 6035-6039 (1992).

[13] M. Ree, C.W. Chu and M.J. Goldberg, "Internal Stress Behavior in Polymer Thin Films: Effects of Polymer Chain Rigidity and Orientation", Proc. of ACS PMSE Div, **69**, pp. 312-313 (1993).

[14] S.C. Noe, J.Y. Pan, and S.D. Senturia, "Planar Optical Waveguide Study of Polyimide Anisotropy including Moisture and Stress Effects", *Proceedings of the Fourth International Conference on Polyimides*, C. Feger, M.M. Khojasteh, M.S. Htoo, Eds., Society of Plastics Engineers, pp. 587-600 (1991).

[15] G. Elsner, J. Kempf, J.W. Bartha and H.H. Wagner, "Anisotropy of Thermal Expansion of Thin Polyimide Films", *Thin Solid Films*, **185**(1), pp. 189-197 (1990).

[16] S.M. Arora, V.H. Desai and K.B. Sundaram, "The Effect of Processing Parameters on the Environmental Stability of YBaCuO Superconductor", *Journal of Materials Science*, **28**, pp. 454-460 (1993).

[17] G.G. Stoney, "The Tension of Metallic Films deposited by Electrolysis", Proc. Royal Society, A82, pp. 172-175 (1909).

[18] W.A. Brantley, J. Appl. Phys. **44**, pp. 534 (1973)

[19] A. Brenner and S. Senderoff, "Calculation of Stress in Electrodeposits from the Curvature of a Plated Strip", *Journal of Research of the National Bureau of Standards*, **42**, pp. 105-133 (1949).

[20] J.T. Pan and I. Blech, "*In Situ* Stress Measurement of Refractory Metal Silicides During Sintering", *J. Appl. Phys.*, **55** (8), pp. 2874-2880 (1984).

[21] G.H. Olsen and M. Ettenberg, J. Appl. Phys. **48**, pp. 2543 (1977)

[22] R.J. Jaccodine and W.A. Schlegel, J. Appl. Phys. **37**, pp. 2429 (1966)

[23] C.L. Bauer and R.J. Farris, *Polyimides: Materials, Chemistry and Characterization*, Elsevier Science Publishers B. V., Amsterdam, (1989)

[24] A.K. Sinha, H.J. Levinstein, and T.E. Smith, J. Appl. Phys. **49** (4), pp. 2423 (1978)

[25] T.G. Tessier, G.M. Adema, and I. Turlik, *Proc. Elec. Component Conf.*, IEEE, pp. 127 (1989)

[26] J.-H. Jou and P.-T. Huang, Macromolecules, **24**, pp. 3796 (1991)

[27] G. Elsner, J. Appl. Poly. Sci., **34**, pp. 815 (1987)

[28] B.T. Merriman, J.D. Craig, A.E. Nader, D.L. Goff, M.T. Pottiger, and W.J. Lautenberger, *Proc. Elec. Component Conf.*, IEEE, pp. 155 (1989)

[29] Center for Information and Numerical Data Analysis and Synthesis (CINDAS) Microelectronic Material Database, Purdue University.

[30] B. Sinno, *Mechanical and Dielectric Characerization of Electronic Grade Polymers at Subambient Temperatures*, M.S. Thesis, Georgia Institute of Technology (1995).

[31] P.K. Tien, *Applied Optics*, **10**, pp. 2395 (1971).

[32] A.C. Adams, D.P. Schinke, and C.D. Capio, *J. Electrochemical Society:Solid State Science and Technology*, **126**, pp. 1539 (1979).

[33] L. Lin, *Molecular Orientation Studies of Spin-Coated Polyimide Films*, Ph.D. Thesis, Georgia Institiute of Technology (1994)

[34] S. Numata, S. Oohara, J. Imaizumi and N. Kinjo, "Thermal Expansion Behavior of Various Aromatic Polyimides", *Polymer Journal*, **17**(8), pp. 981-983 (1985).

[35] S. Numata, K. Fujisaki and N. Kinjo, "Re-examination of the Relationship Between Packing Coefficient and Thermal Expansion Coefficient for Aromatic Polyimides", *Polymer*, **28**(13), pp. 2282-2288 (1989).

[36] M. Ree, C.W. Chu and M.J. Goldberg, "Internal Stress Behavior in Polymer Thin Films: Effects of Polymer Chain Rigidity and Orientation", *Proceedings of ACS Division of Polymeric Materials Science and Engineering,* **69**, pp. 312-313 (1993).

[37] J.C. Coburn, M.T. Pottiger, S.C. Noe, and S.D. Senturia, "Stresses in Polyimide Coatings", *Journal of Polymer Science, Part B: Polymer Physics*, **32**(7), pp. 1271-1283 (1994).

CHAPTER 3

POLYNORBORNENE, A LOW COST, HIGH PERFORMANCE DIELECT

Summary

A new class of materials derived from addition polymers of cyclic olefins is described. The general properties of these polymers include Tg greater than 350 °C, dielectric constant less than 2.6, low moisture absorption and good elongation-to-break. These materials have also been modified to have excellent adhesion to commonly used materials such as silica and aluminum. In addition, excellent adhesion has been achieved to copper and noble metals such as gold and silver. These polymers are shown to adhere even in the absence of an adhesion promoter or tie layer on the metal (e.g. titanium, tantalum, chromium) and to remain as adherent films even after being placed in boiling water for 2 hours. These materials are expected to demonstrate utility in electronic applications and interconnection by offering superior performance over traditional materials while reducing the device manufacturing cost.

Background

Within the microelectronics industry, there is an ongoing trend toward miniaturization coupled with higher performance. One technique to increase the interconnection density and achieve miniaturization without semiconductor redesign is to use multichip modules (MCMs).

There are basic approaches to multichip modules: MCM-L (laminate), in which the chips are mounted on a multilayer laminated surface; MCM-C (ceramic) where a multilayered co-fired substrate and dielectric layer are used; and MCM-D (deposited) technology where organic thin film dielectric materials are deposited on ceramic or silicon substrates. MCM-L is the most widely used technology; however, the routing density is limited, which constrains final component density and speed. MCM-C is a proven "mature" technology; however, the performance is limited by the high dielectric constant (4.0 to 7.0) and high electrical resistance. MCM-D technology

resolves these two issues; however, the current organic dielectric materials have several inherent performance limitations.

Current Materials

Microelectronic manufacturers have historically selected polyimide dielectric materials based on the high glass transition temperature (Tg) and thermal oxidative stability. However, polyimides have several fundamental shortcomings that limit the performance and reliability of MCMs. First, the dielectric constants are higher than desired, generally 3.0 to 3.5 Second, the water absorption levels are as high as 3% which leads to (i) an increase in the dielectric constant, (ii) reliability problems caused by corrosion, and (iii) a tendency to solvate ionic contaminates. Since the dielectric constant of water is 78, this water absorption phenomena can drastically increase the dielectric constant of the film. These high dielectric constants lead to capacitance delays and limit the overall device performance. Conductor corrosion can also occur, particularly with copper. Third, the polyimide materials are inherently anisotropic; i.e., electrical performance differs in the x, y and z directions. One common measure of anisotropy is the film birefringence. Polyimide (PMDA-ODA) has a reported birefringence of approximately 0.085 for a 2 mm film spun-coated and thermally imidized on a silicon wafer with a thermally grown oxide layer[1]. Furthermore, the imidization curing reaction takes place in-situ, and the copper conductor layers may be exposed to the polyamic acid precursor. In turn, this acid aggravates copper ion migration, which must be mitigated with the use of passivation layers to provide sufficient adhesion to assure device reliability. Thus, in order to address some of the reliability concerns, extra process steps must be performed.

Compared to polyimide (PI), benzocyclobutene (BCB) offers a lower dielectric constant, 2.7, and a lower moisture absorption, 0.23%; however, adhesion promotion layers are still typically required because the metal-polymer interfacial strength is low and films peel off the substrate with minimal effort, particularly with copper. In addition, many of the conventional polymers are reacted or cured on the substrate via imidization

or B-staging. As such, the final electrical performance, Tg, and thermal stability are processing dependent.

Thus, there exists a need in the microelectronics industry for a thermally stable, non-corrosive, low dielectric constant polymer with good solvent resistance, low moisture absorption, high glass transition temperature, good mechanical performance, and excellent adhesive properties, particularly to copper. In addition, the desired dielectric material should use environmentally friendly solvents. The final thermal and electrical performance should not be affected by manufacturing or post processing conditions.

New Olefin Materials

Recently, a new class of high glass transition temperature, olefinic polymers have been discovered at BFGoodrich (BFG) that provides many of the desired features. This polymer family, based principally on polynorbornene, is produced via a new transition metal catalyzed polymerization which enables us to control the polymerization of bulky, cyclic monomers to form saturated polymers with high Tg's. The norbornene polymer microstructure can be changed by controlling the enchainment of the monomers; both 2,3 and 2,7 addition has been observed[2]. This mechanism allows tailored molecular weights which can be specifically controlled from tens of thousands to several million enabling polymers to be designed to specific applications. As such, we are currently developing a family of dielectric materials for use as interlayer dielectric thin films. Attributes that make these polynorbornene polymers particularly attractive in microelectronics include (I) excellent thermal and electrical performance, (ii) adhesion to conductors and substrates without the use of adhesion promoters, (iii) very low moisture content, (iv) low dielectric constant, and (v) simple solution processing. These polymers appear to be quite isotropic from birefringence measurements using a prism coupler technique. Films which are nominally 2 μm thick after being spun onto oxidized silicon wafers exhibit birefringence on the order of 0.0031 ± 0.0001, more than 20 times lower than

that observed for PMDA-ODA as mentioned above. The refractive index was measured to be 1.505 for this sample, and free standing films are clear and colorless. The BFG dielectric polymers offer improved performance with lower manufacturing costs compared to other dielectric materials.

The family of polynorbornenes can be described as amorphous, hydrocarbon polymers that exhibit high Tg (> 350 °C) and excellent thermal and electrical stability.

Figure 1: Dynamic Mechanical Temperature Scan of BFG polymer

These highly transparent polymers are readily soluble in a range of common solvents. Of particular interest are decalin and mesitylene. Polynorbornene dielectric polymers have a high glass transition temperature due to the very stiff polymer backbone resulting from the steric crowding of the bulky saturated cyclic groups, as shown below. The group "R" represents specific functional groups which provide adhesion and sites for crosslinking.

Figure 2: Generic Polynorbornene Structure

At room temperature, the mechanical properties include an elongation-to-break of approximately 10% and a tensile modulus of approximately 2 GPa. At elevated temperatures, the high Tg provides mechanical stability, enabling the use of several soldering techniques. The thermal stability of the BFG polymer is excellent with the onset of degradation at 435°C (5% weight loss as determined by thermal gravimetric analysis {TGA} in Argon, using a 10 °C/min ramp rate.

Figure 3: Thermo-gravimetric Scan of BFG polymer

The hydrocarbon nature of polynorbornene yields dielectric thin films with very low moisture absorption (< 0.1 %) and low dielectric constants (< 2.6 at 10 kHz

The dielectric constants were measured by constructing capacitors using sputtered metal and standard photolithography. The film thickness was determined using a Metricon 2010 prism coupler. In order for these measurements to be made, the film must withstand exposure to photoresist (Microposit® SC 1827 from Shipley), developer (Microposit® 354 from Shipley), PAN etch (phosphoric, acetic, and nitric acid mix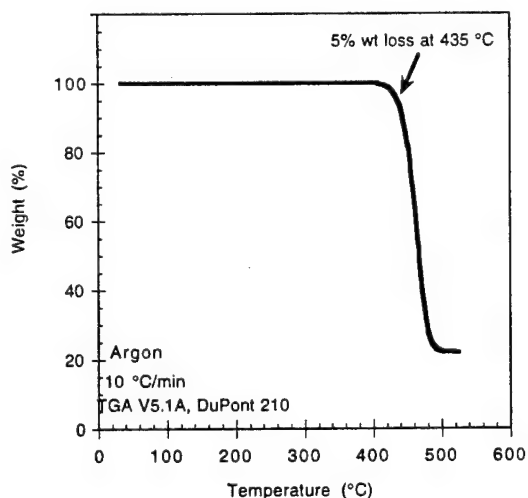ture), acetone, isopropanol and other commonly used solvents. These polymers survived unaffected, with no evidence of cracking or crazing.

Preliminary studies regarding reactive ion etch (RIE) characteristics have centered on use of a photoresist mask. The results have been most successful to date with thin films (< 2 µm) using an oxygen and CHF_3 gas mixture with between 6-12% (by volume) of the fluorinated gas. Figure 4 shows an etched feature where the RIE pressure was 450 mTorr at 300 W rf power for 2 minutes. The photoresist mask is evident on top of the polymer in the left side of Fig. 4, and the center channel shows where the polymer has been etched cleanly from the wafer surface.
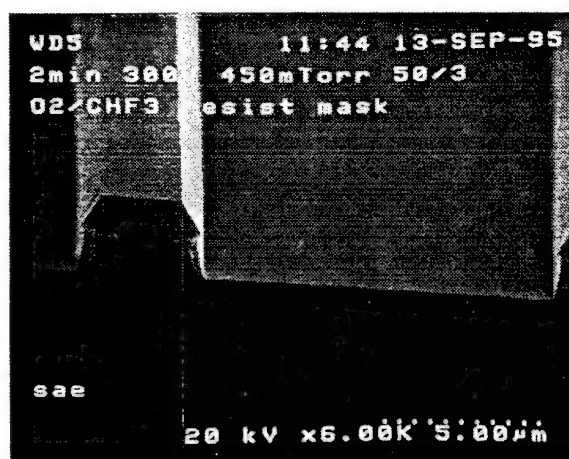

Figure 4: Reactive Ion Etch Micrograph of BFG polymer

The polynorbornene dielectric polymers are fully polymerized before use in electronic packaging; therefore, the base polymer properties are not as dependent on the processing temperatures. Light cross linking can be achieved to enable multi-layer processing. These polymers, are expected to be

benign towards copper since no strong interactions are anticipated due to their hydrocarbon nature and low moisture absorption. For example, no carboxylic acid intermediate or decomposition product is present, as with polyimides. This may eliminate the need for passivation layers and tie layers when using copper.

The polynorbornene dielectric polymers can be produced with excellent adhesion to copper, gold, silver, silicon, and silica without the use of adhesion promoters. Simple solutions of the polynorbornene dielectric polymers are applied by spin coating onto substrates using hydrocarbon or halogenated solvents. These films are then dried and cured at elevated temperatures, typically above 250°C. The adhesion of these films is then tested by using a diamond scribe to form a cross-hatched pattern, then Scotch™ tape is used to try to pull away any of the cross-hatched sections. The polymer passes this test if none of the film is removed or delaminated. The BFG polymer passes the Scotch™ tape test for oxidized silicon and aluminum. The intriguing result is that the BFG polymer also passes this test when coated onto bare copper, gold and silver without any adhesion promoter and in the absence of any tie layer (such as chromium, titanium, tantalum). These films remain adherent and continue to pass the Scotch™ tape test even after being placed in boiling water for 2 hours. Likewise, metal sputtered on top of the polymer survives these adhesion tests, as do additional layers of the polymer. This combination of attributes for the dielectric material leads to the elimination of manufacturing steps, and thus reduces the overall manufacturing costs.

Conclusions

Thus, the new polynorbornene interlayer dielectric polymers from BFG offer the microelectronics producer several important performance and processing advantages over the existing materials at a reduced manufacturing cost. Electrical performance can be dramatically increased, along with increased reliability. The pertinent comparative properties are shown in Table 1. At this time, BFG is interested in industry

feedback on potential uses and in discussions concerning specific needs and requirements for these experimental polymers.   Table   1:   BFG's Polynorbornene Dielectric Polymers vs. Current Materials.

Dielectric Material	Moisture Absorption Weight %	Coefficient of Thermal Expansion ppm/°C	Glass Transition Temperature °C	Dielectric Constant
BFG's PNB	< 0.1	50	> 350	2.4-2.6
BCB Cyclotene® CY3022-57	0.23	65	> 350	2.7
Typical PI Pyralin® 2540	2-3	33 (in-plane) [3] 129 (through-plane)	430	3.5
Low Stress PI Pyralin® 2611	0.5	3 (in-plane) [3] 148 (through-plane)	330	2.9
Fluorinated-PI Pyralin® 2566	1.5	60	290	3.0
Silica	---	2-4	>800	3.8 - 4.2

References

[1] J.C Coburn, M.T. Pottiger, S.C. Noe and S.D. Senturia, J. Polym. Sci: Part B: Polym. Phys., **32**, 1271 (1994).

[2] B.L. Goodall, G.M. Benedikt, L.H. McIntosh, D.A. Barnes, L.F. Rhodes "Addition Polymers Derived from Norbornene-Functional Monomers and Process Therefor" WO 95/14048

[3] M.T. Pottiger and J.C. Coburn, Polym. for Microelectronics; ACS Symposium Series; American Chemical Society: Washington, D.C., (1992)

CHAPTER 4

CHARACTERIZATION OF STRESS-TEMPERATURE BEHAVIOR OF BENZOCYCLOBUTENE FILMS

Abstract

Stresses developed between a low coefficient of thermal expansion (CTE) substrate and a high CTE polymer dielectric is a significant reliability issue in microelectronic packaging. Reliable measurements of the CTE of spin-cast polymer films are necessary for proper characterization of stresses in devices. This work examines the effect of film thickness on spin-cast benzocyclobutene (BCB) films. No thickness dependence was observed for either the in-plane CTE or biaxial modulus of the BCB films. The CTE and biaxial modulus calculated for spin-cast BCB agrees well with values reported for bulk BCB samples.

Introduction

Polymeric insulators for use as interlevel dielectrics in electronic applications or in electronic packaging have been extensively studied and documented. [1-6] However, most of these applications operate at or just above room temperature. The stress developed between high coefficient of thermal expansion (CTE) polymer insulators and low CTE substrate materials vary with temperature. [7,8] Several factors enter into the magnitude of the stress in the film. The Young's modulus of the film, the magnitude of the CTE mismatch between the film and the substrate, the glass transition temperature of the polymer film, the cure temperature of the film, and the humidity all affect the magnitude of the stress in the film. [9,10] The emergence of new electronic applications that operate at temperatures significantly higher or lower than room temperature place new demands on the stress behavior of polymer dielectric films. High temperature applications of multichip packaging, such as in the automotive and aerospace industries, require multichip modules that will not delaminate or otherwise fail during a reasonable operational lifetime. In order to

50

minimize the probability of mechanical failure at the dielectric-substrate interface, low stress is desirable. In particular, low residual stresses at room temperature can be achieved by reducing the CTE mismatch between the film and the substrate or by reducing the biaxial modulus of the film.

Achieving low stress dielectric polymer films in high temperature applications is relatively simple becaue the polymeric dielectric is usually under tensile stress at room temperature. The thermal stress developed between the high CTE film and the low CTE substrate decreases as the temperature rises above room temperature. In fact, the stress in the film disappears upon reaching either the glass transition temperature or the cure temperature, whichever is lower. [3]

Benzocyclobutene (BCB) is one of the commercially available materials which has excellent chracteristics as an interlevel dielectric for high speed packaging. BCB is a thermosetting material with low optical anisotropy. This low anisotropy of BCB is believed to hold for mechanical and dielectric properties as well. [11,12] In this study, a comprehensive examination of the stress of BCB thin films has been performed. In particular, the effect of film thickness on the in-plane CTE and Young's modulus of spin-coated BCB films was examined.

Experimental

The residual stress of BCB films were measured with a Flexus F2320 stress measurement system (Tencor Instruments, Sunnyvale, CA). In the Flexus system, the Stoney equation is used to determine the film stress in two dimensions:

$$\sigma = -\frac{E}{(1-v)}\frac{h^2}{6Rt}$$

(1)

where s is the average film stress, $E/(1-n)$ is the biaxial modulus of the substrate $(1.805 \times 10^{11}$ Pa for <100> silicon wafers [13]), h is the substrate thickness, t is the film thickness, and R is the substrate radius of curvature. The Stoney equation for biaxially strained films obtained in Equation 1 has been verified by numerous independent sources for measurement of a thin film on a thick substrate.[14-23] The radius R must be corrected for the initial curvature of the bare wafer. The uncoated

wafer is scanned for the initial radius R_1, before deposition of the polymers, and then scanned again to determine R_2 after deposition of the film. Since the stress is proportional to $1/R$, it follows that:

$$\frac{1}{R}=\frac{1}{R_2}-\frac{1}{R_1}$$

(2)

To calculate the film CTE and biaxial modulus, the following equation is utilized[23]:

$$\frac{d\sigma}{dT}=\frac{E}{(1-v)_{film}}(\alpha_{sub}-\alpha_{film})$$

(3)

where ds/dT is the slope of the stress versus temperature plot that is generated by the Flexus. Equation 3 has two unknowns, namely the biaxial modulus of the film, $[E/(1-v)]_{film}$, and the CTE of the film, α_{film}. In order to solve for both unknowns, we need to perform temperature cycles with BCB on at least two different substrates.

In this work, BCB films were spin-cast in approximately 1, 5, and 15 micrometers thickness on three different substrates: 100 mm diameter <100> silicon substrate, 40 mm diameter gallium arsenide substrate, and 75 mm diameter 2024-T3 aluminum substrate. The silicon and GaAs substrates are microelectronic substrates. The aluminum substrate was necessary for the accurate calculation of the film properties because its mechanical properties are very different from silicon and GaAs. Aluminum has a significantly higher CTE (ca. 22.7 ppm/°C [24]) than silicon and GaAs (ca. 3 and 6 ppm/°C respectively [25]). Ideally, a substrate with a CTE greater than that of the BCB film would be desirable to allow interpolation of the CTE of the polymer film. However, no materials with CTEs greater than 60 ppm/°C (the CTE of bulk BCB) were available for this purpose; therefore, some error may be associated with the calculated CTEs because of the required extrapolation of the film CTE.

Prior to film deposition, the bare substrates were temperature cycled in the Flexus F2320 to observe the radius of curvature as a function of temperature. In the

case of silicon and gallium arsenide substrates, the room temperature curvature was assumed constant throughout the temperature range. For the aluminum substrate, a temperature dependence of the radius of curvature was observed and was incorporated into the calculation of the effective radius used in the stress calculation by allowing R_1 in Equation 2 to be a function of temperature. This temperature dependence of the bare aluminum wafer is most likely due to a deformed surface layer created during polishing of the wafer. Substrate Young's modulus, Poisson's ratio and CTE used in the stress calculations were obtained from the CINDAS database in the case of silicon and gallium arsenide, and from the Metal's Handbook in the case of aluminum. [24,25]

Film thicknesses were determined using a Metricon 2010 prism coupler system (Metricon Corporation, Pennington, NJ). [26] This system utilizes polarized laser light to non-destructively determine the index of refraction and film thickness.

Results

The stress as a function of temperature for 14.61 micrometer thick BCB films on silicon, gallium arsenide and aluminum substrates are shown in Figure 1. The stresses are highest for the silicon data and lowest for the aluminum data, reflective of the difference in the CTE mismatch between the film and substrate. Some curvature is seen in stress versus temperature plot of the BCB on aluminum data set. This curvature may be due to changes in the bare substrate curvature with temperature. The slopes from the stress-temperature plots are shown in Table 1. The slope for the aluminum substrate was for the temperature interval from 25°C to 80°C. Using the data in Table 1 in Equation 3, the calculated in-plane CTE and biaxial modulus are 53.75 ± 13.64 ppm/°C and 4.290 ± 1.469 GPa, respectively. The ranges are the 95% confidence intervals calculated on the linear regression.

Figure 1. Stress as a Function of Temperature for Approximately Fifteen
Micrometer Thick BCB.

Table 1. Calculated Slopes for Data in Figure 1.

Substrate	Substrate CTE (ppm/°C)	Slope (MPa/°C)
Silicon	2.87	-0.204
GaAs	5.9	-0.222
Aluminu m	22.7	-0.131

The stress as a function of temperature for approximately five micrometer thick BCB films on silicon, gallium arsenide and aluminum substrates were measured and the slopes (ds/dT) are shown in Table 2. The measured stress linearly changes for all three substrates with very little scatter. The average thickness of the films is 5.33 μm. The calculated in-plane CTE and biaxial modulus from the data in Table 2 are 63.31 ± 13.64 ppm/°C and 2.642 ± 0.619 GPa, respectively.

The stress as a function of temperature for approximately one micrometer thick BCB on silicon, gallium arsenide and aluminum substrates showed more scatter in the data due to the relatively small changes in the radius of curvature with temperature. A small change in the radius results in a noticeable change in the calculated stress. The slopes of the stress-temperature measurements are shown in Table 3. The average thickness of the tested samples is 1.36 μm. Three measurements of the stress as a function of temperature on silicon were performed to examine the reproducibility of the data as well as to estimate the expected error in the calculated slopes between runs. The average slope on the silicon substrates is -0.162 MPa/°C with a standard deviation of 0.019 MPa/°C. Using the results in Table 3 with equation 3, the calculated CTE and biaxial modulus are 55.84 ± 10.72 ppm/°C and 2.937 ± 1.227 GPa.

Table 2. Calculated Slopes for the Stress-Temperature Measurements for 5 mm BCB Films.

Substrate	Substrate CTE (ppm/°C)	Slope (MPa/°C)
Silicon	2.87	-0.166
Aluminum	22.7	-0.108
GaAs	5.9	-0.145

Table 3. Results for Stress as a Function of Temperature for 1 mm Thick BCB Films

Substrate	Substrate CTE (ppm/°C)	Slope (MPa/°C)
Silicon	2.87	-0.143
GaAs	5.9	-0.124
Silicon	2.87	-0.180
Silicon	2.87	-0.163
Aluminum	22.7	-0.101

Discussion

Each of the three data sets obtained in this work yielded an in-plane CTE and biaxial modulus comparable to the bulk literature values for BCB of 52-60 ppm/°C and 3 GPa. [27,28] The average of the calculated in-plane CTEs is 57.63 ppm/°C which lies in the range of the literature values of CTE for BCB with a standard deviation of 12.67 ppm/°C. The average biaxial modulus of the three data sets is 3.312 GPa with a standard deviation of 1.105 GPa, very close to the literature value of 3 GPa. [28] These results indicate that there is little or no thickness dependence on the in-plane mechanical properties of in-situ BCB films. It should be noted that the in-plane CTE calculated is a material property, not the actual displacement which the film undergoes. The calculation of the film stress assumes that the film expands and contracts perfectly with the substrate and that the curvature results from the stresses induced by the higher CTE film being constrained by the low CTE substrate. Therefore, in the case of a BCB film on a silicon substrate, the film expands and contracts in the in-plane direction at the same rate as silicon (2.87 ppm/°C) while still having an in-plane CTE of 52-60 ppm/°C.

Only one previous author, Elsner et al[29], has attempted to calculate in-plane mechanical properties for polymer films using wafer curvature measurements. In his work, Elsner utilized silicon and fused quartz substrates to determine the CTE and biaxial modulus of Probimide 293 films. The CTE obtained by Elsner was quite different from the reported value of CTE for Probimide 293 reported by OCG, with Elsner reporting a CTE of 8 ppm/°C, compared to a value of 30-40 ppm/°C reported by OCG. [30] In his work, Elsner attributed the poor correlation to differences between the thin spin-cast films and the thicker films used in the OCG measurements. In this study, we show that spin-cast and thick films of BCB do yield similar values. The similarity of the substrate CTEs in Elsner's work (silicon has a CTE of about 3 ppm/°C and fused quartz has a CTE of 0.5-2 ppm/°C) may have caused considerable error in the analyses. Better results are obtained when a wider range of substrate CTEs are available as shown by the BCB measurements in this work.

Conclusions

Measurements of stress as a function of temperature for BCB films were performed using silicon, gallium arsenide and aluminum substrates. Using this data, the coefficient of thermal expansion and biaxial modulus of spin-cast BCB was calculated. The in-plane CTE of spin cast BCB was found to be 57.63±12.67 ppm/°C and a biaxial modulus of 3.312±1.105 GPa, compared to values of 52-60 ppm/°C and 3 GPa reported previously for bulk BCB. The accuracy of the measurements is good because of the large range of substrate CTEs [silicon (2.87 ppm/°C) and aluminum (22.7 ppm/°C)]. Ideally, substrates which have CTEs which bracket the CTE of the thin-film should be used; however, in the case of polymers with CTEs ranging from 35-60 ppm/°C, finding a suitable substrate material with a CTE greater than 60 ppm/°C is very difficult. Results from this work show that three substrates with CTEs less than that of the thin-film can be successfully used to calculate polymer film CTE.

---

[1] P. Garrou, *Proc. IEEE*, **80**(12), pp. 1942 (1992)

[2] T. G. Tessier, G. M. Adema, and I. Turlik, *Proc. Elec. Component Conf.*, IEEE, pp. 127 (1989)

[3] B. T. Merriman, J. D. Craig, A. E. Nader, D. L. Goff, M. T. Pottiger, and W. J.Lautenberger, *Proc. Elec. Component Conf.*, IEEE, pp. 155 (1989)

[4] D. L. Goff, E. L. Yuan, H. Long, and H. J. Neuhaus, *Polymers for Electronics Packaging and Interconnection,* pp. 93 (1989)

[5] J.-H. Jou. and P.-T. Huang, *Macromolecules* **24**, pp. 3796 (1991)

[6] G. Elsner, *J. Appl. Poly. Sci.* **34**, pp. 815 (1987)

[7] M. Ree, T.L. Nunes and G. Czornyj, "Residual Stress Behaviour of Isomeric PMDA-ODA Polyimides", *Polymer*, **33**(6), pp. 1228-1236 (1992).

[8] J.-H. Jou and C.-S. Chung, "Curing Effect on the Relaxation Modulus and Thermal Expansion Coefficient of Rodlike Polyimide Films", *Macromolecules*, **25**, pp. 6035-6039 (1992).

[9] M. Ree, C.W. Chu and M.J. Goldberg, "Internal Stress Behavior in Polymer Thin Films: Effects of Polymer Chain Rigidity and Orientation", Proc. of ACS PMSE Div, **69**, pp. 312-313 (1993).

[10] S.C. Noe, J.Y. Pan, and S.D. Senturia, "Planar Optical Waveguide Study of Polyimide Anisotropy including Moisture and Stress Effects", *Proceedings of the Fourth International Conference on Polyimides*, C. Feger, M.M. Khojasteh, M.S. Htoo, Eds., Society of Plastics Engineers, pp. 587-600 (1991).

[11] T.C. Hodge, Ph.D. Thesis, Georgia Institute of Technology (1996).

[12] S.A. Weinberg, *In-Plane Permittivity of Spin-Coated Polymer Films*, M.S. Thesis, Georgia Institute of Technology, 1996.

[13] W.A. Brantley, *J. Appl. Phys.* **44**, pp. 534 (1973)

[14] A. Brenner and S. Senderoff, "Calculation of Stress in Electrodeposits from the Curvature of a Plated Strip", *Journal of Research of the National Bureau of Standards*, **42**, pp. 105-133 (1949).

[15] J.T. Pan and I. Blech, "*In Situ* Stress Measurement of Refractory Metal Silicides During Sintering", *J. Appl. Phys.*, **55** (8), pp. 2874-2880 (1984).

[16] G.H. Olsen and M. Ettenberg, *J. Appl. Phys.* **48**, pp. 2543 (1977)

[17] R.J. Jaccodine and W.A. Schlegel, *J. Appl. Phys.* **37**, pp. 2429 (1966)

[18] C.L. Bauer and R.J. Farris, *Polyimides: Materials, Chemistry and Characterization*, Elsevier Science Publishers B. V., Amsterdam, (1989)

[19] A.K. Sinha, H.J. Levinstein, and T.E. Smith, *J. Appl. Phys.* **49** (4), pp. 2423 (1978)

[20] T.G. Tessier, G.M. Adema, and I. Turlik, *Proc. Elec. Component Conf.*, IEEE, pp. 127 (1989)

[21] J.-H. Jou and P.-T. Huang, *Macromolecules*, **24**, pp. 3796 (1991)

[22] G. Elsner, *J. Appl. Poly. Sci.*, **34**, pp. 815 (1987)

[23] B.T. Merriman, J.D. Craig, A.E. Nader, D.L. Goff, M.T. Pottiger, and W.J. Lautenberger, *Proc. Elec. Component Conf.*, IEEE, pp. 155 (1989)

[24] *Metals Handbook Ninth Edition*, Vol. 2 "Properties and Selection: Nonferrous Alloys and Pure Metals", American Society for Metals, pp. 72-78 (1979)

[25] Center for Information and Numerical Data Analysis and Synthesis (CINDAS) Microelectronic Material Database, Purdue University.

[26] A.C. Adams, D.P. Schinke, and C.D. Capio, *Journal of the Electrochemical Society: Solid State Science and Technology*, **126**, pp. 1539-1543 (1979).

[27] D. Burdeaux, P. Townsend, J. Carr, P.E. Garrou, *J. Electronic Materials*, **19**, pp. 1357, (1990).

[28] P.E. Garrou, et al., in *Proc. ECTC*, (1992); also *IEEE Trans. Components, Hybrids, Manuf. Technol.*, pp. 770 (1992).

[29] G. Elsner, J. Kempf, J.W. Bartha and H.H. Wagner, "Anisotropy of Thermal Expansion of Thin Polyimide Films", *Thin Solid Films*, **185**(1), pp. 189-197 (1990).

[30] OCG Probimide 293 Product Information Sheets, OCG Microelectronic Materials, Inc., W. Paterson, NJ.

CHAPTER 5

PECVD Silicon Dioxide Deposited at Low Temperatures

Abstract

Thin silicon dioxide films are commonly used as insulating layers in metal-insulator structures, such as integrated circuits and multi-chip modules. These films are either thermally grown or deposited by thermally or plasma-enhanced chemical vapor deposition. The advantage of PECVD is that lower deposition temperatures can be used avoiding defect formation, diffusion, and degradation of the metal layer. However, the low deposition temperature of the PECVD process has a negative effect on the quality of the silicon dioxide. Oxides produced at low temperatures contain more silanol and water impurities and are more porous than those deposited at higher temperatures. The deposition parameters, including substrate temperature, RF power, pressure, and reactant gas flow rate, affect the silanol and water concentration by altering the plasma conditions. The substrate temperature has the largest effect on the silanol concentration of the oxide. Using a large RF power, high pressure, and low nitrous oxide to silane ratio will minimize the silanol concentration at a given temperature. This will minimize the dielectric constant and maximize the etch resistance of the oxide produced.

Introduction

Thin silicon dioxide films are commonly used as insulating layers in metal-insulator structures, such as integrated circuits and multi-chip modules. These films are either thermally grown through the oxidation of silicon or deposited by thermally or plasma enhanced chemical vapor deposition (PECVD). The advantage of PECVD is that lower deposition temperatures can be used avoiding defect formation, diffusion, and degradation of metal layers.

However, the low deposition temperature of the PECVD process has a negative effect on the quality of the silicon dioxide. Oxides produced at low temperatures contain significantly more silanol and water impurities and are more porous than those deposited at higher temperatures (1). The primary goal of this study is to examine the effects of   the added silanol and water concentrations on

61

the film properties including permittivity, loss, refractive index, wet etch rate, and residual stress to determine the composition of the PECVD oxide best suited for use as an interlevel dielectric. By correlating the film properties and the silanol and water concentration, the film composition and structure that exhibits desirable properties, including a low permittivity and loss can be determined.

The deposition parameters including the substrate temperature, RF power level, reactor pressure, and reactant gas flow rates affect the composition and structure of the growing film by altering the deposition process. In certain cases, it is desirable to deposit the silicon dioxide at as low a temperature as possible to avoid adverse effects of elevated temperatures, such as metal recrystallization and polymer degradation. Therefore, the other deposition parameters must be manipulated to produce the best possible composition and properties. Another goal of this research is to use the correlations between the film composition and properties along with the relationships between the deposition parameters and film composition to examine the effects of the deposition parameters on the properties. Much of the previous literature has evaluated the effects of the deposition parameters on film properties (1). However, the effect of substrate temperature, RF power, and pressure on the permittivity and loss has not been reported. Similarly, the effect of pressure on the refractive index, etch rate, and residual stress has not been reported for the PECVD of silicon dioxide from silane and nitrous oxide.

Experimental

The silicon dioxide films were deposited in a Plasma-Therm 700 Series batch reactor using nitrous oxide and two percent silane in nitrogen. The frequency of the applied field was 13.56 MHz. The distance between electrodes was 2.29 cm. The electrode diameter was 28 cm. For each set of conditions, films approximately 5 mm thick were deposited on bare and gold coated 100 mm diameter (100)-oriented silicon wafers.

In this experiment, the deposition parameters were varied in a reduced factorial experiment. The conditions are presented in Table 1. Films were deposited using these sixteen different combinations of the high and low settings for each of the five factors or parameters.

After deposition, the measured properties including impurity

62

Table 1. Deposition Ranges for Reduced Factorial Experiment

Parameter	Range
Substrate Temperature	200 - 400 °C
RF Power	20 - 150 W
Pressure	0.25 - 1.80 Torr
Two Percent Silane in Nitrogen	200 - 400 sccm
Nitrous Oxide Flow Rate	400 - 900 sccm

concentrations, permittivity, loss, refractive index, wet etch rate, and residual stress, were averaged at the high and low settings of each parameter. The difference between these averages indicates the magnitude of the effect of the deposition parameter on the measured property.

A Perkin-Elmer 1600-FTIR was used to obtain the infrared spectra. The silanol and water concentrations were determined from the infrared OH absorption bands at 3650 and 3330 cm^{-1} using Equations 1 and 2 obtained from gravimetric analysis (2).

$$S = (179 \ A_{3650} - 41 \ A_{3330}) \qquad\qquad [1]$$

$$W = (-14 \ A_{3650} + 89 \ A_{3330}) \qquad\qquad [2]$$

S is the concentration of silanol in weight percent, W is the water weight percent, and A_n is the optical density per micron of film at a wavenumber of n.

Parallel-plate capacitors were fabricated to evaluate the permittivity and loss. A Keithley 590 CV analyzer and a HP 4263A LCR meter were used to measure the capacitance and conductance at a frequency of 100 kHz. The film thickness was measured across the wafers using a Metricon 2010 Prism Coupler. The capacitor diameters were measured using a Dektak 3030 Surface Profilometer. The permittivity and loss were then calculated from these measurements using Equations 3 and 4 (3)

$$e' = CL/e_0 A \qquad\qquad [3]$$

$$e'' = GL/we_0 A \qquad\qquad [4]$$

where e' is the permittivity, e" is the loss, C is the capacitance, G is the conductance, L is the film thickness, w is the measurement frequency in radians/sec, e_0 is the permittivity of free space, and A is the capacitor area.

A Metricon 2010 Prism Coupler was used to determine the thickness

and index of refraction of the films on blank silicon substrates.

To determine the wet etch rate, a strip of the oxide was covered with black wax and submerged in a solution of 49% $HF:H_2O$ (15:1 by volume). The height of the unetched strip was measured with a Dektak 3030 Surface Profilometer to determine the etch rate.

A Flexus F2320 was used to measure the change of the radius of curvature of the bare silicon substrate due to the stress in the silicon dioxide film. The Flexus measures the translation of a laser beam as a function of position across the wafer. Then, the average radius is determined from a linear regression where the slope is equal to $2/R_1$ and R_1 is the average radius of curvature of the substrate. The average radius of the silicon wafer is obtained in the same manner after deposition. The effective radius is then determined using Equation 6.

$$1/R = 1/R_1 - 1/R_2 \tag{6}$$

R_2 is the average radius of curvature after deposition and R is the effective radius of curvature. The residual stress is then calculated using Equation 7 (4)

$$s = Eh^2/(1-n)6Rt \tag{7}$$

where s is the film stress, $E/(1-n)$ is the biaxial elastic modulus of the silicon, h is the thickness of the substrate, and t is the film thickness.

Results

Film Composition.-The completeness of the silicon-oxygen bond formation and the residual silanol and water concentrations are the primary quantities of interest in establishing the film composition. The silanol concentration of the films was between 1 and 6 weight percent, and the water concentration of the films was less than 5 weight percent. These concentrations are similar to those found in the literature (1). The water concentration appears to vary with the silanol concentration (Fig. 1). Since the water molecules hydrogen bond to silanol groups

65

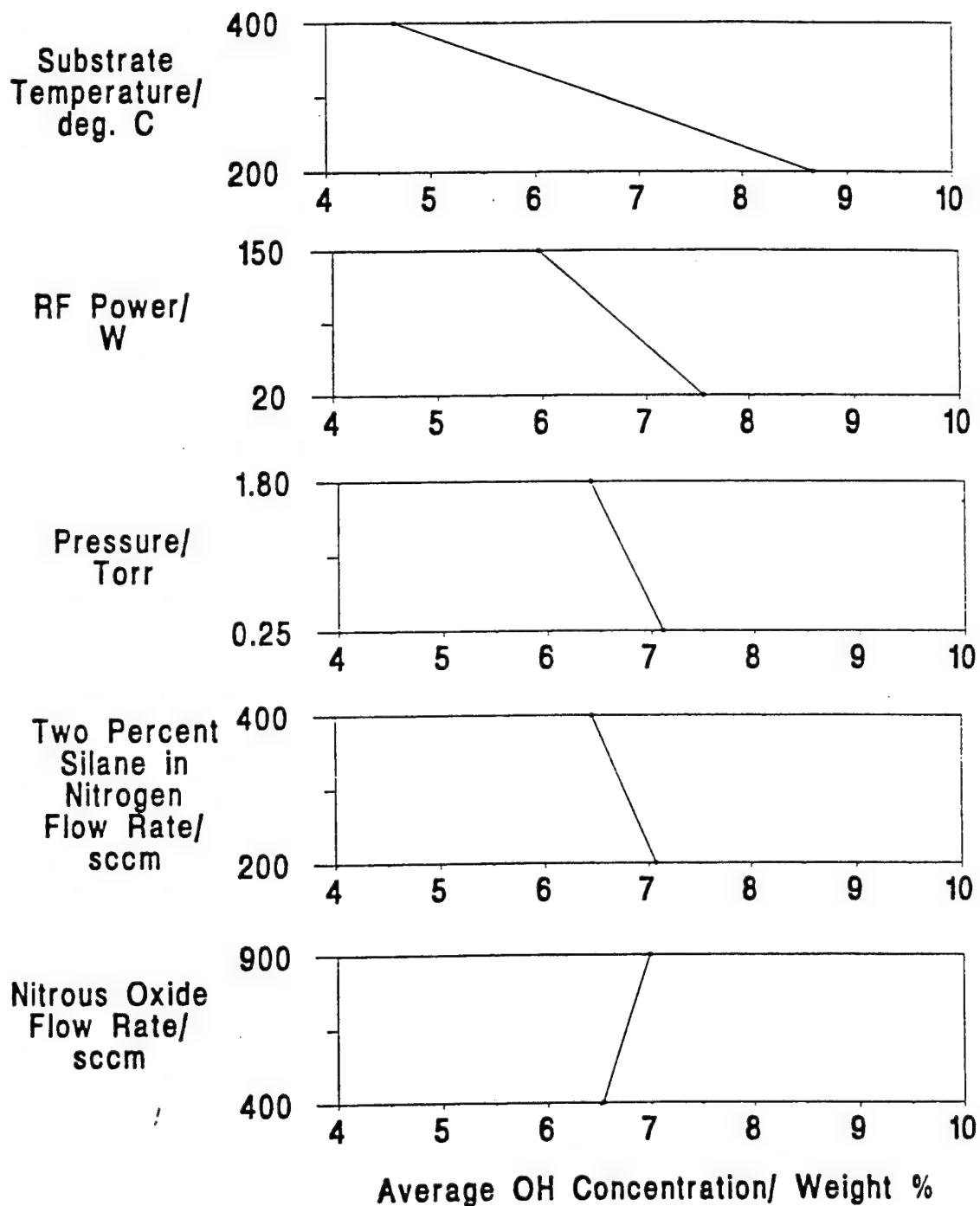Fig. 1. Water concentration vs. silanol concentration.

and the film becomes less dense as the silanol concentration increases, an increase in the water concentration with increasing silanol concentration seems reasonable.

The substrate temperature has the largest effect on the extent of silicon dioxide bonding and the silanol and water concentration in the film. Raising the substrate temperature from 200 to 400°C causes the average OH concentration (the sum of the silanol and water concentrations) to fall from 8.7 to 4.7 weight percent (Fig. 2). Previous studies have shown that the substrate temperature has the largest influence on the impurity concentration. Chapple-Sokol (5) proposes that a thermally activated surface phenomenon both limits the formation and promotes the removal of silanol and water impurities. Increased substrate temperature also promotes the rearrangement of the atoms on the surface. The removal of silanol and water impurities leads to more complete silicon dioxide bonding. Films with lower impurity concentrations and more complete silicon dioxide bonding also have a higher density.

An increase in the RF power from 20 to 150 W causes the average OH concentration to fall from 7.6 to 6.0 weight percent (Fig. 2). The RF power affects the deposition process in two ways. First, the RF power determines the extent of decomposition of the gas phase molecules. Silicon dioxide is formed by the reaction of silane derivatives formed in the plasma with oxygen atoms. Previous studies have shown that the decomposition of silane occurs more readily than the decomposition of nitrous oxide so that increasing the RF power increases the concentration of oxygen radicals (6). This facilitates more complete conversion of the precursors, more complete silicon dioxide bonding, and lower silanol concentrations. Second, the RF power also affects the positive ion bombardment. Increasing the RF power increases both the ion current and the energy of the bombarding ions. This increases the rate of the surface reactions, increases the mobility of the species on the surface, and enhances the desorption of by-products from the surface (7). The result is more complete silicon dioxide bonding, lower impurity concentrations, and higher density. Thus, increasing the RF power leads to lower impurity concentrations by increasing the relative oxygen concentration and enhancing the ion bombardment.

The average OH concentration drops from 7.1 to 6.4 weight

67

Fig. 2. Effect of the deposition parameters on OH concentration.

percent when the reactor pressure is increased from 0.25 to 1.8 Torr (Fig. 2). The effect of pressure on the deposition process is the combination of two effects. First, increasing the reactor pressure causes a decrease in the energy of the bombarding ions. Increasing the pressure decreases the mean free path of the ions. Therefore, the ions experience a larger number of collisions and lose more of their energy at high pressure. The lower ion energy reduces the effects of ion bombardment and results in less complete silicon dioxide bonding, larger impurity concentrations, and lower density (7). Second, the residence time of the species in the plasma increases with increasing pressure. Studies by Pai et al (8) have shown that increasing the residence time leads to the formation of an oxide that contains less hydrogen. They attribute this effect to an increase in the concentration of oxygen radicals. A larger concentration of oxygen radicals causes more complete reaction of the precursor molecules, decreasing the silanol concentration. Thus, increasing the reactor pressure leads to two competing effects. The observed drop in impurity concentration indicates that in this situation the increase in residence time from 0.12 msec to 0.84 has a larger effect on film composition than the decrease in the ion bombardment energy.

Decreasing the feed rate of silane in nitrogen or increasing the flow rate of nitrous oxide causes the average OH concentration to rise from 6.5 to 7.0. The nitrous oxide to silane ratio sets the relative concentrations of the reactants. As previously mentioned, the decomposition of silane occurs more readily than the decomposition of nitrous oxide, and the number of oxygen radicals must be significantly in excess of the number of silane molecules to produce near stoichiometric oxides. For these reasons, the ratio of nitrous oxide to silane must be large. The absence of Si-H peaks in the IR spectra of these oxides suggests that the excess of nitrous oxide was sufficient. However, as the excess of nitrous oxide in the feed increases, the silicon dioxide bonding is less complete, and the silanol concentration increases because silane is the limiting reagent. This agrees with the observations of Adams who found that increasing the nitrous oxide to silane ratio increases the silanol concentration of the films (1).

Permittivity and Loss.-The density   of metal-insulator circuitry is limited by,
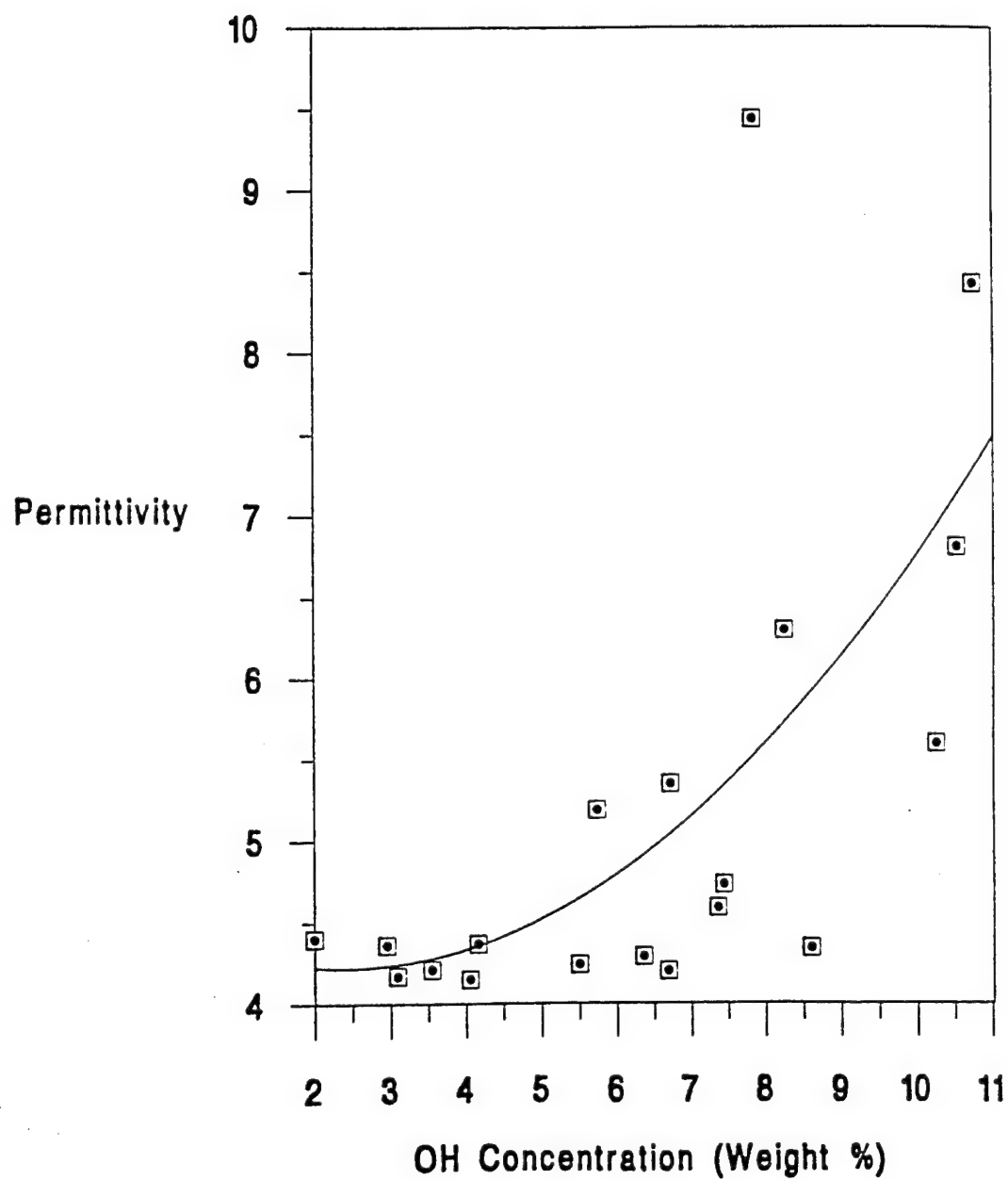
along with other factors, the complex dielectric constant of the dielectric. Thus, the permittivity and loss of a material are of primary importance when evaluating a material for use in metal-insulator structures. Permittivity is a measure of the polarization of the dielectric in an electric field, and loss is a measure of the energy losses associated with polarization. A decrease in the film density causes a decrease in the permittivity and loss assuming that the silicon dioxide quality remains constant and gases fill the free volume. The hydroxyl group of the silanol and water are more polar than silicon dioxide so that an increase in polarity with increasing silanol and water concentration is expected to increase the permittivity and loss. However, the increase may be somewhat offset by the decrease in density associated with inclusion of silanol and water impurities in the silicon dioxide lattice.

The permittivity of the films at 100 kHz increased from 4.2 to 10 as the OH concentration rose from 2 to 11 weight percent (Fig. 3). The loss at 100 kHz increased from 0.02 to 0.4 as the OH concentration rose from 2 to 11 weight percent (Fig. 4). Thus, the increase in polarity has a larger effect on the permittivity and loss than the decrease in density.

The effects of the deposition parameters on permittivity and loss correlate with their effects on the silanol and water concentration. Increasing the substrate temperature, increasing the RF power, increasing the pressure, or decreasing the nitrous oxide to silane ratio decreases the permittivity and the loss. However, the effect of pressure on loss is larger than the effect of RF power on loss even though the RF power exhibited a larger effect on the OH concentration.

Refractive Index.-The refractive index is the ratio of the speed of light in a vacuum to the speed of light in the material and is proportional to the square root of the permittivity at high frequency. As the density of the material increases, the speed of light in the material decreases and the refractive index increases. Similarly, an increase in the polarity of the molecules in a material decreases the speed of light and increases the refractive index and dielectric constant. An increase in the silanol and water concentration causes a decrease in the film density due to the inclusion of these species into the silicon dioxide lattice. However, water and the hydroxyl groups of the silanol are more   polar than silicon dioxide and are expected to

70

Fig. 3. Permittivity at 100 kHz vs. OH concentration (wt%).

increase the refractive index. The refractive index was found to decrease from 1.47 to 1.45 as the impurity concentration of the films increases from 2 to 11 weight percent (Fig. 5). The decrease in density has a larger effect on the refractive index than the increase in polarity, and the permittivity and loss appear to be more sensitive to the polarity changes than the refractive index. At high frequency, the loss mechanisms are not active.

The effects of the deposition parameters on the refractive index correlate with their effect on impurity concentration and film density. The substrate temperature had the largest effect on refractive index. The average refractive index increased from when the temperature was increased, increasing the RF power, increasing the pressure or decreasing the nitrous oxide to silane ratio causes the silanol and water concentration to fall and the average refractive index to rise.

However, the relative size of the effects of the deposition parameters on refractive index does not exactly correlate with their effects on OH concentration. Although the RF power has a larger effect on the OH concentration than the pressure, the RF power and pressure exhibit nearly identical effects on the refractive index. As is the case with loss, the additional change can be accounted for by enhanced film densification with increasing reactor pressure.

Wet Etch Rate.-The wet etch rate of the films in dilute HF is a function of the extent of silicon dioxide bonding and porosity. Less complete silicon dioxide bonding reduces the number of silicon-oxygen bonds resulting in a smaller number of bonds to be broken in order to etch the film. The etch rates range from 600 to 42000 Å/min as the OH concentration increased from 2 to 11 weight percent (Fig. 6).

The effects of the deposition parameters on etch rate generally are similar to their effect on silanol concentration and film density. Increasing the substrate temperature causes more complete silicon dioxide bonding, lower impurity concentrations, and higher density. Similarly, increasing the RF power or pressure decreased the OH concentration and the average etch rate. However, increasing the reactor pressure causes a larger decrease in the wet etch rate than is suggested by the corresponding decrease in OH concentration.

The wet etch rate, refractive index, and loss data indicate that

Fig. 4. Loss at 100 kHz vs. OH concentration (wt%).
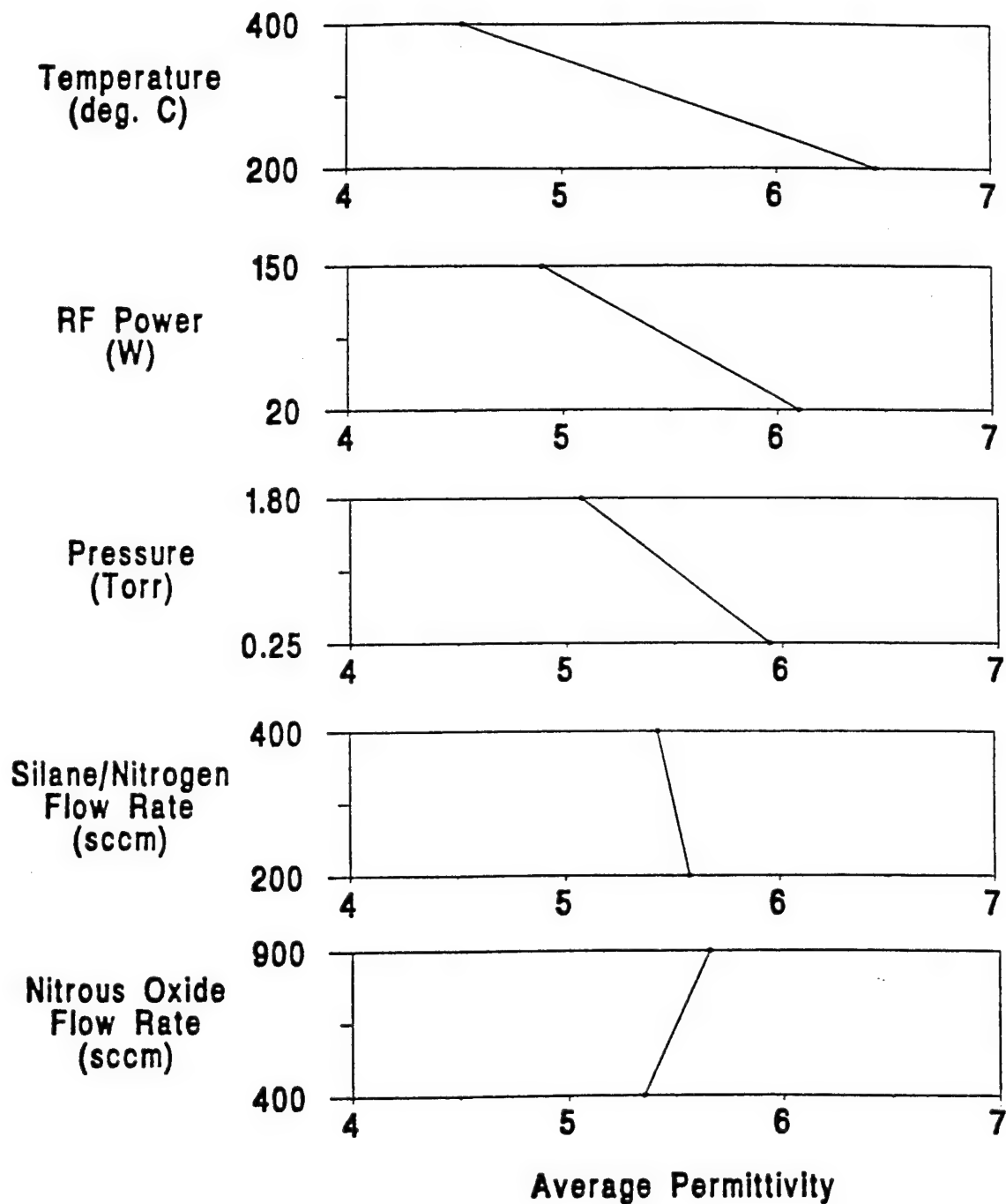
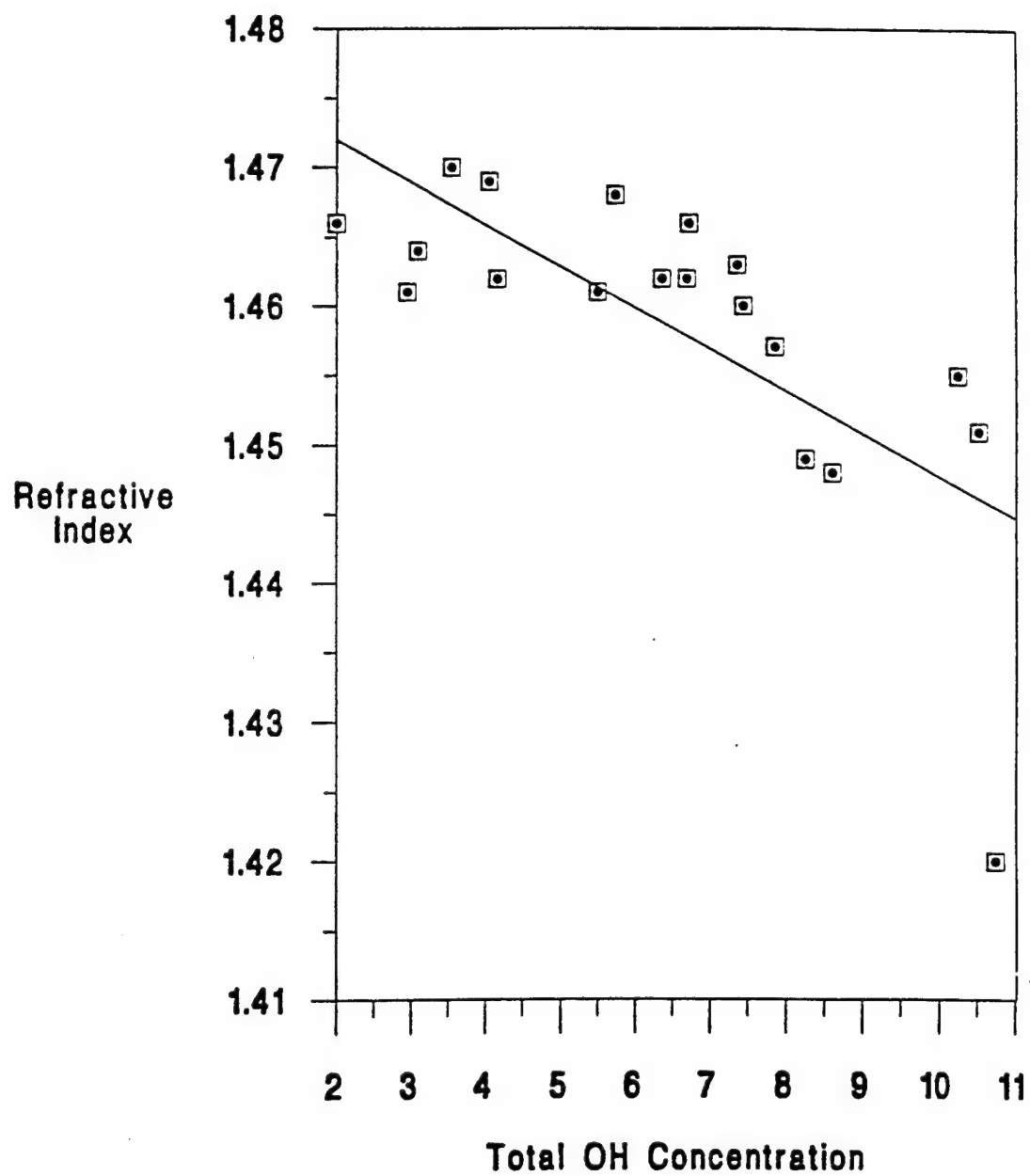Fig. 5. Refractive index vs. OH concentration (wt%).

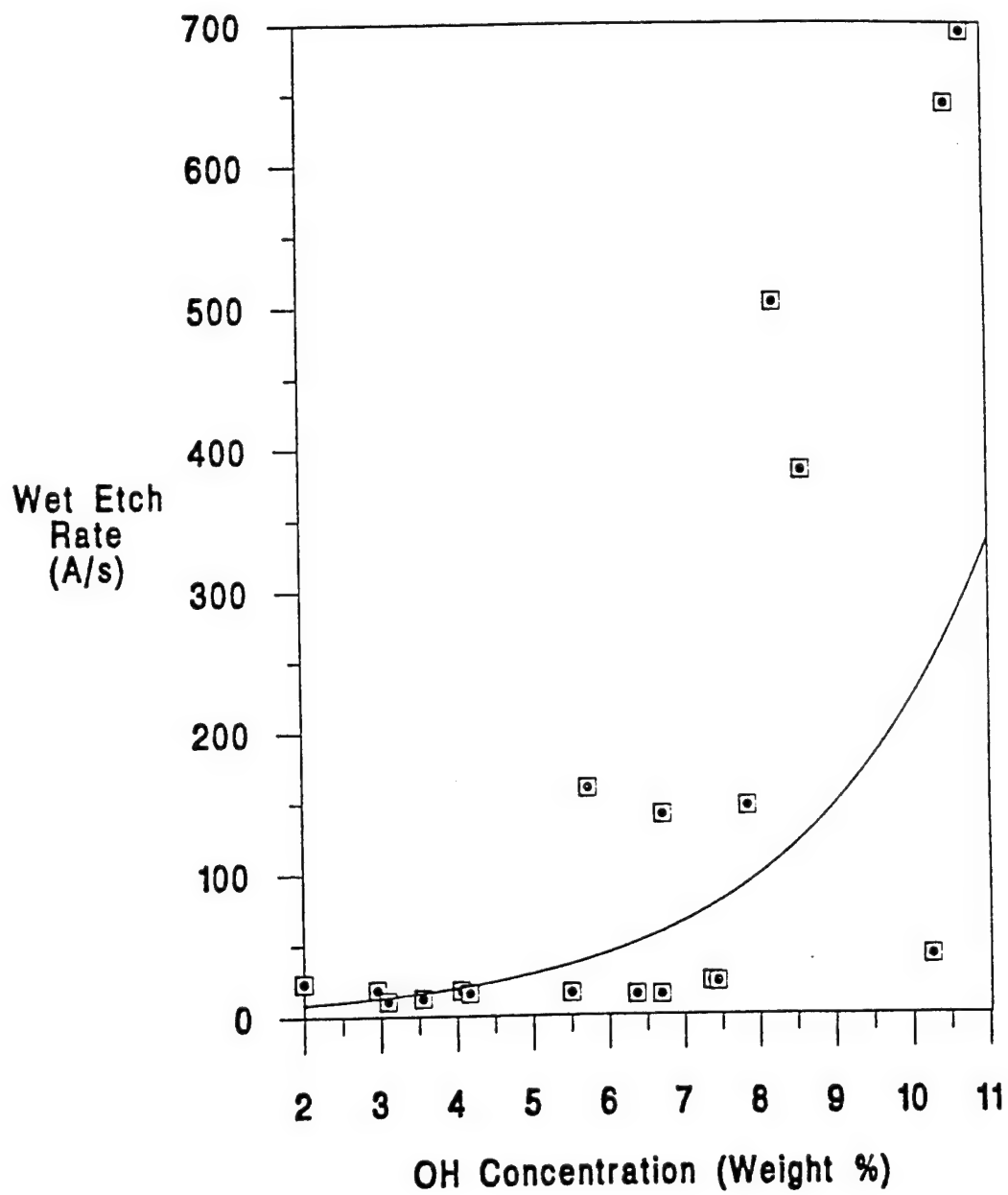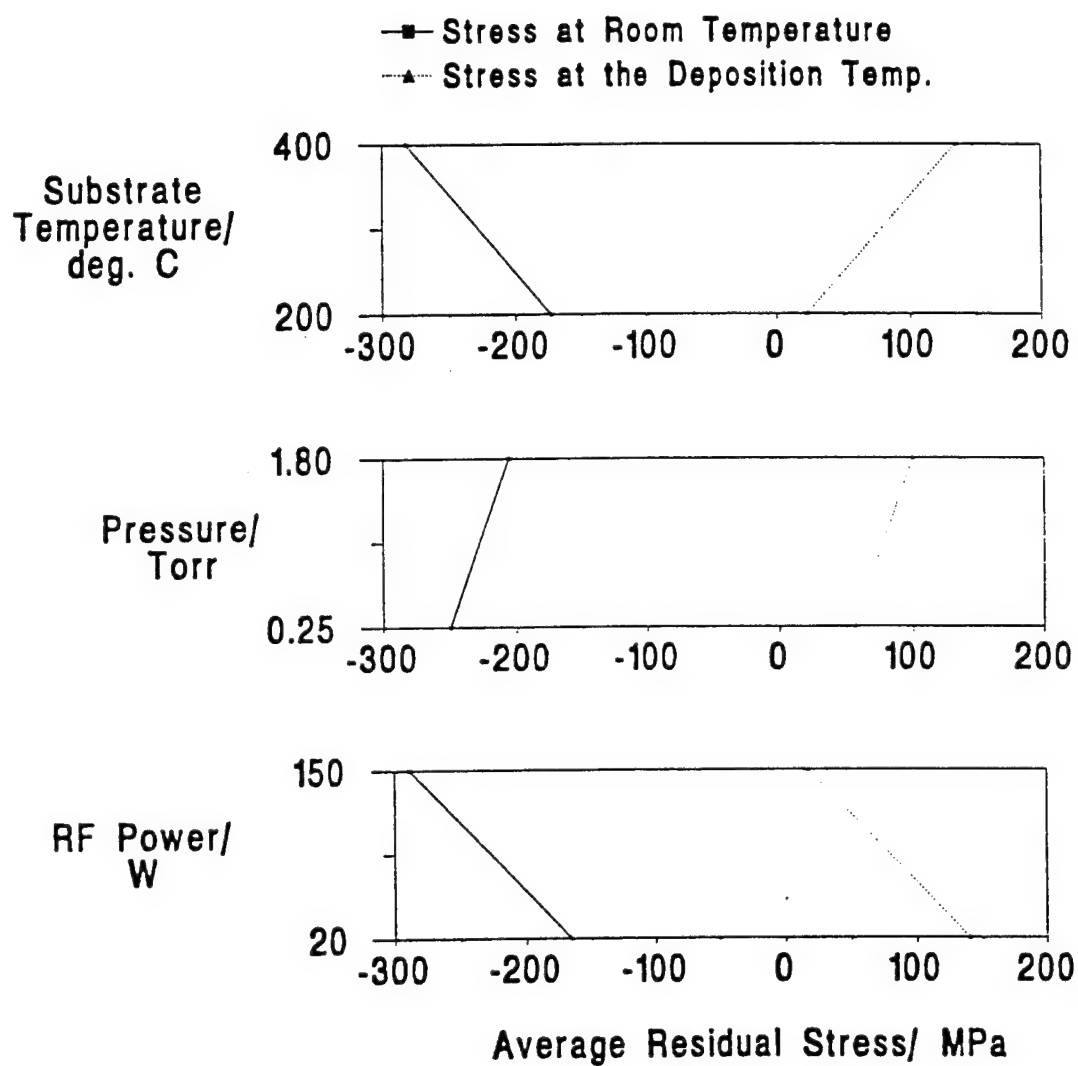Fig. 6. Wet etch rate (Å/min) vs. OH concentration (wt%).

Fig. 7. Effect of the deposition parameters on the residual stress (MPa). The negative sign indicates a compressive stress.

the reactor pressure has a larger effect than its concentration effect suggests. In each case, the additional change can be accounted for by enhanced film densification with increasing reactor pressure. Increasing the reactor pressure causes an increase in the residence time which leads to the formation of a film that contains less hydrogen. Pai (8) attributes this effect to an increase in the oxygen radical concentration. The increase in reactor pressure not only leads to the formation of a film containing less silanol, but must also facilitate the formation of a denser film. Then, the large changes in the loss, refractive index and wet etch rate can be attributed to enhanced film densification.

Residual Stress.-The residual stress of a film on silicon is a function of the film composition, structure, and the thermal history of the film and substrate. The films deposited in this study are under 30 to 400 MPa compressive stress at room temperature. An increase in the substrate temperature causes the residual stress at room temperature to rise from 173 to 282 MPa compressive (Fig. 7). A compressive residual stress builds upon cooling because of the CTE mismatch between the silicon dioxide and silicon. Since the films deposited at high temperature are cooled over a greater temperature range, they exhibit a higher compressive stress at room temperature.

Increasing the RF power or decreasing the pressure causes the room temperature residual stress to become more compressive (Fig. 7). Previous studies have shown that additional ion flux causes the film to relax laterally resulting in greater compressive stress (7). Thus, increasing the RF power or decreasing the reactor pressure enhances the ion bombardment causing the residual stress to become more compressive.

The silane and nitrous oxide flow rates exhibit no significant effect on the residual stress at either the deposition temperature or room temperature. This suggests that either the composition changes are too small to affect the residual stress or that the composition has little effect on the residual stress.

In summary, the results of the previous experiments show that the properties of PECVD oxides with a lower silanol and water concentration are superior to the properties of oxides with a higher impurity content. Minimizing the

77

silanol and water concentration, in turn, minimizes the permittivity and loss, and maximizes the density and etch resistance of the silicon dioxide. The silanol concentration can be limited by the correct choice of the deposition parameters. The conditions that contribute to the formation of silicon dioxide with a low silanol concentration are high substrate temperature (400 °C), high reactor pressure (1.8 Torr), high RF power level (150 W), and a nitrous oxide to silane ratio of 50-100. Films deposited under these conditions have an OH concentration of approximately 3.0 weight percent and exhibit a permittivity of 4.1, a loss of 0.004, a refractive index of 1.465, and a wet etch rate of 16 Å/s.

However, lower deposition temperatures must be employed in the presence of some materials. With a 200 °C deposition, the silicon dioxide has an OH concentration of 7.4 weight percent, a permittivity of 4.7, a loss of 0.010, a refractive index of 1.460, and a wet etch rate of 26 Å/s. By raising the deposition temperature to only 250 °C, the permittivity and loss can be reduced to 4.3 and 0.006, respectively. Thus, with the correct choice of the RF power level, pressure, and gas flow rates, the impurity content of the silicon dioxide can be limited while the substrate temperature is lowered.

Conclusions

PECVD silicon dioxide films contain more silanol and water and are less dense than films deposited or grown at high temperatures. The extent of silicon dioxide bonding and the residual silanol and water concentrations are the quantities of primary importance when evaluating the film composition. Since the water molecules hydrogen bond to silanol groups and the film becomes less dense as silanol is incorporated into the lattice, an increase in the silanol concentration is accompanied by an increase in the water concentration.

The substrate temperature has the largest effect on the silanol and water impurity concentrations. A thermally activated surface phenomenon inhibits the formation and promotes the removal of impurities causing more complete silicon dioxide bonding. Increasing the RF power increases the relative concentration of oxygen radicals which leads to more complete silicon dioxide bonding. Increasing the RF power also increases the   level of ion bombardment which increases the

rate of surface reactions, increases the mobility of the species on the surface, and enhances the desorption of by-products causing more complete silicon dioxide bonding and lower impurity concentrations. Although increasing the reactor pressure decreases the ion bombardment effects, the corresponding increase in residence time exhibits a larger effect. The concentration of oxygen radicals produced in the plasma increases with residence time leading to more complete silicon dioxide bonding and a lower silanol concentration. Changing the reactant gas flow rates changes the relative amounts of the reactants at the surface. Increasing the nitrous oxide to silane ratio causes less complete silicon dioxide bonding and a larger impurity concentration because silane is the limiting reagent. At very low nitrous oxide to silane ratios, a porous silicon rich film that contains SiH is produced.

The silanol concentration is an important factor in determining the film properties. First, the hydroxyl group of the silanol and water are more polar than silicon dioxide. Thus, an increase in the silanol and water concentration causes an increase the permittivity and loss. Second, the oxide becomes less dense with the inclusion of impurities into the silicon dioxide lattice. Thus, the refractive index decreases as the silanol concentration increases. Similarly, as the extent of silicon dioxide bonding decreases, the number of bonds that must be broken to etch the film decreases. Thus, the wet etch rate increases as the silanol concentration increases.

The residual stress is highly dependent upon the substrate temperature. Upon cooling, the residual stress becomes more compressive because the CTE of silicon dioxide is less than that of silicon. Because the films deposited at higher temperature are cooled over a greater temperature range, they exhibit a larger compressive stress at room temperature. Increasing the RF power or decreasing the reactor pressure enhances the ion bombardment effect which causes the film to relax laterally causing the residual stress to become more compressive.

Although the substrate temperature causes the most significant decrease in impurity concentration, the deposition temperature must be limited if the oxide is to be used in metal-insulator structures. Using a large RF power, high pressure, and low nitrous oxide to silane ratio   will minimize the silanol concentration at a

given temperature. This, in turn, will minimize the dielectric constant and maximize the etch and solvent resistance of the oxide produced.

REFERENCES

1. Adams, A. C., F. B. Alexander, C. D. Capio, and T. E. Smith, J. Electrochem. Soc., 128, 1545 (1981).

2. Pliskin, W.A. and H.S. Lehman, J. Electrochem. Soc., 112, 1013 (1965).

3. Atkins, P. W., Physical Chemistry, Third Edition, W. S. Freeman and Company, New York (1986).

4. Smolinsky, G. and T. P. H. F. Wendling, J. Electrochem. Soc., 132, 950 (1985).

5. Chapple-Sokol, J. D., W. A. Pliskin, R. A. Conti, E. Tierney and J. Batey, J. Electrochem. Soc., 138, 3723 (1991).

6. Smith, D. L. and A. S. Alimonda, J. Electrochem. Soc., 140, 1496 (1993).

7. Hey, H. P. W., B. G. Sluijk and D. G. Hemmes, Solid State Technology, 33, 139 (1990).

8. Pai, P. C., S. S. Chao, Y. Takagi and G. Lucovsky, J. Vac. Sci. Technol. A, 4, 689 (1986).

CHAPTER 6

ELECTRICAL MEASUREMENTS

BACKGROUND

High Frequency Measurements and Data Analysis

<u>Structures Used</u>

A number of different structures were considered for making the high frequency measurements. It was decided to use microstrip structures since only two metal layers separated by a dielectric would be required. This has the advantage that fewer processing steps are required; therefore, structures could be manufactured more quickly and would have a greater chance of surviving the manufacturing process than would more complex structures with additional layers.

A modified version of the microstrip T-resonator described in a paper by Amey et al.[1] was chosen as the test-structure for high-frequency
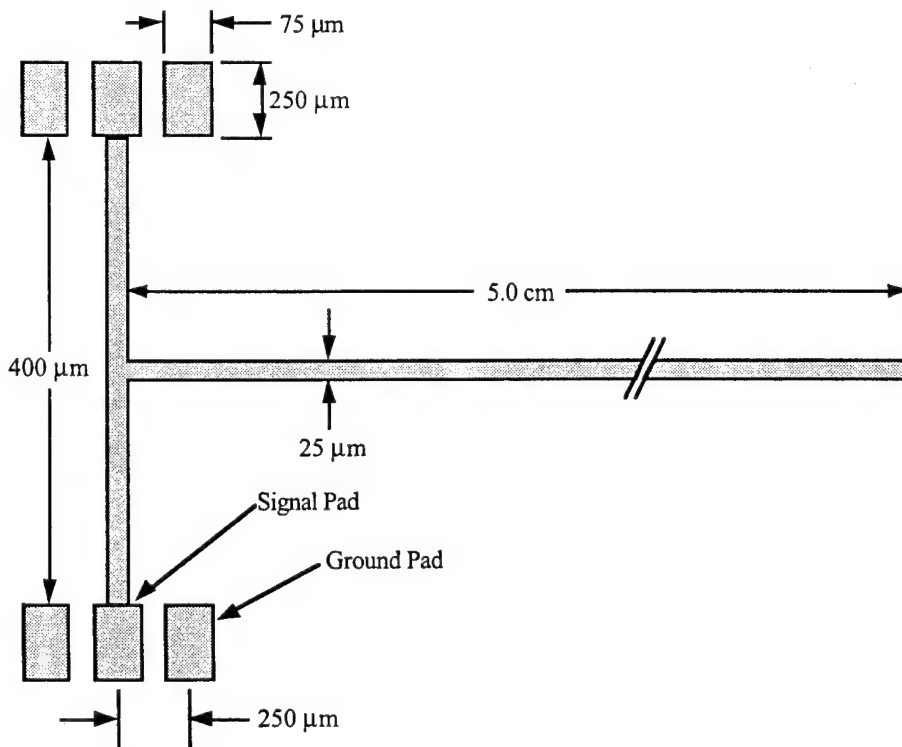

Figure 1: Diagram of a T-resonator (not to scale)

measurements. This structure is shown in Figure 1. The resonant portion or base of the T-resonator consists of a 5.0 cm length of microstrip which is approximately 25 microns wide. The length of this base determines its resonant frequencies. The end of this base can be terminated with either a short-circuit or open-circuit. A short-circuit termination was created by using a via to connect the end of the base to the ground plane. An open-circuit termination was created by simply leaving the end of the base unconnected to anything else. The other end of the base terminated in two symmetrical microstrip arms which form the "T" shape. Each of these arms is 200 microns long and 25 microns wide. Each arm terminates in a signal probe pad which is 75 microns wide and about 100 microns long. On both sides of the signal pad is a ground probe pad of the same size which is connected to the ground plane by a via.

A number of other structures besides the T-resonator were considered and rejected before the T-resonator was finally chosen. Parallel plate capacitors were rejected because at the higher frequencies of interest (above 1 GHz), depending on their size, they can behave as circular resonators. Simple transmission lines were rejected due mainly to limitations of the microwave probes being used. These probes can only be moved to approximately 2 cm apart thus allowing transmission lines of 2 cm maximum length. Transmission lines this short would not be useful for determining the electrical properties of the dielectric material.

A variety of other lightly coupled resonators in other configurations were also considered and rejected for two primary reasons. First of all some of the structures would be difficult to fabricate. The lightly coupled configurations usually required very small and thus hard to fabricate coupling gaps. Some of these structures also required specific values of characteristic impedance for the coupling lines. Since in this project a variety of different dielectrics and metals were used it was not practical to design a specific mask for each possible combination. Second, many of the lightly coupled resonator configurations had to be rejected due to the limitations of maximum probe spacing as described above.

General Measurement Procedures

Equipment Used

The key piece of measuring equipment used to obtain high frequency data was the Hewlett Packard 8510 Network Analyzer. This network analyzer has a frequency range of 45 MHz to 26.5 GHz and was used to measure the S-parameters of the T-resonators.

The second key element was the Design Techniques Ground-Signal-Ground probe tips. These tips were mounted in the micropositioner assembly in a probe station which consisted of a microscope and stage. The probes were connected to the network analyzer by using coaxial cables.

An HP Vectra computer with an HPIB card installed was connected to the network analyzer in order to download the s-parameter data and to analyze the data with suitable computer programs.

HP 8510 Setup

Before any measurements were taken, the network analyzer was calibrated using the full two-port Short-Open-Load-Thru (SOLT) calibration procedure. This is the most accurate SOLT calibration procedure available. The network analyzer which was used was not able to perform TRL or other calibration procedures which are considered more accurate than the SOLT method. The calibration standard used was a Tektronix Cal96 Calibration chip, which included short-circuits, 50-ohm loads, and thru standards in the ground-signal-ground 10-mil pitch configuration required for the probes. For the open standard, the probes were placed on the bare substrate of the calibration chip. After checking the calibration by remeasuring the standards, actual measurements were ready to be performed.

The HP 8510 was set up to measure 801 data points in the frequency range from 1 GHz to 9 GHz. This yielded a data point every 10 MHz. Before the data was stored, 10 frequency sweeps were averaged together to minimize random noise. The temperature of the room in which measurements were

made was typically around 75 degrees Fahrenheit and the relative humidity varied between 40% and 60%.

High Frequency Data Analysis

Once all of the measurements were taken, the raw data was analyzed. The first step was to determine the frequencies at which the resonant nulls occurred. This was done by using a custom C program. The program read in the data and determined the frequencies of the local minimums. These local minimums are the resonant frequencies of the 5 cm long T-resonator base. A resonant frequency occurs where the physical length of the resonator base corresponds to an odd multiple of quarter-wavelengths. The T-resonators fabricated with the physical dimensions previously described typically have four or five resonant frequencies in the frequency range of 1 GHz to 9 GHz.

Figure 2: Schematic of T-resonator as simulated in the Hewlett-Packard Microwave Design System Software

Figure 3: Plot showing measured and simulated T-resonator data

Next a circuit simulator, the Hewlett Packard Microwave Design System, was used to analyze the microstrip T-resonator.

Figure 2 shows a schematic of a typical simulated circuit. This simulator uses distributed models for microstrip structures and requires the physical dimensions of the structures and material parameters as inputs. Initially, the measured physical characteristics such as thicknesses, lengths, and widths were entered into the model. Next, an estimate was made of the dielectric constant and the simulation was run. The simulator was set up to output data at the same frequencies and in the same format as the network analyzer, so the same PC program could be used to extract the resonant frequencies of the simulated T-resonator. The dielectric constant used in the simulator was then adjusted until the simulated resonant frequencies matched the measured resonant frequencies. This dielectric constant was considered the answer for the particular resonator at the particular frequency. Figure 3 shows a plot of the simulated T-resonator S_{21} data along with actual measured data.

The next step was to get a single dielectric constant for the dielectric on a wafer by combining the dielectric constants determined at each frequency for each resonator on that wafer. Ideally, the dielectric constants would be the same for all structures on a wafer. Unfortunately, there are numerous sources of error which are discussed below. Under most conditions a simple average will suffice, but in an effort to determine the sources of the difference and to determine if the differences were statistically significant, an analysis of variance (ANOVA) was performed when possible[2,3]. The ANOVA used separates differences into those caused by random error, those caused by differences in frequency, and those caused by differences in the resonators.

Sources of Error in High Frequency Data

In any experiment there is always some amount of error. By using careful and consistent measurement techniques; however, both human error and systematic error can be kept to a minimum and quantified with an upper bound. Nevertheless, there are some sources of error that cannot be

completely eliminated. In this experiment, there are a number of possible sources of error.

First, the model being used to analyze the microstrip T-resonators is not ideal. Microstrip models are approximations limited mainly by the fact that there is no closed form electromagnetic solution for a wave on a microstrip transmission line. In a wave propagating on a microstrip line, part of the energy traveling along a microstrip line travels in the dielectric below the microstrip and part of the energy travels in the air above the microstrip. Because the dielectric has different properties than the air, the energy traveling in the dielectric is traveling at a slower rate and with a different amount of loss than the energy traveling in the air. This complicated wave is typically approximated by what is known as a quasi-TEM mode, which cannot be described in a closed form equation. Today, the approximations used to describe microstrip and microstrip discontinuities (bends, width changes, gaps, etc.) are quite accurate, but they are not ideal.

Even if the microstrip model were perfect, however, the dimensions of the microstrip are known only to a limited accuracy. Furthermore, the variations in the manufacturing process and materials do not yield perfectly uniform structures. Thus, the accuracy of the distributed models in the circuit simulator are considered sufficient for this application.

The T-resonators are 5 centimeters long, 25 microns wide, and 2 or 3 microns thick. The dielectric is not perfectly planar over the ground plane, and over 5 centimeters the thickness can vary several percent. The metal thickness and width can also vary somewhat over that length. While all of these variations are typically small, they can add up and combine with model error to become significant.

Besides model error and imperfections in the structures themselves, there is of course measurement error. Each measurement of a physical dimension of the T-resonator has some amount of error. By using careful and consistent techniques, and averaging together multiple measurements, this error can be reduced but not eliminated. Moreover, the act of measuring the T-resonators is a semi-destructive process. Each time the probes touch down

on a set of probe pads they leave a small indentation called a footprint. After multiple measurements, especially when the pads are made of a soft metal such as gold, the footprints can significantly alter the shape and therefore the electrical characteristics of the pads.

Therefore, structural imperfections and measurement errors are propagated to the model, which itself increases the amount of error in the answer. It is estimated that the error in the final measured value of the dielectric constant using the procedures described above is on the order of several percent.

Low Frequency Measurement and Data Analysis

Structures used

When the low frequency test structures were being designed, many different types were considered. From a manufacturability standpoint, only structures which consisted of two metal layers separated by a layer of dielectric were seriously considered.

Parallel plate capacitors were one of the first and most obvious possibilities. Capacitors are straightforward to measure and analyze and can yield both the pure real dielectric constant and the loss tangent of the dielectric. While any shape should theoretically work, a simple circular geometry was chosen. While squares or rectangles could also work, the
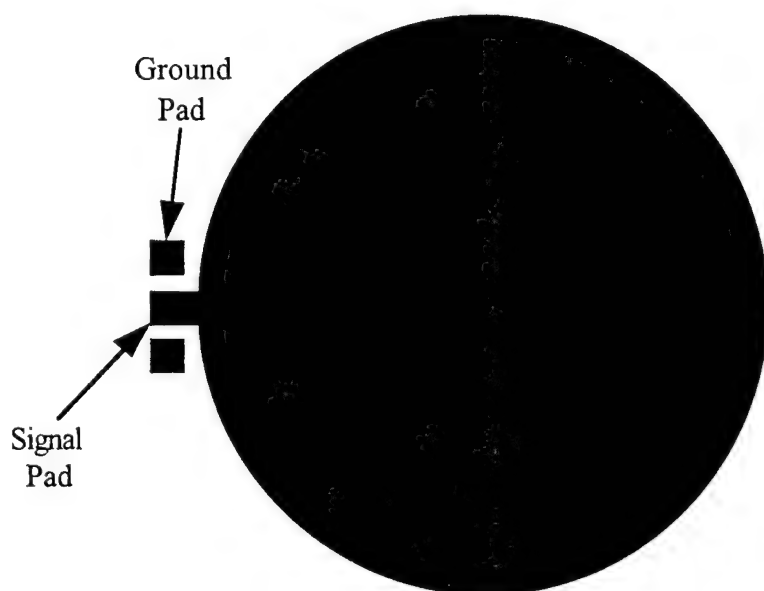

Figure 4: Diagram of a Capacitor (not to scale)

corners would cause strong fringing fields to occur. Additionally, a circle encloses the largest possible area for a given perimeter, thus minimizing fringing fields. Furthermore, the diameter was chosen to be large compared to the dielectric thickness to minimize the effect of the fringing fields.

On the final mask set, three capacitor sizes were chosen. The diameters used were 4.98, 6.98, and 9.88 millimeters. Dielectric thickness ranged from 3 to 8 microns. Metal thickness was usually about 2 to 3 microns. On the mask, there were ten capacitors (3 large, 3 medium, and 4 small). Figure 4 shows a diagram of the top view of a parallel plate capacitor.

Other capacitor types were rejected for the reasons listed above. Resonant structures would have been desirable, however for the resonators to resonate in the low kHz frequencies, the necessary dimensions would have been too large to fit on the wafer. Transmission lines were also considered, but again the problem of narrow probe spacing made their use difficult. Short lines could have been used, but it was believed that the amount of information which could be obtained from them was minimal.

General Measurement Procedures

Equipment Used

The device used to measure the capacitors was the HP 4263A LCR meter. Measurements were taken at 10 kHz. Needle probes were used to contact the probe pads of the capacitors on a probe station.

HP 4263A Setup

The LCR meter was calibrated by using an open and a short. For the short, the probes were placed on a large metallic area (usually the upper plate of a large capacitor) using the same spacing necessary to contact the probe pads. For the short, the probes were placed on top of the open dielectric, again using the probe pad spacing.

Figure 5: Equivalent Circuit for a Capacitor with a Lossy Dielectric

When calibration was complete, the meter was set up to average 128 measurements and display the results as a capacitance in parallel with a conductance.

Low Frequency Data Analysis

Assuming a physical capacitor has a lossy dielectric, the complex permittivity of this lossy dielectric is denoted by:

$$\varepsilon = \varepsilon_o \varepsilon_r = \varepsilon_o (\varepsilon_r' - j\varepsilon_r'') \tag{1}$$

permittivity of the dielectric, ε_r' is the real part of the complex relative permittivity, and ε_r'' is the imaginary part of the complex relative permittivity. where ε_o is the permittivity of free space ($\approx 8.854 \times 10^{-12}$ F/m), ε_r is the complex relative

The capacitance for a parallel plate capacitor is defined as

$$C = \frac{\varepsilon A}{h} \tag{2}$$

where C is the capacitance, A is the area of the plate, and h is the thickness of the dielectric.

The equivalent admittance of this lossy capacitor would then be:

$$Y = j\omega C = \frac{A\omega \varepsilon_o (\varepsilon_r'' + j\varepsilon_r')}{h} \tag{3}$$

where j is the square root of -1, and ω is the radian frequency ($\omega = 2\pi f$).

91

This lossy capacitor can be modeled as a lossless parallel plate capacitor, C', in parallel with a conductance, G', (which represents the loss due to the lossy dielectric) as shown in Figure 5.

When the lossy capacitor is measured using the HP 4263A, the results are output as an ideal capacitor, C', in parallel with a perfect conductance, G'. The admittance of this equivalent circuit is

$$Y = G' + j\omega C' \tag{4}$$

If the real and imaginary parts of **Error! Reference source not found.** and **Error! Reference source not found.** are set equal, the value of the complex relative permittivity can be calculated as follows.

$$\varepsilon_r' = \frac{C'h}{A\varepsilon_o} \tag{5}$$

$$\varepsilon_r'' = \frac{G'h}{A\omega\varepsilon_o} \tag{6}$$

Error! Reference source not found. and **Error! Reference source not found.** describe how to determine both the real and imaginary parts of the complex permittivity from the measured admittance at a particular frequency and the measured physical dimensions of the capacitor, based on a simple model.

Sources of Error in Low Frequency Data

Although the capacitors are much easier to measure and analyze than the T-resonators, error cannot be completely eliminated and may come from many sources.

First of all, the model being used is a simple model which essentially ignores metal loss and fringing fields around the edge of the capacitor. At 10 kHz using gold, silver, or aluminum, the metal loss is assumed to be insignificant. A simple correction for fringing fields around a capacitor increases the apparent radius of the capacitor based on the physical radius and the dielectric thickness. The formula used is $r_{apparent} = r_{physical} + h/2$, where

$r_{apparent}$ is the radius used to calculate the plate area, $r_{physical}$ is the measured radius of the plate, and h is the dielectric thickness.

As with the T-resonators, the dimensions of the capacitors are known only to a limited accuracy, and variations in the manufacturing process and materials do not yield perfectly uniform structures. Because of the non-uniformity in the structures and the large ratio of capacitor area to dielectric thickness, the simple capacitor model described above is considered adequate for this application.

There is still measurement error of course, and the act of measuring the capacitors with the needle probes gradually destroys the probe pads.

The accuracy of the results is estimated to be a few percent.

EXPERIMENTS

Repeatability of High Frequency Measurements

Problem

As mentioned in the section "Sources of Error in High Frequency Data" measuring the T-resonators is a semi-destructive process. The act of probing leaves a footprint on the probe pad which may change the contact resistance at the interface of the probe and the probe pad from measurement to measurement, and thus change the final results. In addition, the amount of force applied to the probe tips may not be exactly the same from measurement to measurement. In order to estimate how much these two factors effect the measurements, an experiment was performed.

Approach

In the experiment, the network analyzer was calibrated as usual. Next a number of T-resonators made with different materials were measured and analyzed multiple times. All measurements were made on the same day to minimize variations due to temperature or humidity changes or HP 8510 instrument drift. All measurements were also made using the same network analyzer calibration.

Results and Discussion

Summarized below are the standard deviations of the resonant frequencies and the corresponding standard deviations in ε_r' due to the resonant frequency variation.

Table 1: Measurement Repeatability Results for Probimide 293 Dielectric with Silver Metallization

Avg. Resonant Frequency (GHz)	Number of Measurements	Resonant Freq. Std. Dev. (GHz)	Resonant Freq. Std. Dev. (%)	ε_r' Std. Dev. (%)
2.801	5	0.008	0.29%	0.69%
4.726	5	0.007	0.15%	0.43%
6.672	5	0.007	0.10%	0.29%
8.659	5	0.035	0.40%	1.09%

Table 2: Measurement Repeatability Results for PI-2566 Dielectric with Aluminum Metallization

Avg. Resonant Frequency (GHz)	Number of Measurements	Resonant Freq. Std. Dev. (GHz)	Resonant Freq. Std. Dev. (%)	ε_r' Std. Dev. (%)
2.569	6	0.004	0.16%	0.33%
4.350	6	0.004	0.09%	0.21%
6.151	6	0.005	0.08%	0.18%
8.021	6	0.008	0.10%	0.25%

Table 3: Measurement Repeatability Results for PI-2611 Dielectric with Gold Metallization

Avg. Resonant Frequency (GHz)	Number of Measurements	Resonant Freq. Std. Dev. (GHz)	Resonant Freq. Std. Dev. (%)	ε_r' Std. Dev. (%)
1.498	10	0.002	0.13%	0.24%
3.116	10	0.004	0.13%	0.27%
4.798	10	0.008	0.17%	0.40%
6.419	10	0.010	0.16%	0.33%
8.198	10	0.014	0.17%	0.40%

The maximum standard deviation in resonant frequency from these data is 0.40%, with a more typical value of standard deviation being below 0.20%. The average standard deviation in dielectric constant (due to variation in resonant frequency) is 0.39%.

Conclusions

There is a small amount of variation in the resonant frequency and consequently of the dielectric constant from measurement to measurement, as expected. However the standard deviation is small enough to conclude that the measurement repeatability is good.

Repeatability of High Frequency Calibration

Problem

While the experiment described above demonstrates good measurement repeatability using a single calibration, it is possible that results could change depending on the calibration itself. Ideally, each time the network analyzer is calibrated, it should provide the exact same results. However, this may not be the case since the calibration standard is subject to the same problems of variable contact resistance and deteriorating probe pads as the actual test structures. To see how repeatable the calibrations are an experiment was performed.

Approach

In the experiment, the network analyzer was calibrated as usual. Next a number of T-resonators made with different materials were measured. Then the network analyzer was recalibrated and the same T-resonators were remeasured. This sequence of calibrating and measuring was performed several times. Then the results were analyzed. All calibrations and measurements were made on the same day to minimize variations due to temperature or humidity changes or HP 8510 instrument drift.

Results and Discussion

The tables below summarize typical results. They show the standard deviations of the resonant frequencies and the corresponding standard deviations in ε_r' due to the resonant frequency variation.

Table 4: Calibration Repeatability Results for PI-2566 Dielectric with Aluminum Metallization (Res. #7)

Avg. Resonant Frequency (GHz)	Number of Calibrations	Resonant Freq. Std. Dev. (GHz)	Resonant Freq. Std. Dev. (%)	ε_r' Std. Dev. (%)
2.548	3	0.004	0.16%	0.27%
4.351	3	0.005	0.11%	0.24%
6.170	3	0.006	0.10%	0.21%
8.048	3	0.017	0.21%	0.50%

Table 5: Calibration Repeatability Results for PI-2611 Dielectric with Gold Metallization (Res. #2)

Avg. Resonant Frequency (GHz)	Number of Calibrations	Resonant Freq. Std. Dev. (GHz)	Resonant Freq. Std. Dev. (%)	ε_r' Std. Dev. (%)
2.299	3	0.006	0.26%	0.57%
3.923	3	0.004	0.10%	0.20%
5.575	3	0.007	0.13%	0.29%
7.290	3	0.011	0.15%	0.36%

Table 6: Calibration Repeatability Results for PI-2611 Dielectric with Silver Metallization (Res. #3)

Avg. Resonant Frequency (GHz)	Number of Calibrations	Resonant Freq. Std. Dev. (GHz)	Resonant Freq. Std. Dev. (%)	ε_r' Std. Dev. (%)
2.455	2	0.003	0.12%	0.26%
4.179	3	0.001	0.02%	0.03%
5.886	3	0.002	0.03%	0.06%
7.657	3	0.003	0.04%	0.09%

The maximum standard deviation in resonant frequency from these data is 0.26%, with a more typical value of standard deviation being below

0.15%. The average standard deviation in dielectric constant (due to variation in resonant frequency) is 0.26%.

Conclusions

Since these values are approximately the same as those obtained from the measurement repeatability experiment previously described, it seems reasonable to conclude that the high frequency calibration procedure is highly repeatable.

Discrepancies Between High and Low Frequency Results

Problem

After a number of measurements had been taken and analyzed, it was noticed that for some samples there seemed to be some significant variation (several percent) from measurement to measurement, and sometimes between the high frequency and low frequency measurements.

Approach

Several possible explanations were considered. The first and most obvious explanation might be problems with either the HP 8510 network analyzer or the HP 4263 LCR meter, or both. However, the repeatability experiments just discussed seem to indicate that the HP 8510 has high precision, and the calibration standards being used should make the measurements highly accurate. According to its manual, the HP 4263 should be accurate to about 0.5% in the configuration needed for these measurements. Measurements of other devices would seem to confirm that estimate. Therefore it seems unlikely that meter problems would account for the differences observed.

Fringing fields, which are ignored in the capacitor model, might be another possible explanation. This seems unlikely, since the radius of the smallest capacitor is about 500 times larger than the dielectric thickness. However as a check, a simple fringing correction was made. The radius used to calculate the area of the plate, $r_{apparent}$, was set equal to the physical radius,

$r_{physical}$, plus half the dielectric thickness, h. Thus $r_{apparent} = r_{physical} + h/2$. When this correction was made on several measurements, the relative dielectric constant was reduced by less than 0.01 units -- a change of less than 0.3%. Since this change is less than the accuracy of the meter, it seems reasonable to continue to ignore fringing fields.

Another possibility was that moisture was being absorbed by the dielectric and that this was effecting the results. Since water in the liquid phase has a dielectric constant of about 80, even a relatively small amount of moisture absorption could significantly effect the results. For example, if the insulator consisted of 99.5% polymer with a dielectric constant of 3.0 and 0.5% water with a dielectric constant of 80.0, the measured dielectric constant would be about 3.4. This measured dielectric constant would be 13% greater than the dielectric constant of the polymer alone. This possibility by itself would not seem to explain the differences between the high and low frequency dielectric constants since all of the test structures are on the same wafer.

There are two possible explanations as to why the dielectric constant appears to be lower at high frequencies. First, the effect could be real. That is, the material (or the water or other contaminant) could have some dielectric relaxation between 10 kHz and 1 GHz (notice there are 5 decades of frequency between the low and high frequency measurements). At first glance this does not seem very likely since most dielectric relaxation's do not occur until the frequency reaches 10's of gigahertz. However, the electrical properties of polymers as a function of frequency are not well understood, so this explanation must still be considered as a possibility. In order to find out for certain, the dielectric constant would have to be measured at frequencies between 10 kHz and 1 GHz. Ideally, the T-resonators should be measured down to 10 kHz and the capacitors should be measured up to 1 GHz. Unfortunately, the T-resonators only resonate at discrete frequencies, and the lower the initial resonant frequency the longer the resonator must be. Thus, the T-resonators cannot realistically provide information below about 1 GHz. The capacitors can be measured at higher frequencies, but since the

impedance of a capacitor is defined as $Z_c = 1 / j\omega C$, as the measurement frequency increases the impedance increases and thus the currents involved become harder and harder to measure accurately.

The second possible explanation is that somehow, the contaminant effects only the capacitance measurements and not the resonant measurements. Water might diffuse rapidly in the vertical direction (i.e. from the exposed surface of the polymer down toward the ground plane) but slowly in a lateral direction. Calculations indicate that it takes only a few minutes for water to diffuse vertically through a few microns of dielectric, however it takes many hours for water to diffuse laterally from the edge of a capacitor all the way to its center. Since the T-resonators are only about 25 microns wide, the amount of water present during a measurement depends on the relative humidity of the immediate environment. On the other hand, for a capacitor, the amount of water between the top plate and the ground plane depends on the amount of humidity over the last several hours or days.

The experiment was performed as follows. First, wafers which had been stored at room conditions for a long period of time were measured at both high and low frequencies. Next, the wafers were baked in an oven in the cleanroom for roughly 1 day. The wafers were then remeasured at both high and low frequencies, and the pre and post-bake results were compared. The results are summarized below.

Table 7: Summary of Baking Experiment Results to determine whether baking wafers for a long period of time affected the high-frequency and low-frequency dielectric constant results.

Lot & Wafer	Material	Low Freq. ε_r' drop after baking	Number of comparisons	High Freq. ε_r' drop after baking	Number of comparisons
Lot 5, W1	PI-2545	0.41	2	0.01	20
Lot 6, W1	PI-2555	0.18	3	0.03	20
Lot 6, W3	PI-2555	0.24	5	0.03	32
Lot 7, W1	PI-2566	0.24	10	0.03	26
Lot 8, W1	PI-2611	0.91	4	0.03	28
Lot 8, W3	PI-2611	0.62	5	0.02	28

Results and Discussion

As Table 7 illustrates, the magnitude of change in the dielectric constant was much greater at low frequency than at high frequency. This would seem to support the hypothesis that the current relative humidity effects the high frequency measurements almost immediately while the low frequency measurements react much more slowly to ambient conditions.

Another possible explanation of the differences observed between the high and low frequency values is anisotropy. If the through-plane dielectric constant, $\varepsilon_{r//}$, is significantly different from the in-plane dielectric constant, $\varepsilon_{r\perp}$, then the apparent overall dielectric constant being measured by the capacitors and the T-resonators could appear to be significantly different. This is due to the importance of fringing fields in both structures.

In the capacitors, as previously discussed, the fringing fields play a relatively minor role. So although the apparent dielectric constant is a weighted average of the through-plane dielectric constant and the in-plane

dielectric constant, the weighting is very strongly towards the through-plane value. On the other hand, in the T-resonators, which are long and thin, the weighting would be more even.

In an attempt to determine if anisotropy was having an effect on the results, a set of simulations was run. First, the dielectric material DuPont PI-2611 was assumed to be anisotropic with a through-plane dielectric constant of $\varepsilon_{r//}$=2.85 and an in-plane dielectric constant of $\varepsilon_{r\perp}$=3.60. Next a T-resonator with the following physical dimensions was assumed (these values were based on an actual T-resonator).

dielectric thickness,	$h = 3.6 \ \mu m$
metal thickness,	$t = 3.3 \ \mu m$
microstrip width,	$w = 23 \ \mu m$
resonator length,	$l = 5.00 \ cm$
metal conductivity	$\sigma = 30.6e6 \ S/m$

According to Hoffman[4], microstrip with an anisotropic substrate can be modeled as an equivalent microstrip with an isotropic substrate with the following modifications:

$$h^* = h\sqrt{\frac{\varepsilon_{r\perp}}{\varepsilon_{r//}}} \qquad\qquad (7)$$

$$\varepsilon_r^* = \sqrt{\varepsilon_{r\perp}\varepsilon_{r//}} \qquad\qquad (8)$$

Table 8: Summary of Results when an anisotropic substrate is assumed to be isotropic.

Resonant Frequency Fo (GHz)	Apparent ε_r'
0.724	3.00
2.362	3.04
4.038	3.06
5.742	3.08
7.464	3.08

With all other physical dimensions being the same. For our case described above, we would have $h^* = 4.05$ μm and $\varepsilon_r^* = 3.20$. A simulation was run using the values of h^* and ε_r^* and the resonant frequencies between 0.5 GHz and 9.0 GHz were obtained. Next, it was assumed that these resonant frequencies were measured and the dielectric constant was solved for using only the physical dimensions of the resonator (i.e. the dielectric was assumed to be isotropic). The results are summarized in Table 8.

As Table 8 illustrates, the apparent ε_r' is a weighted average of the through-plane and in-plane dielectric constants. The apparent ε_r' is close to the through-plane dielectric, but higher because of fringing fields. With the capacitor being used to measure the low frequency value, the apparent ε_r' could be expected to be only slightly above 2.85. It should also be noted that this is an extreme case. Most of the materials that were measured are not expected to be as anisotropic as this material.

In conclusion, while anisotropy can cause the high and low frequency values of dielectric constant to appear different, the effect by itself is not great enough to cause the differences being observed.

Conclusions

As a result of the experiment and the simulation study, it seems that water is the most likely cause of the differences seen between the high frequency and the low frequency results. The baking experiment showed that the low frequency results can vary by several percent depending on the environmental history of the capacitor while the T-resonator results seem to depend more on the immediate environmental conditions.

The anisotropy study showed that strong anisotropy could affect the high frequency results, but the change was relatively small, and the materials being examined in these experiments are thought to be nearly isotropic.

Summary of Results by Type of Dielectric

Below are various tables summarizing the results for the dielectrics studied.

Table 9: Summary of Furnace Cure Results for the Various DuPont Polyimides Studied

Polyimide Name	Cure Temp	Metal	Avg ε_r (1-9 GHz)	Avg ε_r (10 kHz)
PI-B	365	Silver	2.74	3.00
PI-B	365	Gold	2.65	2.72
PI-C'	365	Silver	2.79	3.12
PI-C'	365	Gold	2.72	2.92
PI-2545	350	Gold	3.36	3.29
PI-2555	350	Gold	3.14	3.21
PI-2566	350	Gold	2.86	3.21
PI-2566	350	Silver	3.30	3.25
PI-2566		Aluminum	3.31	3.21
PI-2611	350	Gold	3.39	3.34
PI-2611	380	Gold	3.05	3.46

All materials measured under room conditions.

Table 10: Summary of Furnace Cure Results for OCG Probimide 293 (Preimidized Polyimide)

Cure Temp	Cure Time	Metal	Avg ε_r (1-9 GHz)	Avg ε_r (10 kHz)
260	18 min.	Gold	3.17	3.26
360	1 hr.	Gold	3.06	3.04
360	1 hr.	Silver	3.15	3.08

All materials measured under room conditions.

Table 11: Summary of Rapid Cure Results for Dow Cyclotene 3022

Cure Temp	Cure Time	Metal	Avg ε_r (1-9 GHz)	Avg ε_r (10 kHz)
300	6 sec.	Silver	2.85	2.98
260	60 sec.	Silver	2.80	N/A

All materials measured under room conditions.

Table 12: Summary of Results for Ultradel 7501

Cure Method	Cure Temp	Cure Time	Avg ε_r (1-9 GHz)	Avg ε_r (10 kHz)
Hot Plate	375	5 sec.	3.06	3.29
Furnace	360	1 hr.	3.09	3.19

All materials processed with silver metallization and measured under room conditions. (Note that these materials were not processed according to the manufacturer's recommendations)

Table 13: Summary of Materials Processed Only One Way

Dielectric Name	Metal	Cure Temp.	Avg ε_r (1-9 GHz)	Avg ε_r (10 kHz)
EL-5010[*]	Gold	350	3.34	3.47
EL-5512[*]	Gold	350	3.09	3.15
PIQ-L100[á]	Gold	380	3.13	2.88
Ultradel 4208	Gold	350	3.07	3.35

[*] Manufactured by National Starch and Chemical Company
[á] Manufactured by Hitachi

Summary of Moisture Uptake Experiments

Below, the results for further moisture uptake experiments are summarized. In this set of experiments, wafers were first measured after being exposed to room conditions for a long period of time. Then the wafers were soaked in deionized water for 24 hours and the measurements were repeated. Finally, the wafers were baked for 24 hours and measured again.

Table 14: Summary of High Frequency (1 GHz to 9 GHz) Results for Moisture Uptake Experiments

Dielectric Name	ε_r' After Baking	ε_r' After Exposure to Room Conditions	ε_r' After Soaking in DI water
PI-2555	3.00	3.06	3.13
PI-2566	2.79	2.77	2.78
Cyclotene 3022	2.78	2.80	2.79
Probimide 293	3.00	3.01	3.00
Ultradel 7501 (Rapid Cured)	2.94	2.87	2.90
Ultradel 7501	3.09	3.15	3.09

Table 15: Summary of Low Frequency (10 kHz) Results for Moisture Uptake Experiments

Dielectric Name	ε_r' After Baking	ε_r' After Exposure to Room Conditions	ε_r' After Soaking in DI water
PI-2555	3.26	3.25	3.33
PI-2566	3.16	3.22	3.52
Cyclotene 3022	2.94	2.96	3.03
Probimide 293	2.97	3.18	3.52
Ultradel 7501 (Rapid Cured)	3.20	3.40	5.85
Ultradel 7501	N/A	3.24	5.27

SUMMARY AND CONCLUSIONS

What Questions Were and Were Not Answered

This study showed that microstrip T-resonators are useful as an in-situ test structure for measuring the high frequency dielectric constant (but not the loss) of thin film materials. With careful attention to tolerances in the test structures, this method is accurate to a few percent in the frequency range from 1 GHz to 10 GHz.

A number of dielectrics were examined under various curing and environmental conditions, and the conclusions from these experiments are discussed in more detail in below.

One property that was not examined at all in this set of experiments was long term reliability. The results described in this chapter were obtained while the test structures were relatively new and maintained in favorable conditions. Before any of these materials are used in an actual multi-chip module application, the long term reliability of the dielectric-metal combination under realistic conditions should be examined carefully.

Another property that is important to consider before using any of these materials is manufacturability and cost. While some of the materials have been around for a long time, others examined in this paper are either

prototypes or relatively new. No effort has been made to address the cost or manufacturability of any of these materials.

Advantages and Disadvantages of the Various Dieletrics

Of the materials examined, the ones with the lowest average high-frequency dielectric constant were:

1)	DuPont prototype polyimide PI-B		2.73
2)	DuPont prototype polyimide PI-C'		2.77
3)	Dow Cyclotene 3022 (rapidly cured)		2.83
4)	Ultradel 7501		3.07
5)	DuPont PI-2566	3.10	
6)	OCG's Probimide 293	3.15	

(Note that in this list, the averages shown were sometimes calculated by combining results from different lots using the same dielectric.)

As the list shows, the materials have very similar high frequency dielectric constants. The dielectric constant differences alone are not sufficiently conclusive to justify the use of one material over another. Other factors such as dielectric loss, long-term reliability, mechanical properties, ease of manufacturing, and cost are also important to consider before choosing a material for an application.

Rapid Curing

Of the materials that were cured under different conditions, rapid curing did not seem to effect the electrical properties significantly. The dielectric constants did not change more than a few percent between the furnace cure and the rapid cure. While this study did not examine how rapid curing effects long term reliability or mechanical properties of the dielectric, the electrical properties seem quite acceptable. If long term reliability and the mechanical properties prove acceptable for actual applications, the ability to rapid cure a dielectric provides a definite manufacturing advantage.

Advantages and Disadvantages of the Various Metals Used

Gold and silver were both used as conductors for the test structures. Although silver has a higher conductivity than gold, silver will oxidize and corrode while gold will not. Silver migration problems have also been known for many years. During the course of these experiments however, the silver presented no problems due to oxidation and its lower overall loss afforded a definite measurement advantage when measuring the long thin microstrip resonators. When gold and silver test structures were used to measure the same dielectric, no difference in the dielectric properties were observed.

As far as manufacturability, gold was perhaps slightly easier to work with than silver. This is true primarily because gold is used more commonly than silver and so there is a larger knowledge base (at least in the Georgia Tech Microelectronics Research Center) regarding its processing properties and characteristics.

Thus, ignoring any long term reliability issues (which were not considered), the higher conductivity of silver presents some definite advantages over gold when using microstrip T-resonators as an in-situ structure for measuring the dielectric properties of thin films.

Moisture Absorption

If controlling the dielectric constant to within a few percent is important, moisture absorption by the polymers studied can definitely become a problem. As was demonstrated in the baking experiment discussed earlier, a very small amount of water can raise the dielectric constant by tens of percent. The fact that water appears to diffuse at different rates in the vertical and horizontal directions could also cause potential problems.

Anisotropy

While strong anisotropy could have a small effect on the measurement of dielectric constant, it seems unlikely that the effect would be significant for most applications. With the test structures used in this experiment (capacitors and T-resonators), it is not possible to determine whether a

dielectric is anisotropic. Anisotropy could be a possible explanation for small differences observed between the low frequency and high frequency dielectric constant results, but it is not the most likely explanation. The polymers studied in this paper are believed to be nearly isotropic.

Is This High Frequency Method Useful

This high frequency technique utilizing T-resonators is useful for measuring the high frequency dielectric properties of thin films in-situ. The method does have certain drawbacks. First, the accuracy is limited by the uniformity of the structure, the accuracy of the physical measurements, and the accuracy of the microstrip model being used. The resonator must be quite long in order to get results down to the low gigahertz frequency range. The length and small cross-sectional area of the resonating section means that as the frequency increases, the increasing metal loss causes the resonant nulls to become indistinguishable and thus creates an effective upper frequency limit. However, shorter resonators could probably be used to extend the high frequency limit. The large metal loss prohibits accurate determination of the dielectric loss of low loss materials at high frequencies. This, however, is not a major disadvantage if the properties are to be used by circuit designers since in an actual application the metal loss would be the dominant loss factor. Another disadvantage is that a given resonator gives results only at a few discrete frequencies. However, data at intermediate frequencies could be obtained by using a variety of different length resonators.

In its favor, the T-resonator use only a three layer structure which is as easy to manufacture as a parallel plate capacitor. While not as simple as a capacitor to analyze, the T-resonator is not difficult to measure and analyze.

Suggestions for Further Study

While this project answered many questions, it also raised a number of questions. First, it would be very desirable to measure the electrical properties in the frequency range between 10 kHz and 1 GHz. While it seems unlikely that a dielectric relaxation would occur in that frequency range, such

an assumption can not be made with confidence until measurements are made. It would also be preferable to make these measurements using both capacitors and resonant structures. In order to do this, the test structures may need to be redesigned slightly. Smaller capacitors would increase the measurable frequency range, while longer resonators could resonate at frequencies lower than a gigahertz.

A way of determining the absolute accuracy of the method would also be useful. Although the precision of the T-resonator method seemed acceptable, and the high and low frequency results agreed reasonably well, it was not possible to determine the actual accuracy of the T-resonator method. This was because no dielectric material whose thin-film properties are well known in the range from 1 GHz to 10 GHz was measured. In order to get an idea of how accurate the method really is, such a material would have to be measured.

It would also be desirable to try other resonator configurations. A probe station different from the one used would be necessary, but it would be useful to see if other resonator configurations provided better results than a T-resonator. Lightly coupled linear configurations should be tried, and a circular resonator could potentially resonate at lower frequencies than linear resonators, while remaining reasonably compact.

How to measure the loss of thin films at high frequencies is perhaps the most important question which remains to be answered. Fabricating the resonators with high temperature superconductors could be a solution to this problem. Using conventional metals, and reducing the temperature until they act like superconductors is probably not viable because the dielectric properties would probably change with temperature as well, and the mechanical stresses (due to different coefficients of thermal expansion for the silicon substrate, dielectric, and metal) would probably destroy the test structures.

Finally, it would be nice to perform more thorough tests regarding moisture absorption be the dielectrics. The tests mentioned in this paper

indicate that moisture definitely effect the measurements, but it may not be the complete answer.

REFERENCES

[1] D.J. Amey and J.P. Curilla, "Microwave Properties of Ceramic Materials," *41st ECTC Conference*, May, 1991.

[2] D.C. Montgomery, *Design and Analysis of Experiments, Third Edition*, John Wiley & Sons, Inc., New York, 1991.

[3] G.E.P. Box, W.G. Hunter, and J.S. Hunter, *Statistics For Experimenters: An Introduction to Design, Data Analysis, and Model Building*, John Wiley & Sons, Inc., New York, 1978.

[4] R.K. Hoffman, *Handbook of Microwave Integrated Circuits*, Artech House, Inc., Norwood, Massachusetts, 1987.

Chapter 7

Autocatalytic Deposition of Gold in a Nonalkaline Electroless Bath

Background

In the past decade, multi-chip modules (MCMs) have become increasingly important in the electronics industry. MCMs show improvement in size and weight over conventional printed wiring boards. Thin film MCMs allow for greater signal speed and packaging density than single-chip packaging.

MCM technology uses the sequential deposition of thin film metal-insulator layers. A conducting material and an insulator are deposited and patterned to produce these multilayer structures. Four general technologies are used in depositing the conducting metal: physical vapor deposition (PVD), chemical vapor deposition (CVD), electroplating and electroless plating. PVD techniques, including evaporation and sputtering, are blanket deposition methods requiring several processing steps. CVD techniques for deposition of gold films generally use toxic organometallic gold complexes and deposit films with impurities. Conventional electroplating is an inexpensive method for depositing metals, but requires an external current source and a contiguous ground plane of metal. In contrast, electroless plating uses a galvanic deposition reaction making the contiguous ground plane unnecessary. Electroless plating selectively deposits metal onto patterned metal surfaces only, decreasing the expense and waste associated with unselective PVD techniques. Electroless processes are particularly useful when electrically isolated metal islands are formed.

In the microelectronics industry, electroless plating is a common method of depositing metal chemically and selectively. Electroless gold plating baths are used to form electrical gold contacts and to deposit gold into via holes, the vertical connections in multilayered microelectronic structures. Gold is an excellent choice because of its high corrosion resistance, good electrical

and thermal conductivity, low coefficient of thermal expansion, reasonable ductility and high purity.

Electroless gold plating consists of two simultaneous electrochemical reactions occurring on a gold surface. The gold complex, AuL_m^n, reduces to form gold.

$$AuL_m^a + ne^- \rightarrow Au + m\ L^{(a-n)/m} \tag{1}$$

The catalytic oxidation of a reducing agent, R, supplies the necessary electrons for the reduction reaction.

$$R \xrightarrow{\ Au\ } R^{+n} + ne^- \tag{2}$$

The relative potentials of the redox couples are important in determining the rate of the heterogeneous reaction. The redox potential of the reducing agent must be negative of the reduction potential of the gold complex. The gold complex is reduced homogeneously if the redox potential of the reducing agent is too far negative of the gold complex reduction potential. The homogeneous production of gold in solution is an undesirable side reaction. The subsequent autocatalytic deposition of gold on the forming particulates quickly depletes the electroless bath of the reactants.

An essential characteristic of the electroless gold plating bath for this application is that it uses a nonalkaline electrolyte. The dielectric materials in microelectronics must be stable in the bath, thus nonalkaline solutions are highly desirable. Electroless gold plating baths have mostly been limited to operating at pHs above 11 and temperatures above 60°C ([1,2,3,4,5]).

Gold cyanide is the most widely used gold complex in electroless gold plating baths ([1-6]). The electroless reduction of gold cyanide occurs either at high pH or on substrates other than gold ([1-7]). Gold cyanide has a high stability constant of 10^{39} and reduces as follows ([7,8]):

$$Au(CN)_2^- + e \rightarrow Au + 2\ CN^- \tag{3}$$

Chapter 7

Autocatalytic Deposition of Gold in a Nonalkaline Electroless Bath

Background

In the past decade, multi-chip modules (MCMs) have become increasingly important in the electronics industry. MCMs show improvement in size and weight over conventional printed wiring boards. Thin film MCMs allow for greater signal speed and packaging density than single-chip packaging.

MCM technology uses the sequential deposition of thin film metal-insulator layers. A conducting material and an insulator are deposited and patterned to produce these multilayer structures. Four general technologies are used in depositing the conducting metal: physical vapor deposition (PVD), chemical vapor deposition (CVD), electroplating and electroless plating. PVD techniques, including evaporation and sputtering, are blanket deposition methods requiring several processing steps. CVD techniques for deposition of gold films generally use toxic organometallic gold complexes and deposit films with impurities. Conventional electroplating is an inexpensive method for depositing metals, but requires an external current source and a contiguous ground plane of metal. In contrast, electroless plating uses a galvanic deposition reaction making the contiguous ground plane unnecessary. Electroless plating selectively deposits metal onto patterned metal surfaces only, decreasing the expense and waste associated with unselective PVD techniques. Electroless processes are particularly useful when electrically isolated metal islands are formed.

In the microelectronics industry, electroless plating is a common method of depositing metal chemically and selectively. Electroless gold plating baths are used to form electrical gold contacts and to deposit gold into via holes, the vertical connections in multilayered microelectronic structures. Gold is an excellent choice because of its high corrosion resistance, good electrical

and thermal conductivity, low coefficient of thermal expansion, reasonable ductility and high purity.

Electroless gold plating consists of two simultaneous electrochemical reactions occurring on a gold surface. The gold complex, $AuL_m{}^n$, reduces to form gold.

$$AuL_m{}^a + ne^- \longrightarrow Au + m\ L^{(a-n)/m}$$ (1)

The catalytic oxidation of a reducing agent, R, supplies the necessary electrons for the reduction reaction.

$$R \xrightarrow{\ Au\ } R^{+n} + ne^-$$ (2)

The relative potentials of the redox couples are important in determining the rate of the heterogeneous reaction. The redox potential of the reducing agent must be negative of the reduction potential of the gold complex. The gold complex is reduced homogeneously if the redox potential of the reducing agent is too far negative of the gold complex reduction potential. The homogeneous production of gold in solution is an undesirable side reaction. The subsequent autocatalytic deposition of gold on the forming particulates quickly depletes the electroless bath of the reactants.

An essential characteristic of the electroless gold plating bath for this application is that it uses a nonalkaline electrolyte. The dielectric materials in microelectronics must be stable in the bath, thus nonalkaline solutions are highly desirable. Electroless gold plating baths have mostly been limited to operating at pHs above 11 and temperatures above 60°C ([-12345]).

Gold cyanide is the most widely used gold complex in electroless gold plating baths (1-[6]). The electroless reduction of gold cyanide occurs either at high pH or on substrates other than gold (1-7). Gold cyanide has a high stability constant of 10^{39} and reduces as follows ([7],[8]):

$$Au(CN)_2{}^- + e \longrightarrow Au + 2\ CN^-$$ (3)

The standard formal potential of the electroreduction of gold cyanide is -0.61 V vs. NHE (9). The number of reducing agents which oxidize near the gold cyanide reduction potential in nonalkaline solutions is limited.

Alternate gold complexes, such as gold (I) sulfite and gold (III) chloride, have been used in electroless baths only sparingly (1, [9]-[1011], 19). The low stability of these gold complexes often result in premature bath failure with the homogeneous production of gold. Solutions to overcoming this problem, as proposed by past investigators, are rarely explained or understood (10-12, 19). Continued development of noncyanide electroless gold baths is driven by the environmental need for decreased toxicity, as well as the application demands of chemically reducing a gold complex in nonalkaline conditions.

Review of Electroless Gold Plating Baths

The most commonly used electroless gold plating bath, designed by Okinaka, uses potassium borohydride to autocatalytically reduce potassium gold cyanide to gold at pH > 13 (1, 5, 6, 12). Borohydride hydrolyzes to metaborate ions at pHs below 12, decreasing the activity of the bath (5). Okinaka proposed that the hydrolysis intermediate, BH_3OH^-, is the species responsible for reducing gold cyanide to gold (5). Both BH_3OH^- and gold cyanide remained reasonable stable in solution for several days at high pH (1). According to Okinaka, the autocatalytic reaction between BH_3OH^- and gold cyanide deposited gold at 1.5 μm/hr at 70°C with mild agitation (1). Extensive studies have been done to determine the effects of reactant concentrations and solution conditions on the deposition rate and bath stability. The recommended borohydride/gold cyanide electroless bath has excess cyanide and operates at pH < 13 (6).

Borohydride has been used as a reducing agent in other electroless baths at pH > 13 ([12]-[131415]). A recently developed bath used a combination of hydrazine and DMAB as reductants for gold cyanide. Iacovangelo investigated the oxidation of hydrazine and DMAB at high pH and concluded that hydrazine alone did not reduce gold cyanide on gold substrates (2, [16]). No evidence of electroless autocatalytic gold deposition has been reported for the alkaline, hydrazine/gold cyanide electroless bath (2, 3, 17). Gold cyanide is reduced by hydrazine on nickel substrates at pH >6 and

T>90°C (1, [17]). Optimal operating condition for this bath is 80°C and pH=12 (18).

Okinaka and Mathe have listed many reducing agents for electroless gold deposition on metals other than gold (19). Gold cyanide is reduced by hydroxylamine hydrochloride on n-GaAs substrates in a nonalkaline electroless bath (7). Hypophosphite reduces gold cyanide on nickel substrates at pH=7 (1). Mathe tested numerous bath formulations to distinguish between "electroless" deposition of gold on different metal substrates, and autocatalytic deposition of gold on gold substrates ([18]). Electroless gold deposition occurred using the following reducing agents with gold cyanide: hydrazine, dimethylamine borane, hydroxylamine, formaldehyde, hypophosphite, ascorbic acid and cyanoborohydride (1, 19). Many of these reducing agents, hydrazine, formaldehyde, and hypophosphite in particular, are known to electrolessly deposit other metals such as copper, nickel and silver (1, [19-20212223242526]).

Electroless gold plating baths have been formulated using other gold complexes or mixtures of gold complexes with several complexing agents. Gold (III) chloride has a low stability constant and can be autocatalytically reduced only by weak reducing agents, such as ether-substituted tertiary amine boranes, tertiary and secondary amine boranes, at high pH (1). Ascorbic acid has been found to autocatalytically reduced gold (III) chloride to gold at pH=6 and 60°C, in the presence of excess thiosulfate and sulfite ions (11-12). This electroless bath deposits gold onto gold at approximately 2 μm/hr in the first hour and 1.2 μm/hr for the next 3 hours (11). Gold (I) sulfite electroless baths have been developed using hypophosphite, formaldehyde, hydrazine, borohydride and dimethylamine borane as reducing agents (1, 19). The hypophosphite and formaldehyde baths deposit gold onto gold surfaces, the other baths deposit gold onto different metal surfaces (1). These electroless baths require excess sulfite ions and pHs above 9 in order to remain stable (1).

Additives in electroless baths are found to (1) stabilize the bath or prevent particulate growth of metal in solution, (2) inhibit the electroless deposition for improved control of deposition rate and uniformity, (3) accelerate deposition by activating the surface or consuming inhibitors and (4) modify

the deposit properties (19, 22). Excess complexing agents are an example of stabilizing additives. Cyanides, thiosulfates, sulfites, EDTA and fluorides are cited as stabilizers for electroless baths (1, 19, 20, 28). Heterocompounds containing nitrogen and sulfur, such as mercaptobenzothiazole, are used as inhibitors/stabilizers (1, 28). Thallous, palladium and lead salts are commonly added to activate surfaces for electroless deposition of gold or to change deposit characteristics (1, 7, 13, 17, 22, 29). Boric acid and succinic acid have been used as accelerators in copper and gold electroless baths (19, 20). Carbonate and triethanol amine have been added to electroless gold baths to promote the oxidation of the reducing agent, increase deposition rates and improve stability (2, 29, 30). Inhibition of undesirable reductant decomposition has been attributed to the hydroquinone addition in the thiourea electroless gold bath (10). The effect of these additives is seldom understood on a fundamental level and usually characterized as a qualitative change in bulk deposit properties or overall bath performance.

Research Objectives

The objective of this investigation was to design an electroless gold plating bath that autocatalytically deposits gold onto a gold substrate at a pH compatible with polymers, silicon dioxide and photoresist. An electroless bath's performance is contingent upon the reducing agent and gold complex chosen, as well as the bath operating conditions. The reducing agent and gold complex are chosen for the electroless bath based on several criteria. The redox potential of the reducing agent must be more negative than the reduction potential of the gold complex in nonalkaline media. The oxidation of the reductant on the gold surface must be more favorable than on other surfaces, such as polymers or silicon dioxide. Both the reducing agent and the gold complex need to be soluble and stable in solution over the expected lifetime of the bath. Preferably, the reducing agent and the gold complex should have acceptable toxicity, be reasonably inexpensive and available.

The primary objective of this investigation was to develop a nonalkaline electroless gold plating bath. Homogeneous production of gold must be suppressed in this electroless bath and heterogeneous deposition of gold must occur only on exposed gold surfaces. Preferably, gold is deposited at a constant rate greater than 0.5 μm/hr, the electroless bath remains stable and
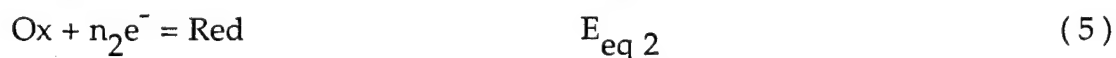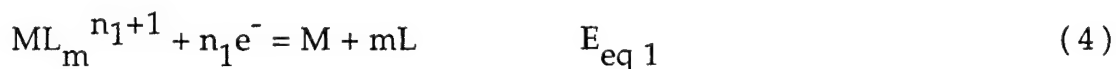
active for at least four hours and the deposit is uniform, conductive and adherent to gold.

Approach

Electroless Theory

Electroless deposition is a chemical redox reaction that produces a metal deposit on a specific substrate. The redox reaction is the reduction of a metal complex by a reducing agent. The oxidation of the reducing agent and the reduction of a metal complex occur without an external current source. The chemical potential difference between the reducing agent and the metal complex drive the reaction forward. The reducing agent is typically adsorbed onto the substrate, which is either a conductive or nonconductive material. Reduction of the metal complex may occur at sites other than reductant adsorption sites, if the substrate is conductive. Electrons donated by the metal complex reduction travel across the conductive substrate from the reduction site to the site of the adsorbed reducing agent. The metal complex is reduced at the adsorbed site of the reducing agent if the substrate is nonconductive.

The oxidation and reduction reactions are:

$$ML_m^{n_1+1} + n_1e^- = M + mL \qquad\qquad E_{eq\ 1} \qquad\qquad\qquad (4)$$

$$Ox + n_2e^- = Red \qquad\qquad E_{eq\ 2} \qquad\qquad\qquad (5)$$

where M is the metal anion, L is the ligand in the metal complex, Red is the reducing agent, Ox is the oxidized form of the reducing agent, n is the number of electrons transferred and E_{eq} is the redox potential. These reactions occur simultaneously and proceed until each reaction establishes an electrochemical equilibrium with its own electrochemical potential. The net reaction between (2-1) and (2-2) is:

$$ML_m^{n+1} + Red = M + mL + Ox \qquad\qquad\qquad (6)$$

The rate of the electroless deposition can be determined if the current-overpotential relationships for the reducing agent and the metal

complex are known. The mixed potential theory is used in conjunction with cyclic voltammetry in predicting electroless bath behavior. Voltammograms of the reducing agent oxidation in the absence of the metal complex and the metal complex reduction in the absence of the reducing agent are obtained in solutions, otherwise similar to the electroless solution.

The catalytic activity of the substrate metal and the depositing metal are key to initiating and continuing the electroless deposition. Reducing agents are chosen based on: (a) the affinity of the dissociating species for chemisorption onto the metal substrate, (b) the subsequent deposit of the metal, and (c) their equilibrium potentials. Controlling the selectivity of the metal reduction necessitates sufficient catalytic activity of the substrate and electroless deposit for the overall oxidation of the reducing agent.

Bath Reactant Selection

The challenge in developing an electroless bath is selecting an appropriate reducing agent and metal complex combination. The choice for the metal complex is dependent upon the choice for the reducing agent, and vice versa. Criteria used for selecting metal complexes and reducing agents include the potential difference between equilibrium potential, the catalytic activity of the metal for the reducing agent oxidation reaction and the exchange current measured at the mixed potential.

Electroless solutions are prepared at different conditions to test and confirm predictions made by applying the mixed potential theory. Electroless bath performance is assessed on the basis of the following criteria: the thickness of the electroless deposit in a given area of the substrate, the bath stability during the experiment, the adhesion of the electroless deposit to the substrate, the uniformity in thickness of the deposit, and the conductivity of a deposit.

The adhesion and uniformity of the deposit are measured qualitatively. A simple assessment of the adhesion and uniformity is sufficient for comparing electroless bath performance. The conductivity of the deposit quantifies the practicality of using a particular electroless bath.

Investigation of Electrochemical Processes

Partial electrochemical reactions of the reducing agents and metal complexes are investigated in the selection process of electroless bath

reactants. Analysis of current voltage responses gives thermodynamic and kinetic information about the electron transfer reaction at the electrode/surface interface and any chemical reactions that occur homogeneously prior to or proceeding after the electron transfer reaction.

Results and Discussion

<u>Selection of a Gold Complex</u>

The development of an electroless gold bath requires selecting a gold complex with adequate chemical stability and modest reduction potential. The electroreduction reactions of gold (I) cyanide and gold (I) thiosulfate were studied on gold electrodes, in order to simulate the partial gold complex reduction to gold in the electroless deposition reaction.

Electroreduction of Gold Cyanide and Gold Thiosulfate

The electrochemical reduction of gold cyanide on a stationary gold electrode was investigated in a citrate buffer (pH=4.7) at 80°C. The reduction voltammograms of 0.05 M gold cyanide, 0.065 M gold cyanide and 0.1 M gold cyanide were obtained with a potential sweep rate of 100 mV/sec. The gold cyanide reduction voltammograms show small anodic currents in the potential range of 0.3 V vs. SCE to 0.0 V vs. SCE, see Fig. 1. The current increased in the cathodic direction as the potential was swept in the negative direction and reached a diffusion controlled peak current near -0.3 V vs. SCE, see Fig. 1. The large potential difference between the onset potential and the peak potential is characteristic of an irreversible reaction. The peak currents and peak potentials are less defined at the lower concentrations, see Fig. 1. The cathodic current decreases as the potential is swept past the peak potential, but the decrease in current does not appear to be proportional to $t^{-1/2}$. The general shape of the reduction voltammogram is not typical of reversible electron transfer reactions.

In contrast, the gold thiosulfate electroreduction was investigated in a citrate buffer solution (pH=6.4) at a rotating gold disk electrode. Gold thiosulfate reduction voltammograms were obtained for different concentrations with a potential sweep rate of 100 mV/sec and an electrode rotation rate of 200 RPM at 25°C. The gold thiosulfate reduction voltammogram occurs in the potential range of 0.15 V vs. SCE to -0.3 V vs. SCE. The reduction voltammogram shows increasing current as the potential is swept in the negative direction, until the current reaches a limiting value, see Fig. 2. The limiting current increases with concentration, see Fig. 2. A plot of the limiting current, at -0.25 V vs. SCE, against gold thiosulfate

121

Fig. 1:   Reduction of Gold (I) Cyanide. Current-Potential Variation with
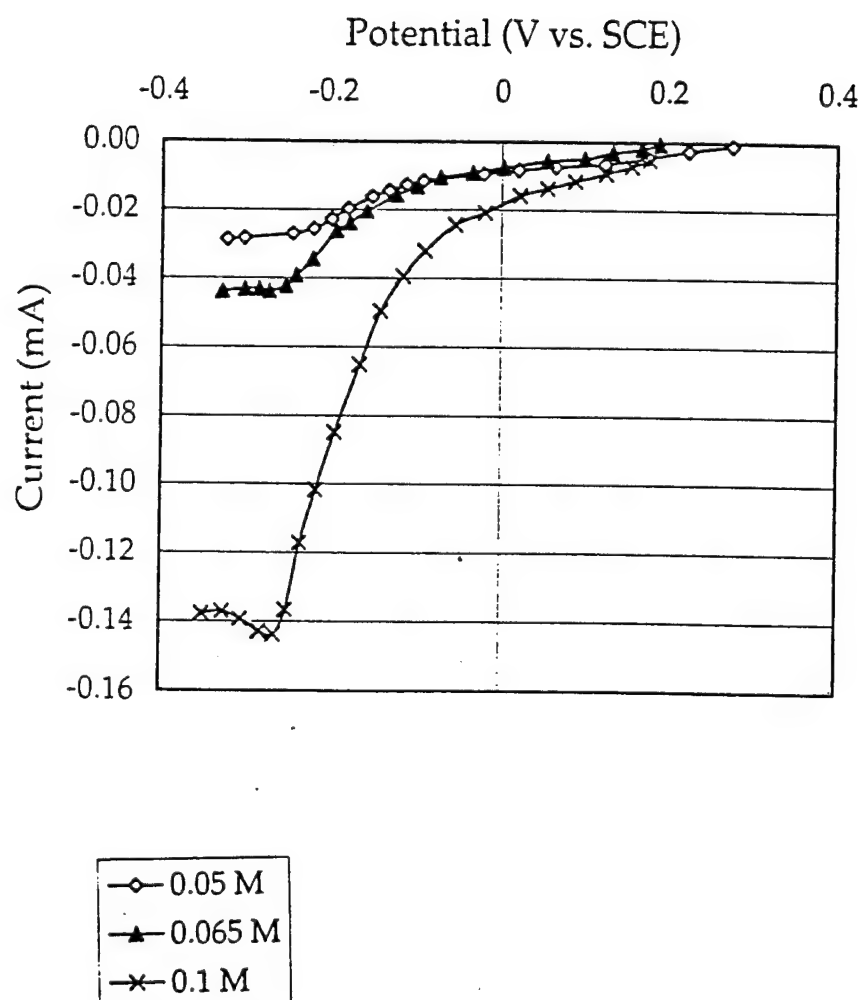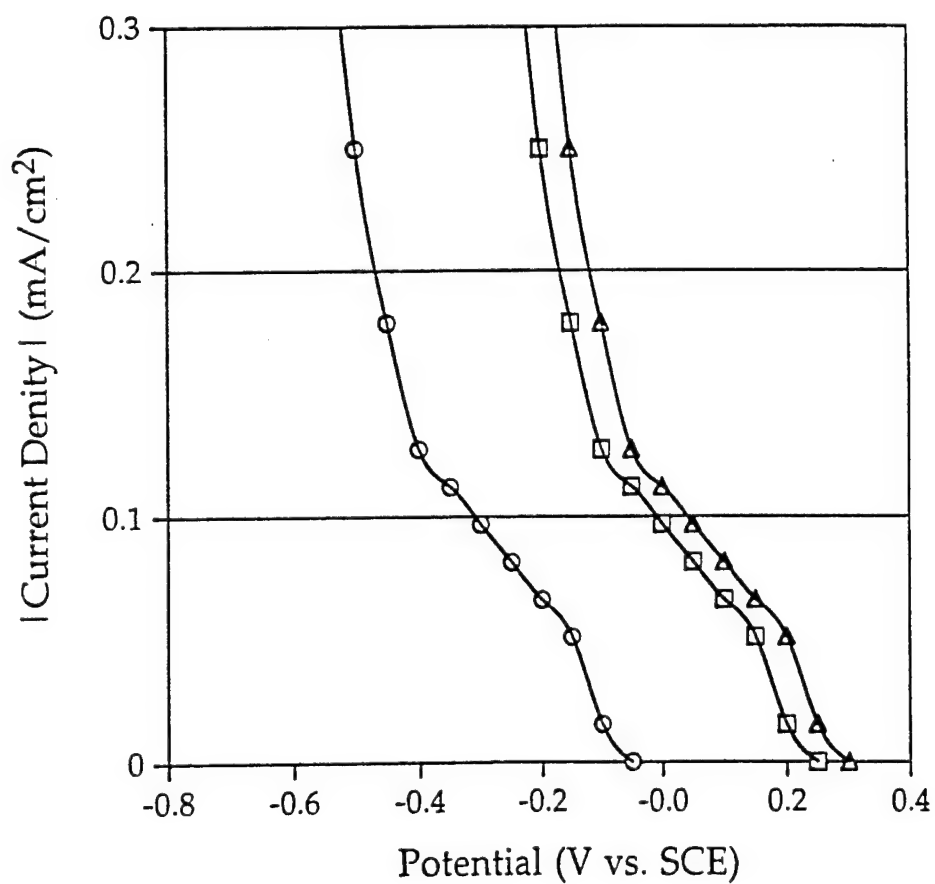Concentration.   100   mV/sec,   0   RPM,   pH=4.7,80°C   on   Gold   Disk.

Fig. 2:   Reduction of 0.1 M Gold (I) Cyanide. Current Density-Potential
Variation with pH and Concentration.   100 mV/sec, 0 RPM, 25°C on Gold
Disk.

Δ	pH=3.2
□	pH=4.7
O	pH=6.4

concentration is linear, see Fig. 3. The increase in current with concentration is observed at a stationary gold electrode, as well. The current potential voltammogram shows a single diffusion limited peak near -0.2 V vs. SCE, see Fig. 4. The peak potential is -0.192 V vs. SCE at a sweep rate of 100 mV/sec and does not change with concentration, see Fig. 4.

Measurement of the peak potential must account for the overpotential due to solution resistance. Excess potassium chloride (1.2 N KCl) was used as the supporting electrolyte in all voltammetric experiments. The solution resistance for 1.2 N KCl, with the reference and working electrodes less than 2 cm apart, was calculated to be 32 Ω. The uncompensated solution resistance of a 1.2 N KCl solution was measured with a EG&G PARC Model 273 potentiostat to be 30 Ω ± 2 Ω. The overpotential due to solution resistance is approximately 8 mV for $|i| \cong 0.25$ mA. Therefore, peak potential measurements are subject to 8 mV (iR_s) variation. The peak potential measured above, for the reduction of gold thiosulfate at 100 mV/sec on a stationary gold electrode is -0.192 ± 0.008 V vs. SCE.

Reduction voltammograms of 0.01 M gold thiosulfate were obtained at different sweep rates on a stationary gold electrode at pH=6.4, 25°C. The peak current increased and the peak potential moved to more negative potentials as the sweep rate increased, see Fig. 5. The currents measured at potentials more negative than the peak potential do not appear to have a $t^{-1/2}$ decrease. The voltammogram does not have the general shape of a reversible electron transfer reaction. A linear relationship between peak currents and $\upsilon^{1/2}$ over a wide range of sweep rates is seen in Fig. 6. The linearity of the correlation between the peak current and $\upsilon^{1/2}$ is characteristic of reversible or irreversible reaction, not quasi-reversible reactions. The absence of an anodic peak on the reverse sweep shows that the electrochemical reduction of gold thiosulfate is chemically irreversible.

Peak currents and peak potentials at different sweep rates were used to calculate a transfer coefficient for the gold thiosulfate reduction reaction. The natural logarithm of the peak current is proportional to the peak potential for irreversible electron transfer reactions (35):

$$\ln i_p = -\alpha nF/(RT)\, E_p + [\ln(0.227\, nFACk^o) + \alpha nF/(RT)\, E^{o\prime}] \qquad (7)$$

Fig. 3:   Reduction of Gold (I) Thiosulfate.   Limiting Current Variation with Concentration.   100 mV/sec, 200 RPM, pH=6.4, 25°C on Gold Disk.
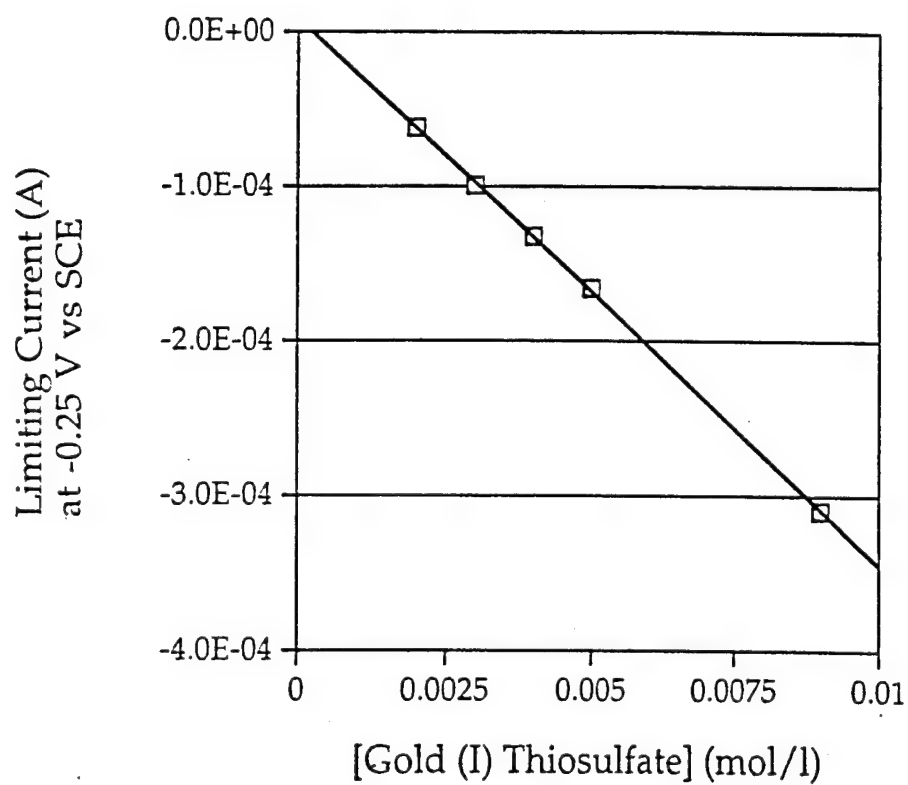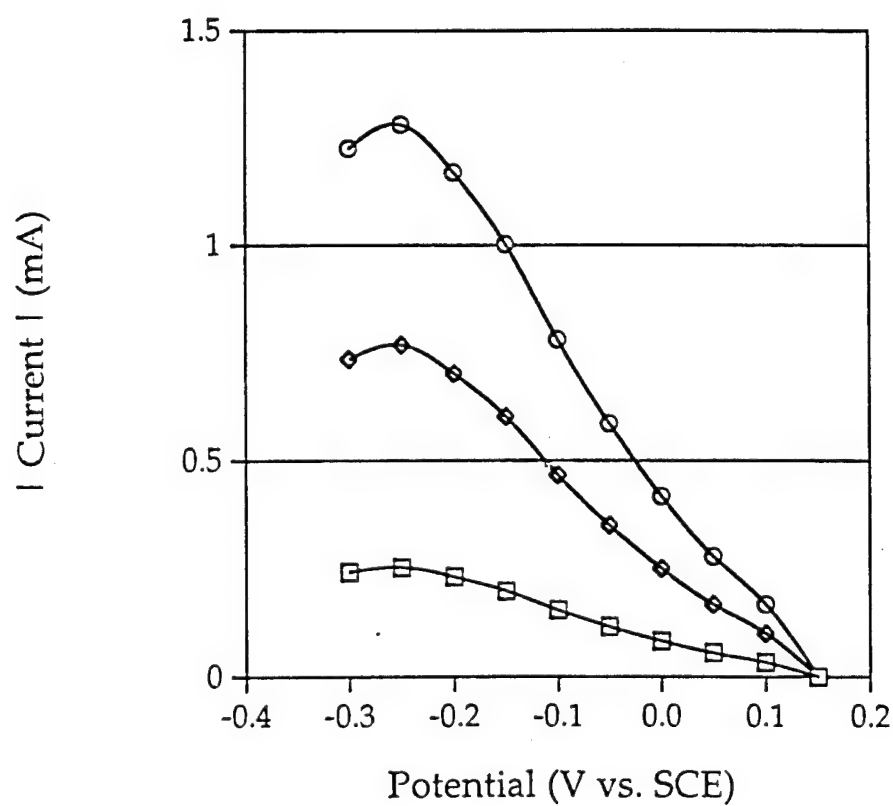

[Gold (I) Thiosulfate] (mol/l)

Fig. 4: Reduction of Gold (I) Thiosulfate. Absolute Value of Current Density-Potential Variation with Concentration. 100 mV/sec, 0 RPM, pH,=6.4, 25°C on Gold Disk.

□   0.01 M Gold (I) Thiosulfate

◇   0.03 M Gold (I) Thiosulfate

○   0.05 M Gold (I) Thiosulfate

Fig. 5:   Reduction of 0.01 M Gold (I) Thiosulfate. Current-Potential Variation with Sweep Rate. 0 RPM, pH=6.4, 25°C on Gold Disk.

Fig. 6: Reduction of 0.01 M Gold (I) Thiosulfate. Peak Current Variation with Square Root of the Potential Sweep Rate. 0 RPM, pH=6.4, 25°C on Gold Disk.

A plot of ln i_p vs E_p has a theoretical slope of $-\alpha nF/RT$ and is shown in Fig. 7. The number of electrons transferred in the gold thiosulfate reduction reaction is assumed to be one (n=1). The calculated transfer coefficient is 0.28 with a standard error of 0.06. No reported transfer coefficients of the gold thiosulfate reduction reaction are available for comparison. A low transfer coefficient signifies that the electrochemical reaction activation complex is more similar to the reactant than the product, in structure. Therefore, the low transfer coefficient of gold thiosulfate suggests that the gold thiosulfate activation complex has a structure more like the bidentate complex than the thiosulfate ion.

The equation describing the irreversible peak current as a function of $D^{1/2}$ and $\upsilon^{1/2}$ was used to calculate a diffusion coefficient of 7.01×10^{-6} cm^2/sec with a standard error of 0.13×10^{-6} cm^2/sec. No reported diffusion coefficients of gold thiosulfate are available for comparison. The calculated gold thiosulfate diffusion coefficient is lower than the estimated diffusion coefficient of thiosulfate, 1.08×10^{-5} cm^2/sec. The size of the hydrated gold thiosulfate complex may be larger than the size of the hydrated thiosulfate ion. Thus, gold thiosulfate may have slower mobility than thiosulfate.

The reduction of 0.01 M gold thiosulfate was investigated on a rotating gold electrode at different rotation rates. Voltammograms were obtained with a potential sweep rate of 100 mV/sec (pH=6.4, 25°C). The variation in the current-potential voltammogram with rotation rate is seen as an increase in limiting current with increasing rotation rate, see Fig. 8. The reduction of gold thiosulfate has an onset potential near 0.15 V vs. SCE. Currents increased to a limiting current near -0.2 V vs. SCE.

Measured currents at different potentials along the gold thiosulfate reduction voltammogram give kinetic information about the electrochemical reduction reaction. Currents were measured at six potentials (-0.35 V, -0.3 V, -0.25 V, -0.2 V, -0.15 V, -0.1 V and -0.05 V vs. SCE) along the current-potential curve. Voltammograms were corrected for background current and digitized. Currents are expected to have errors less than 10 μA and potentials are expected to have errors less than 8 mV (see iR_s discussion above). A linear plot of $1/i$ vs. $1/\omega^{1/2}$ at limiting currents (E $\leq$ -0.2 V vs. SCE) shows the

Fig. 7: Reduction of 0.01 M Gold (I) Thiosulfate. Logarithmic Variation of Peak Current with Potential. 0 RPM, pH=6.4, 25°C on Gold Disk.
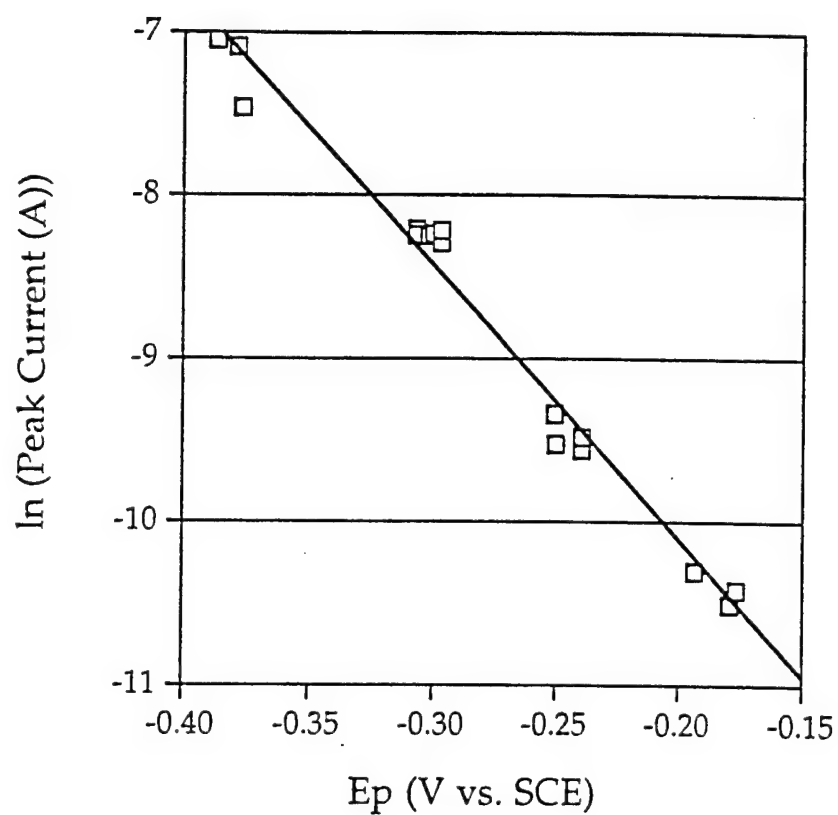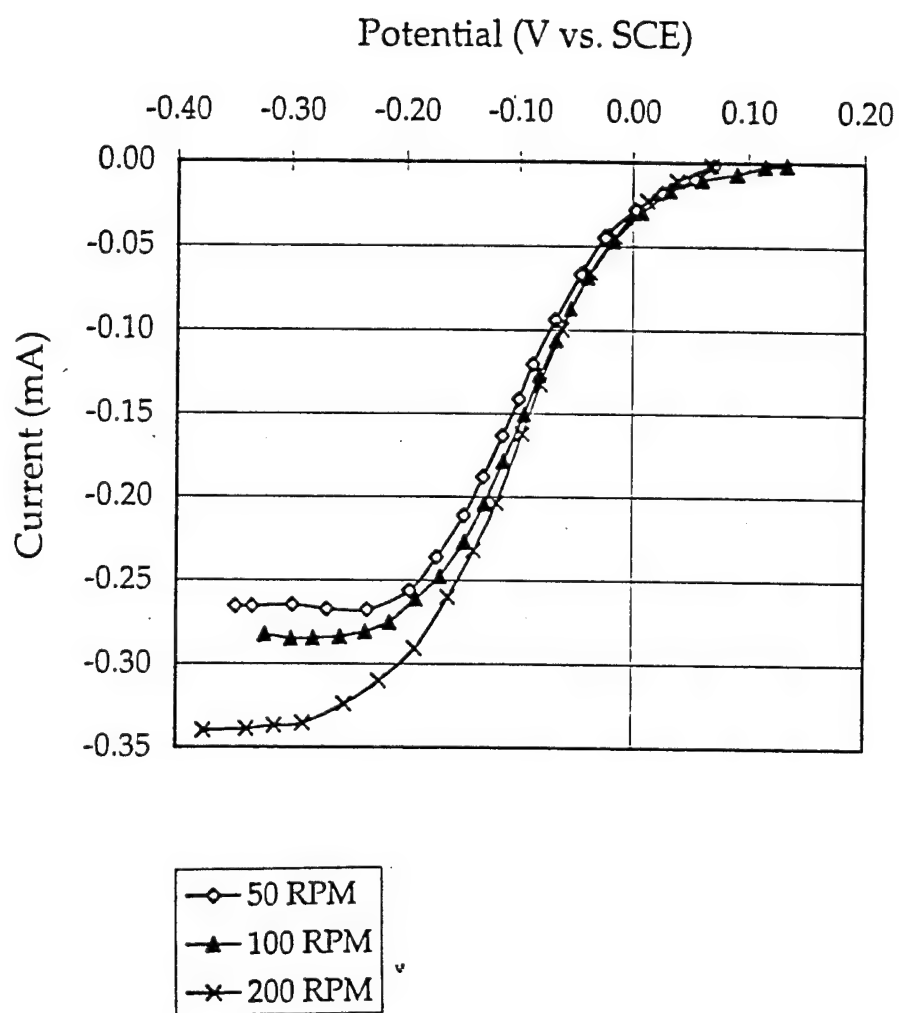
Fig. 8:   Reduction of 0.01 M Gold Thiosulfate.   Current-Potential
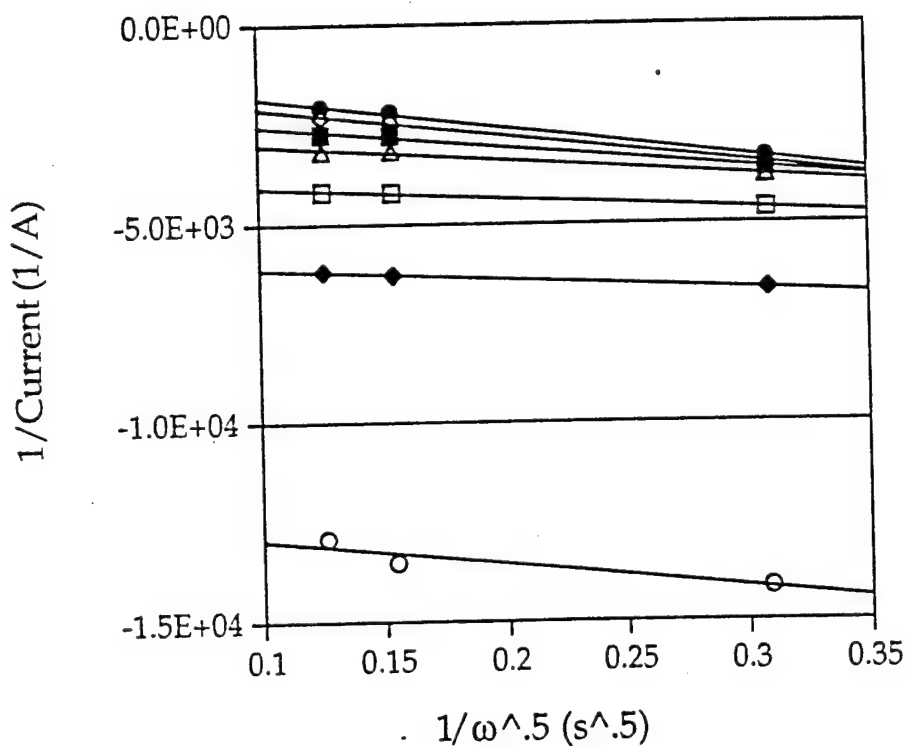Variation with RPM. 100 mV/sec, pH=6.4, 25°C on Gold Disk.

y-intercept does not go through (0,0), see Fig. 9. At very fast rotation rates $(1/\omega^{1/2} \rightarrow 0)$ the inverse current (at $E \leq -0.2$ V vs. SCE) approaches the inverse of the kinetic controlled current, i_k. Therefore, the gold thiosulfate reduction reaction is limited by electrochemical kinetics, as well as mass transfer.

The currents measured at -0.35 V, -0.3 V, -0.25 V, -0.2 V, -0.15 V, -0.1 V and -0.05 V vs. SCE increased with rotation rate, see Fig. 8 and Fig. 9. The value of $1/i$ at $1/\omega^{1/2} = 0$ is measured at different potentials and is equivalent to the inverse current in the absence of mass transfer effects, $1/i_k$. The kinetic current, i_k, is completely, kinetically controlled and is proportional to the heterogeneous electrochemical rate constant, $k_f(E)$, for the reduction. Y-intercepts from Fig. 9 were used to calculate the heterogeneous rate constants at -0.35 V, -0.3 V, -0.25 V, -0.2 V, -0.15 V, -0.1 V and -0.05 V vs. SCE.

Determination of the heterogeneous rate constants requires knowing the standard formal reduction potential for gold thiosulfate. The accuracy of the standard heterogeneous rate constant, calculated for the electroreduction of gold thiosulfate, is limited by the certainty of the gold thiosulfate standard formal potential. For, example, a 100 mV deviation in the gold thiosulfate formal potential changes the calculated heterogeneous standard rate constant by an order of magnitude.

Three standard formal potentials for the gold thiosulfate reduction reaction are available for this investigation. The standard formal potential of gold thiosulfate has been reported by Pouradier and Gadet to be 0.15 V vs. NHE, which is equivalent to -0.09 V vs. SCE (9, [27]). This standard formal potential was experimentally determined by measuring the rest (equilibrium) potential of gold thiosulfate solutions with various thiosulfate concentrations (32). The standard formal potential was calculated by correcting the rest (equilibrium) potential for the gold thiosulfate and thiosulfate concentrations. The problem with this method is that rest potentials fluctuate with small changes in reactant concentrations and electrode surface anomalies. In this particular case, the electroreduction of gold thiosulfate, in a voltammetric experiment, results in a small depletion of gold thiosulfate in solution, a small increase in thiosulfate concentration in solution and deposition of a gold film on the working electrode. The measured rest potentials may depend upon

132

Fig. 9: Reduction of 0.01 M Gold (I) Thiosulfate. Inverse Current Variation with Inverse Rotation Rate. 100 mV/sec, pH=6.4, 25°C on Gold Disk.

●	at -0.35 V vs. SCE	◇	at -0.3 V vs. SCE
■	at -0.25 V vs. SCE	△	at -0.2 V vs. SCE
□	at -0.15 V vs. SCE	◆	at -0.1 V vs. SCE
○	at -0.05 V vs. SCE		

the number of consecutive electroreduction experiments performed with gold thiosulfate.

Another standard formal potential was determined in this investigation. Rest potentials of 0.01 M gold thiosulfate solutions were measured as a function of thiosulfate concentration. The activity coefficients of gold thiosulfate and thiosulfate were assumed to be one. Fifteen standard formal potentials were calculated by correcting the rest potentials for gold thiosulfate and thiosulfate concentrations. The average standard formal potential for the electroreduction of gold thiosulfate is -0.09 V vs. SCE ± 0.005 V vs. SCE (± 2σ). The experimental standard formal potential determined in this investigation agrees well with the experimental standard formal potential reported in literature. Both experimental standard formal potentials are subject to the limitations outlined above.

A third standard formal potential was calculated by using the Nernst equation for the reduction of gold ions to gold and assuming a stability constant for gold thiosulfate. The standard formal potential for the reduction of gold ions to gold is 1.44 V vs. SCE (9). The Nernst equation for the gold (I) ion reduction to gold was corrected for the complexation of gold ions with thiosulfate. The problem with this method is that the standard formal potential is dependent upon the stability constant of gold thiosulfate, which is too large to be known very accurately. The gold thiosulfate stability constant has been reported by many sources, without details on how the stability constant was determined, see Ref. (8), (9) and (11). Possibly, an electrochemical technique was used to measure reduction potential shifts with increasing thiosulfate concentration.

Using the Nernst equation and a gold thiosulfate stability constant of 10^{28}, the standard formal potential for gold thiosulfate is calculated to be -0.22 V vs. SCE. This standard formal potential approximates the reduction potential region observed for gold thiosulfate and is subject to the uncertainty of the stability constant. The calculated standard formal potential approaches the standard formal potential found in this investigation and in Pouradier's investigation, if the stability constant is decreased by an order of magnitude.

The standard heterogeneous rate constant and transfer coefficient for the gold thiosulfate reduction reaction were determined using the reported

standard formal potential and the experimental data shown in Fig. 9. A plot of $\ln k_f$ vs. $(E-E^{O'})$ has an intercept equal to $\ln k^O$, where k^O is the standard heterogeneous rate constant for the gold thiosulfate reduction reaction. The slope of $\ln k_f$ vs. $(E-E^{O'})$ is proportional to the transfer coefficient. The relationship between $\ln k_f$ and $(E-E^{O'})$ is linear. The calculated standard heterogeneous rate constant is 1.58×10^{-3} cm/sec with a standard error of 0.8×10^{-3} cm/sec ($\pm 2\sigma$). The calculated transfer coefficient is 0.23 with a standard error of 0.02. This transfer coefficient agrees well with the transfer coefficient calculated in a previous experiment, 0.28 ± 0.06. The high standard heterogeneous rate constant indicates that gold thiosulfate will be reduced at a high exchange current in electroless baths. The irreversibility of the gold thiosulfate reduction reaction is due to the absence of reduction products when the potential is reversed and swept in the anodic direction.

Evaluation of Possible Gold Thiosulfate Reduction Products

Reduction products of gold thiosulfate were determined using a rotating ring disk electrode (RRDE). Three sulfur compounds, thiosulfate, sulfite and dithionite, were investigated as possible products of the gold thiosulfate reduction reaction. The oxidation voltammograms of these sulfur compounds were obtained at pH=9.2, 25°C, 100 mV/s on different stationary electrodes.

The peak potential differences between sulfite and thiosulfate were less than 50 mV for both gold and platinum electrodes, as seen in Table 1. Detection of gold thiosulfate reduction products requires being able to identify the product by comparing the observed oxidation voltammogram with the oxidation voltammograms of sulfite, thiosulfate and dithionite. As mentioned earlier, the complexity of the dithionite oxidation voltammogram facilitates the identification process, if the product is dithionite. However, sulfite and thiosulfate are more likely to be gold thiosulfate reduction products and are less likely to be identified if a platinum or gold electrode is used.
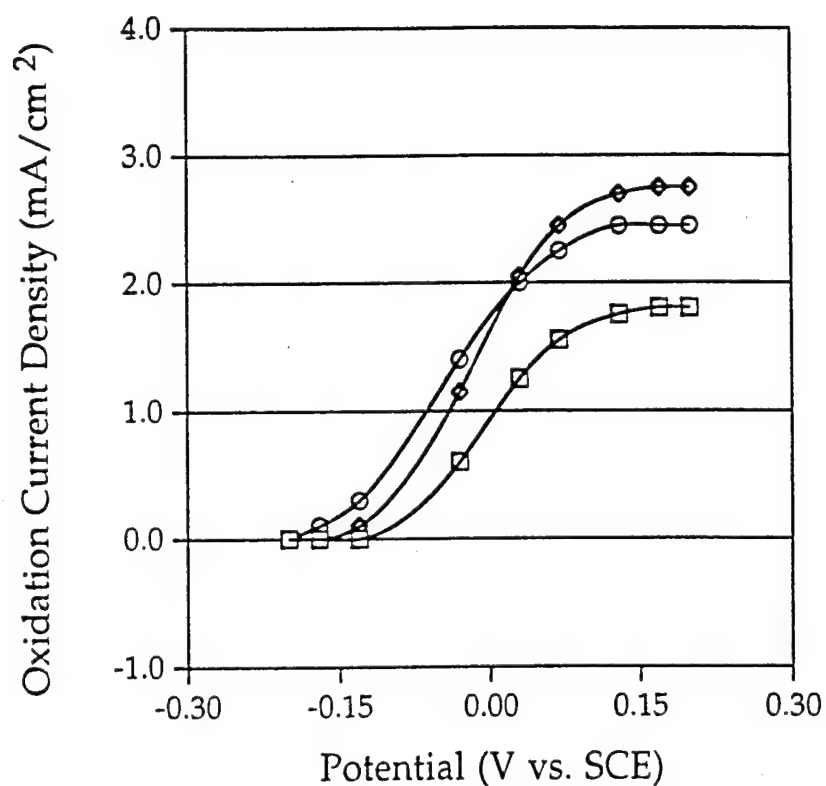
Table 1: Peak Potentials of Oxidation Voltammograms on Different Stationary Electrodes.

Sulfur Compound	Peak Potential on Gold (V vs. SCE) ($\pm 2\sigma$)	Peak Potential on Platinum (V vs. SCE) ($\pm 2\sigma$)	Peak Potential on Mercury (amalgamated gold) (V vs. SCE) ($\pm 2\sigma$)
Sulfite	0.70 ± 0.05	0.72 ± 0.05	0.23 ± 0.05
Thiosulfate	0.75 ± 0.05	0.75 ± 0.05	-0.02 ± 0.05

Using a gold electrode to detect thiosulfate concentration is not significantly more advantageous than using a platinum electrode. This characteristic of platinum and gold electrodes and the similarity between thiosulfate peak potentials on platinum and gold electrodes are interesting to note in lieu of the reported difference in thiosulfate oxidation products. In particular, sulfur is expected to form and passivate the surface as thiosulfate oxidizes on a gold electrode, but this does not occur on a platinum electrode. The passivation of the gold electrode presents a problem only on subsequent potential sweeps, or if the potential is held positive of 0.75 V vs. SCE for any amount of time. The other disadvantage of using a gold electrode is that determination of sulfite concentrations from currents measured on a gold electrode is imprecise. Higher anodic current densities for sulfite are measured on the platinum electrode than on the gold electrode. Therefore, the choice between a gold ring and a platinum ring electrode for detection of gold thiosulfate reduction products is not clear. In addition, the oxidation voltammograms of sulfite and thiosulfate occur within the same potential range on both electrodes. This difficulty in distinguishing between the oxidation voltammograms of sulfite and thiosulfate was overcome by using a gold ring electrode amalgamated with mercury.

The gold thiosulfate reduction product collection experiment was done with a gold disk electrode and an amalgamated gold ring electrode. The RRDE experiment was performed with an electrode rotation rate of 200 RPM in a borate buffer solution (pH=9.2, 25°C). The disk potential was held at open circuit and the potential at the ring electrode was swept in the positive direction with a potential sweep rate of 100 mV/sec. The ring oxidation voltammogram corresponded to the oxidation of gold thiosulfate in the absence of products from the disk, and was used as the baseline current, see Fig. 10. The next oxidation voltammogram at the ring was obtained with the disk potential held at -0.3 V vs. SCE, a potential where gold thiosulfate reduced at the disk, see Fig. 10. Thus, the measured anodic ring current was the sum of the anodic current of the gold thiosulfate oxidation reaction and the anodic current of the oxidation of the disk reduction products. Thiosulfate was identified as the reduction product by matching the

Fig. 10:   Oxidation   of   Gold   Thiosulfate.   Oxidation   Current
Density-Potential Variation with and without Reduction Products.   100
mV/sec, 200 RPM, pH=9.2, 25°C on Amalgamated Gold Ring.

□   Rotating Gold Disk
        at Open Circuit
        (0.01 M Gold Thiosulfate)

◇   Rotating Gold Disk
        at -0.3 V vs. SCE
        (0.01 M Gold Thiosulfate)

○   Rotating Gold Disk
        at Open Circuit
        (0.01 M Thiosulfate)

reduction product oxidation voltammogram to the oxidation of thiosulfate at the same conditions, see Fig. 10. The number of moles of thiosulfate produced for every mole of gold thiosulfate reduced was calculated using the experimental collection efficiency and the concentration-limiting current correlation for the oxidation of thiosulfate on the amalgamated gold electrode. The calculated number of thiosulfate ions produced per gold thiosulfate ion reduced is 1.92 stoichiometric reduction of gold thiosulfate to gold and thiosulfate.

Comparison of Gold Thiosulfate and Gold Cyanide

The reduction voltammograms of gold thiosulfate were studied in order to determine if gold thiosulfate would be a suitable alternate gold complex for use in electroless gold plating baths. Comparison of reduction voltammograms between gold thiosulfate and gold cyanide were used to qualitatively determine the advantages of using gold thiosulfate instead of gold cyanide. The reduction voltammograms of 0.01 M gold thiosulfate and 0.01 M gold cyanide are compared in Fig. 12. The reduction voltammograms were obtained on a stationary gold electrode in a citrate buffer (pH=6.4, 25°C) with a potential sweep rate of 100 mV/sec. The electroreduction of gold thiosulfate occurs at potentials more positive than the electroreduction of gold cyanide see Fig. 12. Since thiosulfate does not protonate at pHs above 4, the gold thiosulfate reduction voltammogram does not shift in potential if the pH is decreased to 4 or increased to 14, see earlier results. However, the cyanide ions in the gold cyanide solution protonate at pHs below 7.5. Earlier results have shown that an increase in pH shifts the gold cyanide reduction potential to more negative potentials. Thus, the potential difference between the gold thiosulfate reduction voltammogram and the gold cyanide reduction voltammogram increases as pH increases. A decrease in the pH of a gold cyanide solution may shift the reduction potential to more positive potentials, but hydrocyanic gas may be released. Therefore, the comparison of voltammograms at practical pHs concludes that gold thiosulfate is easier to reduce than gold cyanide.

The peak currents and the slopes of the current-potential curves are indicative of the rate of the gold complex reduction reaction. The gold thiosulfate reduction voltammogram has a much larger peak current than the

Fig. 11: Reduction of Gold Complexes. Absolute Value of Reduction Current-Potential Comparison Between 0.01 M Gold Thiosulfate and 0.01 M Gold Cyanide. 100 mV/sec, 0 RPM, pH=6.4, 25°C on Gold Disk.

□   Gold (I) Thiosulfate

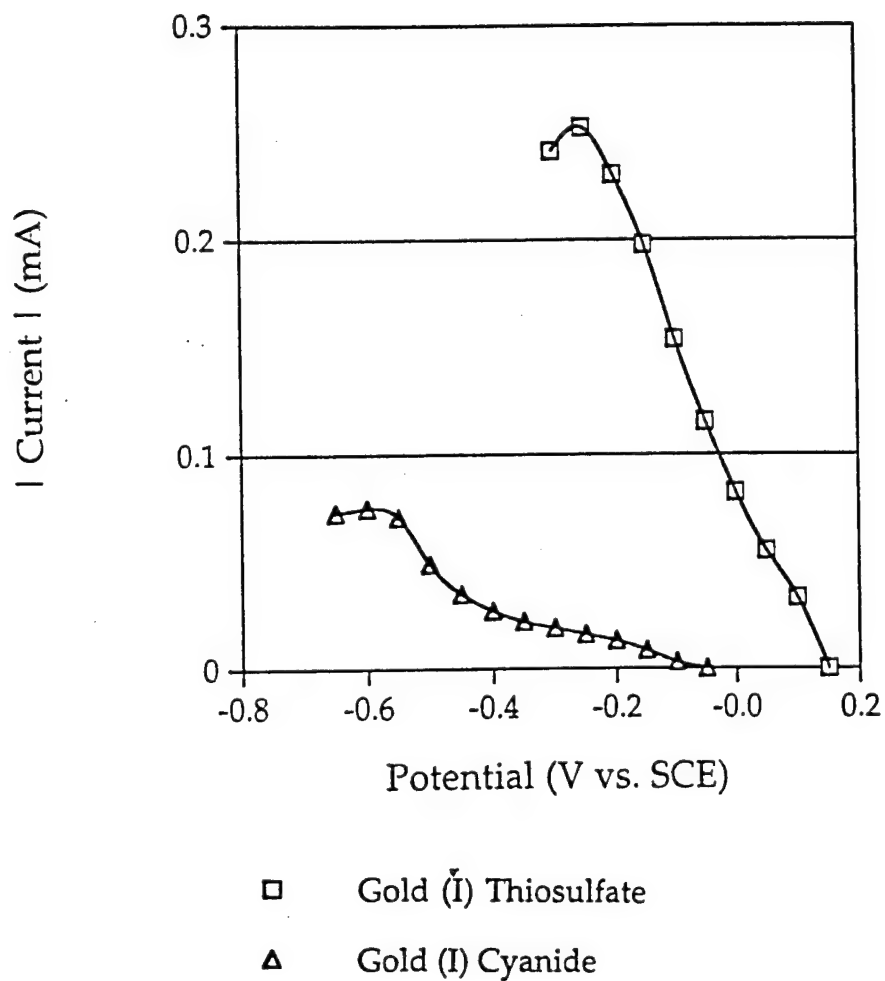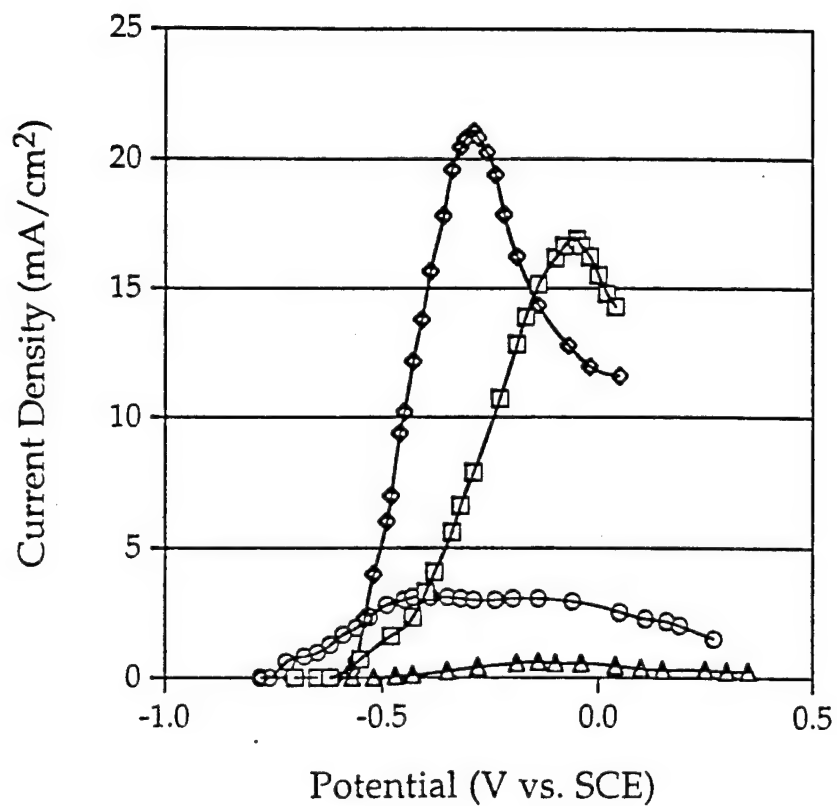△   Gold (I) Cyanide

Fig. 12: Oxidation of 0.01 M Borohydride. Current Density-Potential Variation with pH. 100 mV/sec, 0 RPM, 25°C on Gold Disk.

□   pH=11   ◇   pH=13

○   pH=9.2   △   pH = 7.2

gold cyanide reduction voltammogram. The gold cyanide reduction reaction may be more kinetically limited than the gold thiosulfate reduction reaction. The slope of the current-potential curve for the gold thiosulfate reduction voltammogram is much higher than the slope of the gold cyanide current-potential curve. The exchange current is qualitatively higher for the gold thiosulfate reduction reaction than for the gold cyanide reduction reaction. The higher exchange current for the gold thiosulfate reduction reaction indicates that the electroless deposition of gold is faster if gold thiosulfate is used in the electroless bath. Disproportionation of gold thiosulfate was not observed in gold thiosulfate solutions which were left undisturbed for three days (pH=6.4, 25°C). Reduction voltammograms of the aged solution are identical to reduction voltammograms obtained within five minutes of solution preparation (pH=6.4, 25°C). The solubility and stability of gold thiosulfate were sufficient for an electroless bath gold complex. For all the above reasons, gold thiosulfate was chosen as the gold complex in this investigation.

Selection of Reducing Agent

Reducing agents used in electroless plating applications are selected based on two major criteria. The first criterion is that the redox potential for the oxidation reaction of the reductant must be more negative than the reduction potential for the reduction reaction of the chosen metal complex. A significant potential difference between the reductant and the metal complex is required to drive the metal deposition reaction. This selective chemical reaction is limited to a surface, typically by the reductant oxidation reaction. Thus, the second criterion is that the oxidation of the reductant must be kinetically limited on the metal surface. Other preferred characteristics of the electroless reductant include nontoxicity, solubility, and a high standard heterogeneous electrochemical oxidation rate.

Certain reducing agents have been studied as electroless bath reactants at different bath conditions, by many investigators. Borohydride, hydrazine, hydroxylamine and hypophosphite are the common reductants used in electroless plating of gold, nickel and silver (1-7, 12-18). Lactones, organic heterocyclic molecules with an ene-diol group, have been used in silver electroless plating applications (25). Reducing agents known to be weak and
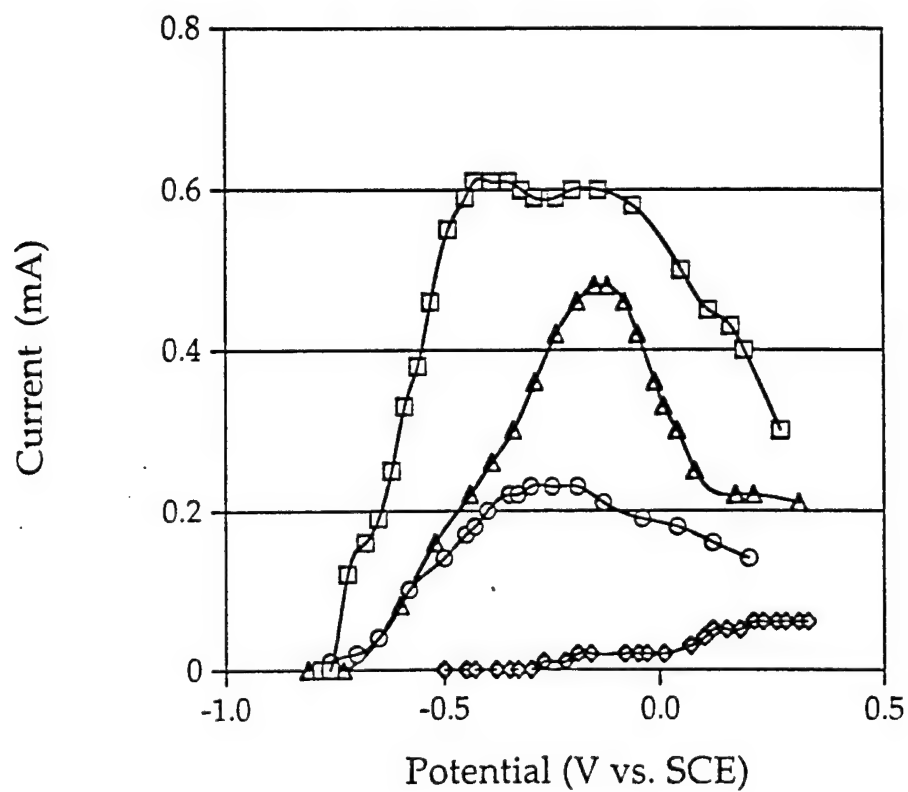
limited in application, dimethlyamine borane and formaldehyde in particular, were eliminated from the list of possible reducing agents. The reducing agents considered as possible gold electroless bath reactants were: borohydride, hydrazine, hydroxylamine, hypophosphite and ascorbic acid. The partial anodic reactions of each of these reductants was studied on a gold electrode at various solution conditions.

Borohydride

The oxidation of borohydride was studied at different pHs on a stationary gold electrode at 25°C. The oxidation voltammograms of 0.01 M borohydride in a strong hydroxide solution (pH=13), sodium hydroxide solution (pH=11), borate buffer solution (pH=9.2), and an ammonium hydroxide/ammonium chloride buffer solution (pH=7.2), with a 100 mV/s potential sweep rate are shown in Fig. 12. Oxidation voltammograms were obtained approximately three minutes after the borohydride dissolution and corrected for background current. Borohydride had the opportunity to hydrolyze during the three minutes prior to the onset of the voltammetric experiment. As expected, the magnitude of the anodic peaks decreased with pH. The lower the pH, the faster the hydrolysis reactions were expected to proceed. The decrease in peak currents with pH is characteristic of a decrease in the electroactive species concentration. The low anodic current densities observed at pH=7.2 suggest that the electroactive species had been consumed in the first three minutes. The anodic current densities measured at pH=9.2 are higher, but show more complicated anodic behavior. The second wave, near -0.01 V vs. SCE, may be the oxidation of the hydrolysis intermediate to metaborate. The production and accumulation of the hydrolysis intermediate occurs in solution as the hydrolysis reaction proceeds. The presence of the hydrolysis intermediate explains the appearance of the second wave.

The increasing concentration of the hydrolysis intermediate with time was studied by observing intermittent voltammograms of the borohydride electro-oxidation in a borate buffer solution (pH=9.2, 25°C) with time, see Fig. 13. The oxidation voltammograms were obtained on a stationary gold disk electrode at a potential sweep rate of 100 mV/sec and corrected for background current. The first oxidation voltammogram (at 3 minutes) shows

Fig. 13 :   Oxidation of 0.01 M Borohydride.   Current-Potential Variation
with Time.   100 mV/sec, 0 RPM, pH=9.2, 25°C on Gold Disk.

the two anodic waves, similar to the two anodic waves seen in the previous experiment (at a different sweep rate), see Fig. 13. The second oxidation voltammogram (at 12 minutes) shows one primary wave with a trace of a preceding anodic wave, see Fig. 13. The loss of the borohydride in the hydrolysis reaction and the production of an electroactive hydrolysis intermediate may explain the decrease in magnitude of the first wave and presence of a larger second anodic wave. The oxidation voltammogram taken approximately ten minutes after the second voltammogram shows a decrease in the anodic current over all potentials, see Fig. 13. The partial hydrolysis of the borohydride hydrolysis intermediate to the electroinactive metaboric acid may explain the anodic current values at 25 minutes. An oxidation voltammogram taken 75 minutes after the borohydride dissolution shows insignificant anodic behavior. This characteristic of borohydride voltammograms supports the idea that borohydride hydrolyzes to an electroinactive species and is ineffective as a reducing agent if the pH is lower than 10.

Ascorbic Acid

The electrochemical oxidation of ascorbic acid was investigated in a citrate buffer (pH=6.4) on a rotating gold electrode at 25°C. Oxidation voltammograms were obtained at a rotation rate of 200 RPM and a potential sweep rate of 100 mV/sec within three minutes after ascorbic acid dissolution. Oxidation voltammograms were corrected for background current. The anodic current of the ascorbic acid oxidation voltammograms increases with increasing concentration, see Fig. 14. The onset potential of ascorbic acid was near -0.15 V vs. SCE, see Fig. 14. The anodic current appears as a single wave approaching a limiting value at potentials beyond 0.4 V vs. SCE, see Fig. 14. The limiting current varies linearly with concentration with a correlation coefficient of 0.997, see Fig. 15. As explained before, the current is directly proportional to concentration for reversible, irreversible and quasi-reversible reactions. Published literature claimed that the ascorbic acid oxidation is a C_rE_r mechanism with the electron transfer reaction proceeding the dissociation of the fully protonated ascorbic acid to monoprotonated ascorbic acid:

$$H_2A = HA^- + H^+ \tag{8}$$

Fig. 14:   Oxidation of Ascorbic Acid. Current-Potential Variation with Concentration. 100 mV/sec, 200 RPM, pH=6.4, 25°C on Gold Disk.
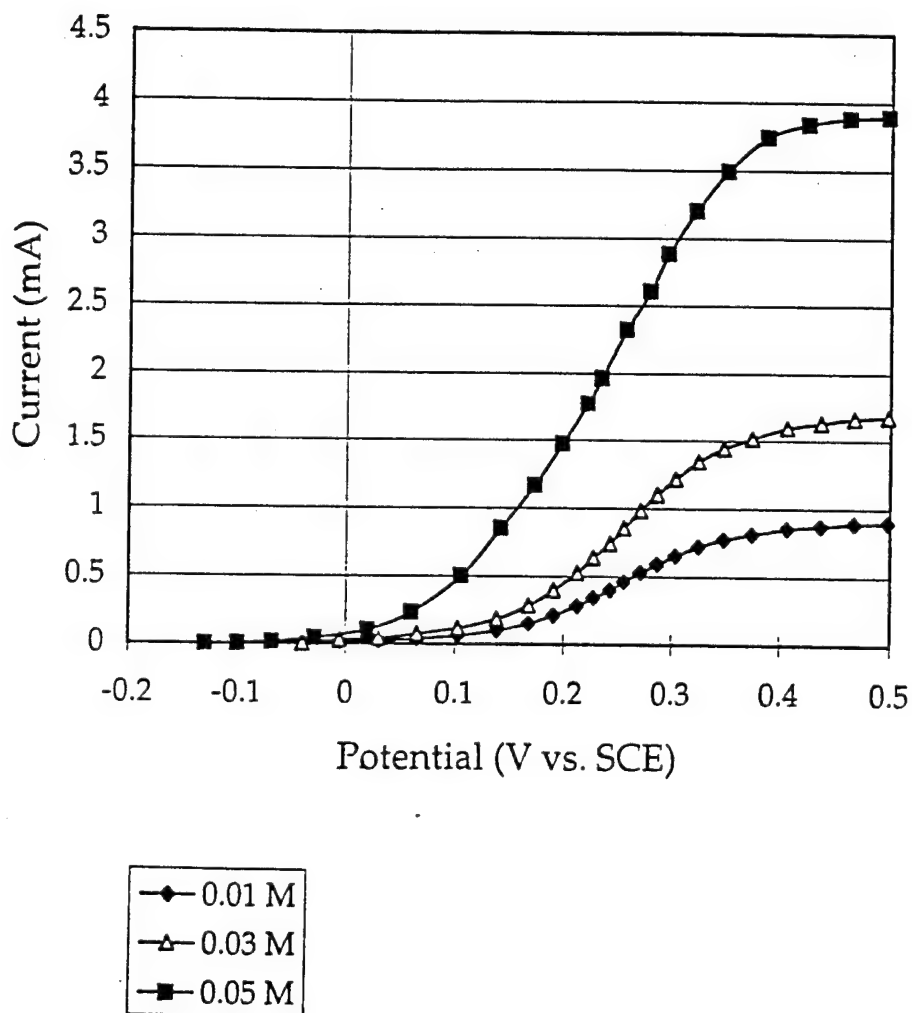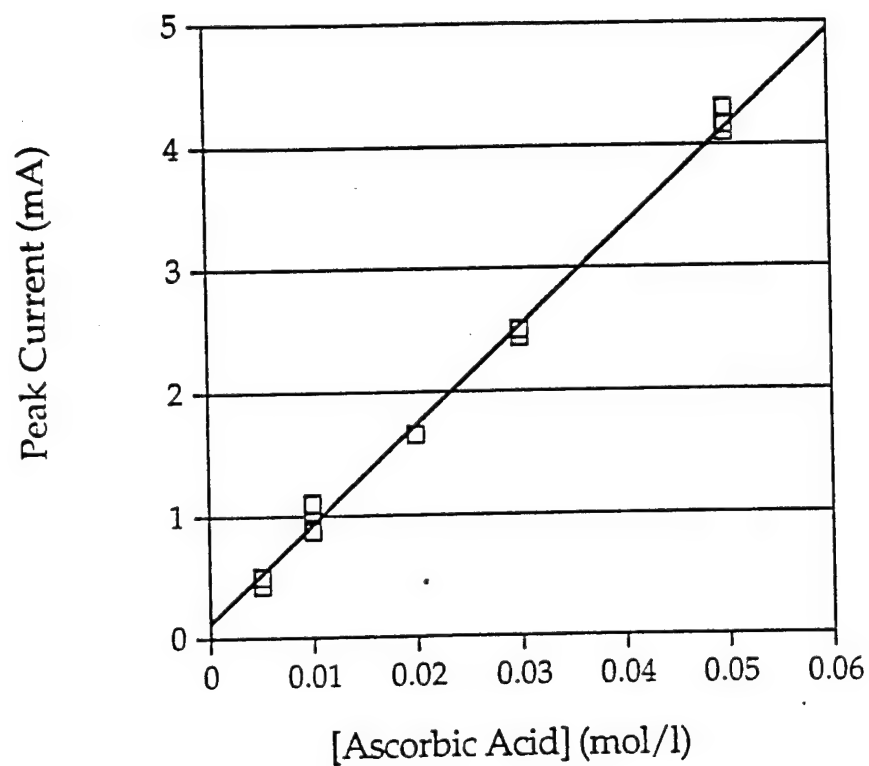
Fig. 15:   Oxidation of Ascorbic Acid.   Peak Current Variation with Concentration.   100 mV/sec, 200 RPM, pH=6.4, 25°C on Gold Disk.

$HA^- = DA + H^+ + 2e$ (9)

The limiting current of the electron transfer reaction in the C_rE_r mechanism becomes directly proportional to $\omega^{1/2}$ at small rotation rates, where ω is the electrode rotation rate in sec^{-1}. The limiting current approaches mass transfer controlled limiting values at small rotation rates and can be evaluated using the Levich equation.

The ascorbic acid oxidation reaction was investigated in a citrate buffer (pH=6.4) on a rotating gold disk electrode. Oxidation voltammograms were obtained at a potential sweep rate of 100 mV/sec at 25°C and corrected for background current. An increase in rotation rate increased the limiting current significantly, see Fig. 16. The limiting current for the ascorbic acid oxidation varies linearly with the square root of the rotation rate in the 200 RPM to 600 RPM range, see Fig. 17. The linear relationship has a slope of 0.877 (mA s$^{.5}$) with a standard error of 0.010 and a correlation coefficient of 0.999. Linear variation in limiting current with the square root of the rotation rate is characteristic of systems obeying the Levich equation. The linearity of the limiting current with $\omega^{1/2}$ at these low rotation rates supports the proposed C_rE_r mechanism. The Levich equation, a valid equation for limiting currents at low rotation rates, was used to calculate an experimental diffusion coefficient of 6.46×10^{-6} cm^2/s with a standard error of 1.1×10^{-7} cm^2/s. The diffusion coefficient found in this investigation is within 2% difference of the experimental diffusion coefficient reported in past investigations (6.34×10^{-6} cm^2/sec). The experimental diffusion coefficient, 6.46×10^{-6} cm^2/sec, is statistically the same number as the reported diffusion coefficient, taking into account the standard error. Diffusion coefficients of electroactive species in aqueous solutions are generally higher, in the range of 1 to 2×10^{-5} cm^2/sec. The low diffusion coefficient of ascorbic acid may be due to its bulky structure and subsequent lower mobility.

Other Reducing Agents

Hydrazine, hydroxylamine and hypophosphite were also considered as possible reducing agents for gold thiosulfate. The reducing agent selected for this investigation was chosen based on the mixed potential analysis and electroless bath performance It was found that gold cyanide is not heterogeneously reduced by the following reducing agents: ascorbic acid,

Fig. 16:   Oxidation of 0.05 M Ascorbic Acid. Current-Potential Variation with RPM. 100 mV/sec, pH=6.4, 25°C on Gold Disk.
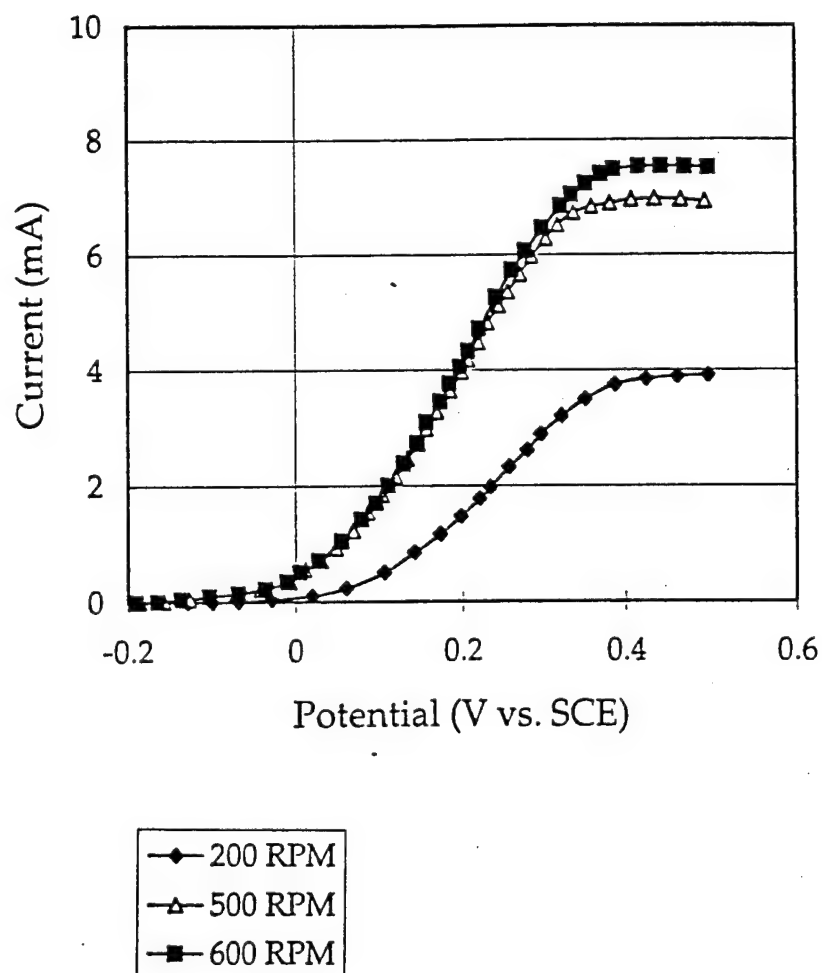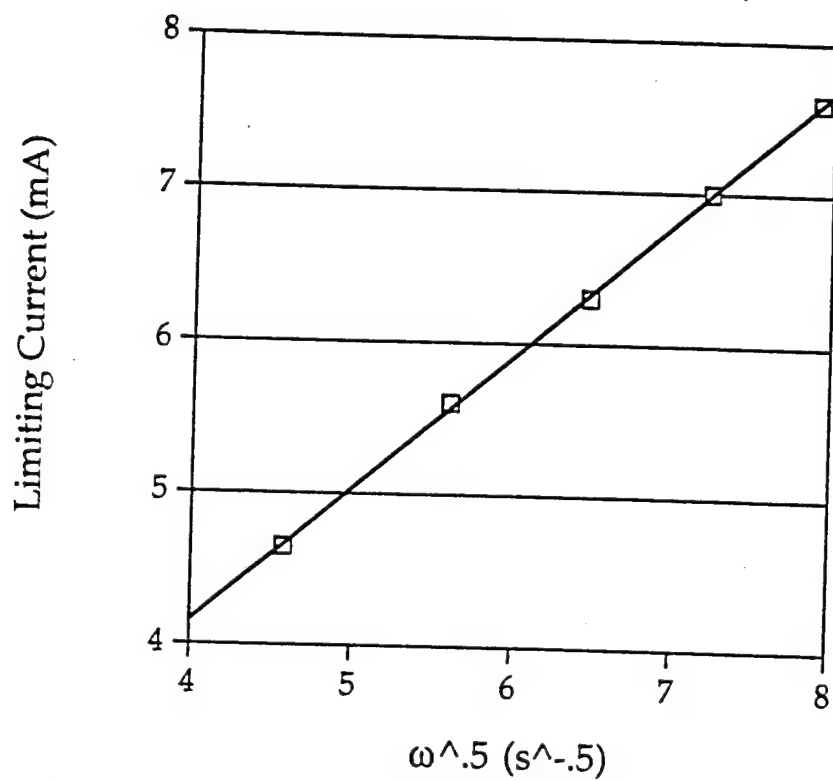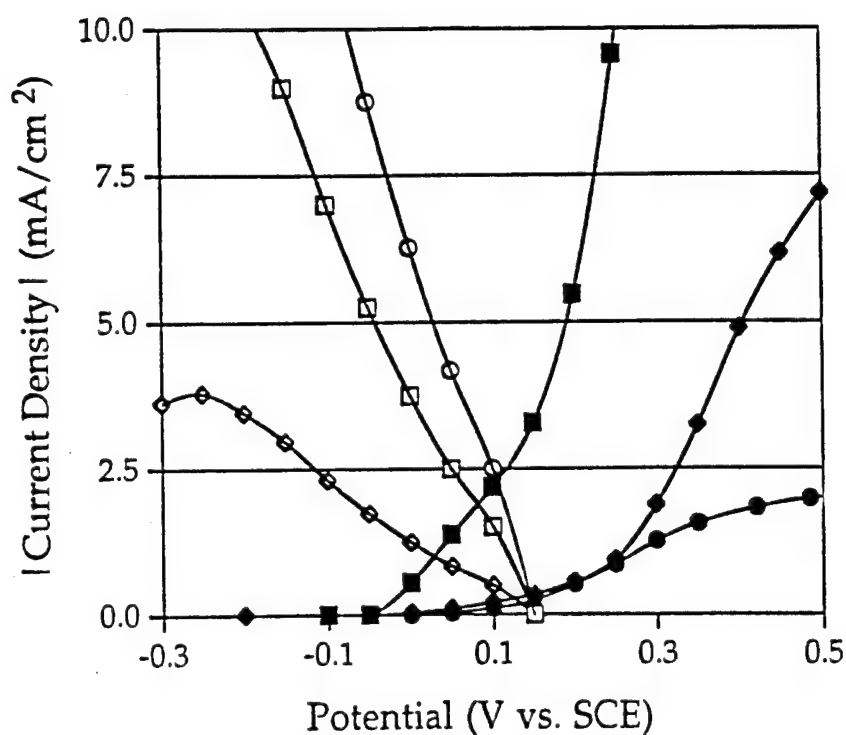
Fig. 17: Oxidation of 0.05 M Ascorbic Acid. Limiting Current Variation with Square Root of Rotation Rate. 100 mV/sec, pH=6.4, 25°C on Gold Disk.

hydrazine, hydroxylamine and hypophosphite. It was found that gold thiosulfate is homogeneously reduced by borohydride.
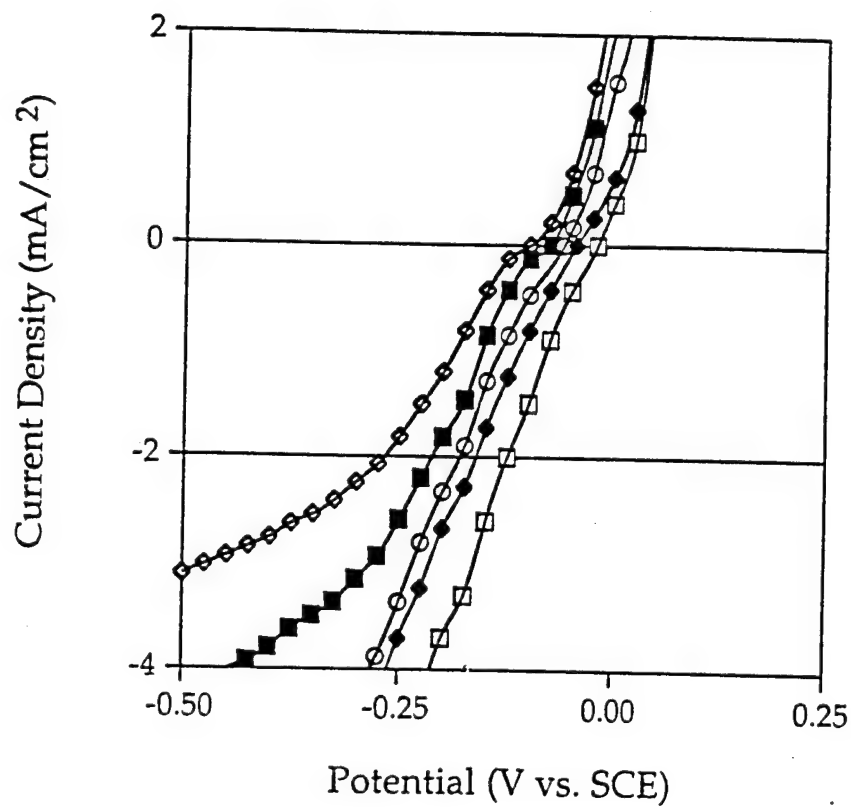
Thus, electroless deposition rates were predicted using the mixed potential theory for the following electroless bath combinations: gold thiosulfate with 0.05 M ascorbic acid, gold thiosulfate with 0.05 M hydrazine and gold thiosulfate with 0.05 M hydroxylamine. Voltammograms obtained at a potential sweep rate of 100 mV/sec on a gold electrode in a citrate buffer solution (pH=6.4) at 30°C were compared in order to determine predicted deposition rates and electroless bath mixed potentials, see Fig. 18. The absolute value of the gold thiosulfate reduction voltammogram at three different concentrations is plotted in Fig. 18. The oxidation voltammograms of the three reducing agents at 0.05 M concentration are superimposed onto Fig. 19. Predicted mixed potentials and deposition rates are listed in Table 2. The predicted deposition rates were higher for baths using ascorbic acid as the reducing agent than for any bath with hydrazine or hydroxylamine as the reducing agent. Hydroxylamine and hydrazine baths were predicted to have similar deposition rates and mixed potentials. The predicted deposition rates increased in the ascorbic acid electroless bath, hydrazine electroless bath and hydroxylamine electroless bath, as the concentration of gold thiosulfate increased. The predicted mixed potential shifted in the negative direction as the gold thiosulfate concentration increased.

Fig. 18:   Mixed   Potential   Diagram.   Current   Density-Potential
Comparison for Different Reducing Agents and Different Gold Thiosulfate
Concentrations. 100 mV/sec, 0 RPM, pH=6.4, 30°C on Gold Disk.

□   0.03 M Gold (I) Thiosulfate

◇   0.01 M Gold (I) Thiosulfate

○   0.05 M Gold (I) Thiosulfate

■   0.05 M Ascorbic Acid

◆   0.05 M Hydrazine

●   0.05 M Hydroxylamine

Fig. 19: Voltammograms of the 0.05 M Ascorbic Acid/0.03 M Gold Thiosulfate Electroless Bath. 100 mV/sec, 0 RPM, pH=6.4, 30°C on Gold Disk.

□   T = 0

◆   T = 30 minutes

○   T = 60 minutes

■   T = 90 minutes

◇   T = 120 minutes

Table 2: Predicted and Actual Electroless Deposition Rates for Different Concentrations of Gold Thiosulfate with 0.05 M Concentration of Ascorbic Acid, Hydrazine or Hydroxylamine in a Citrate Buffer (pH=6.4) and 30°C.

Reductant	[Gold Thiosulfate]	Predicted Deposition Rates	Predicted Mixed Potentials	Actual Deposition Rates
	(mol/l)	μm/hr $\pm 0.03\,\mu$m/hr ($\pm 2\sigma$)	V vs. SCE	μm/hr $\pm 0.03\,\mu$m/hr ($\pm 2\sigma$)
Ascorbic Acid	0.05	1.37	0.11	1.26
Ascorbic Acid	0.03	1.13	0.08	0.89
Ascorbic Acid	0.01	0.59	0.07	0.69
Hydrazine	0.05	0.19	0.12	0.19
Hydrazine	0.03	0.18	0.11	
Hydrazine	0.01	0.15	0.06	
Hydroxyl-amine	0.05	0.13	0.14	0.14
Hydroxyl-amine	0.03	0.12	0.13	
Hydroxyl-amine	0.01	0.11	0.11	

Electroless baths were performed in order to confirm the mixed potential analysis. The electroless baths used a citrate buffer solution (pH=6.4), operated at 30°C with equimolar reactant concentrations of 0.05 M gold thiosulfate and 0.05 M reducing agent. Deposition rates were averaged over the first thirty minutes and measured with a profilometer, see Table 2.

Actual deposition rates for the three electroless baths are compared to the predicted deposition rates and listed in Table 2 with the predicted deposition

rates. The actual initial deposition rate for the 0.05 M ascorbic acid/0.05 M gold thiosulfate electroless bath is high and agrees well with the predicted value. Homogeneous production of gold was observed in the electroless bath 30 minutes after deposition initiation. Lowering the gold thiosulfate concentration in the 0.05 M ascorbic acid electroless bath (pH=6.4, 30°C) proved to be sufficient for suppressing the homogeneous gold production reaction and still have high initial deposition rates. The predicted and actual initial deposition rates decreased with decreasing gold thiosulfate concentration. No homogeneous production of gold was observed in the 0.05 M ascorbic acid/0.03 M gold thiosulfate electroless bath or in the 0.05 M ascorbic acid/0.01 M gold thiosulfate electroless bath during the two hour experiment. A more detailed investigation of the effect of reactant concentration on the ascorbic acid/gold thiosulfate bath follows in the next section, 6.2.3. The actual initial deposition rate for the 0.05 M hydrazine/0.05 M gold thiosulfate electroless bath is low and agrees well with the predicted value. The actual initial deposition rate for the 0.05 M hydroxlamine/0.05 M gold thiosulfate electroless bath is low and agrees well with the predicted value. No homogeneous gold production was observed in the hydrazine and hydroxylamine baths, during the two hour experiment. The electroless bath tests confirmed that ascorbic acid reduces gold thiosulfate at a faster rate than hydrazine or hydroxylamine at pH=6.4 and 30°C. Gold thiosulfate electroless baths with lower concentrations of hydrazine or hydroxylamine were not studied because a decrease in reactant concentration seldom increases the deposition rates.

Two other reducing agents were paired with gold thiosulfate as possible electroless bath reactant combinations. Dithionite was tested as a reducing agent for gold thiosulfate in two alkaline buffered solutions at room temperature, but resulted in homogeneous production of gold. Thus, dithionite is unacceptable in electroless baths and no further tests were prepared. Hypophosphite was tested as a reducing agent for gold thiosulfate in acidic to alkaline buffered electroless baths. No homogeneous or heterogeneous deposition of gold occurred in these three electroless baths. Experimental results confirmed the mixed potential theory prediction of no gold deposition.

The Ascorbic Acid/Gold Thiosulfate Electroless Baths

Ascorbic acid and gold thiosulfate were selected as the most appropriate reducing agent/gold complex pair for a nonalkaline electroless bath. The main reason for this choice was that predicted and actual deposition rates of the ascorbic acid/gold thiosulfate electroless baths were higher than for electroless baths with any other combinations of gold complexes and reducing agents in acidic, neutral or mildly alkaline conditions (i.e. $pH \leq 9.2$). The nontoxicity and stability of the bath are two additional attractive characteristics of the ascorbic acid/gold thiosulfate electroless bath.

The electroless bath with the best deposition rate (0.89 μm/hr) and stability (bath stability for over two hours) had a composition of 0.05 M ascorbic acid/0.03 M gold thiosulfate and operated at pH=6.4, 30°C. If the pH is increased to 7.2 or the temperature is increased to 35°C or the gold thiosulfate concentration is increased to 0.05 M, homogeneous production of gold occurs. If the pH is decreased to 4.6 or temperature is decreased to 25°C or the ascorbic acid concentration is decreased to 0.03 M, deposition rates decrease over 50%.

Electroless Bath Reactions

The objective of this part of the investigation of the ascorbic acid/gold thiosulfate electroless bath was to explain any variations in the bath performance with time and to determine kinetic parameters of all identified significant side reactions. Investigation of possible side reactions and evaluation of their relative reactant consumption rate resulted in the development of a reaction mechanism for the ascorbic acid/gold thiosulfate electroless bath. Kinetic information about the side reactions was compiled from literature sources and experimental data.

Time Varied Performance of the Ascorbic Acid/Gold Thiosulfate Electroless Bath

Previous results have shown that the 0.05 M ascorbic acid/0.03 M gold thiosulfate bath (pH=6.4, 30°C) deposited gold at an initial deposition rate of 0.89 μm/hr and remained stable for the two-hour duration of the experiment. The deposition rates of this bath were measured every thirty minutes for two hours to assess the degradation rate of the bath. The deposition rates decreased from 0.89 ± 0.10 ($\pm 2\sigma$) μm/hr to 0.72 ± 0.07 ($\pm 2\sigma$) μm/hr to 0.61 ± 0.04 ($\pm 2\sigma$) μm/hr to 0.40 ± 0.06 ($\pm 2\sigma$) μm/hr at thirty minute intervals.

Voltammograms of the 0.05 M ascorbic acid/0.03 M gold thiosulfate electroless bath (pH=6.4, 30°C) were taken at each time interval Voltammograms were obtained on a stationary gold electrode with 100 mV/sec potential sweep rate. The voltammograms of the electroless bath were different at each time interval, see Fig. 19. The ascorbic acid concentration decreased with time, explaining the gradual decrease in anodic current. The decrease in cathodic current with time was due to a decrease in gold thiosulfate concentration. The lifetime of the bath was defined as when the deposition of gold ceased, approximately 3.5 hours after immersing the first gold substrate into the electroless bath.

Electroless deposition of gold on sputtered gold substrates was observed at four discrete times using a scanning electron microscope. The grain size of the deposited gold increased with time. The deposited film in the first five minutes was less uniform than after 10 minutes. Grain size was approximately 0.2 μm after 30 minutes.

A four point-probe was used to measure the resistivity of the electroless deposit. Ten resistivity measurements were taken of a one micrometer gold film, deposited in the 0.05 M ascorbic acid/0.03 M gold thiosulfate electroless bath (pH=6.4, 30°C). The average resistivity of the electroless gold deposit is 2.5 μΩ-cm ± 0.05 ($\pm 2\sigma$) μΩ-cm. The percent difference between measured resistivity and referenced bulk resistivity is 1.35%. The adhesion of the electroless gold deposit to the original sputtered gold surface was qualitatively determined using the scotch tape test. Twenty samples of the gold film, deposited in the 0.05 M ascorbic acid/0.03M gold thiosulfate electroless bath (pH=6.4, 30°C), were scored in a one cm^2 region and subjected to the scotch tape test. All samples demonstrated 100% adhesion between the electroless gold deposit and the original sputtered gold surface. Electroless gold plating in 20 μm diameter via holes was successful, with an electroless deposit of 0.62 ± 0.06 ($\pm 2\sigma$) μm grown in one hour.

The electroless gold deposits had desirable characteristics for microelectronic applications. The qualitative assessment of the electroless deposit adhesion to the original gold substrate showed reasonable adhesion between the electroless gold deposit and the sputtered gold surface. This strong adhesion suggests that the deposit formed directly on the gold

substrate. The resistivity of the electroless gold deposit was low, at 2.5 $\mu\Omega$-cm, and approached bulk resistivity of gold. High conductivity and adhesion is advantageous for gold deposits in microelectronic applications. Scanning electron microscope images show a uniform coverage of the deposit onto the selected substrate. The fine grain size of the electroless deposit is desirable for continued scaling of conductor line widths. Deposition of gold at moderate rates into via holes was successful. A slower deposition rate of 0.62 μm/hr into via holes may be explained by the increased difficulty in mass transport of reactants to the gold surface and products away from the gold surface. Previous studies confirmed that both ascorbic acid and gold thiosulfate have low diffusion coefficients. Increasing the convective mass transport of reactants and products would be necessary for depositing gold into via holes of smaller diameter. Although the grain size of the deposit favors smaller deposition regions, deposition rates decreasing with deposition surface area may limit the application of this bath.

A primary goal in the development of an electroless bath is to deposit metal selectively at high constant deposition rates. The rate of the deposition is influenced by the reactant concentration if the solution conditions are maintained. Fluctuations in reactant concentration, pH or temperature will affect bath performance. The 0.05 M ascorbic acid/0.03 M gold thiosulfate electroless bath deposited gold at high initial deposition rates at pH=6.4 and 30°C. A significant decrease in deposition rates occurred over time, with bath pH and temperature maintained.

Explanation of Decreasing Deposition Rates

The thiosulfate concentration increases in the electroless bath as the gold thiosulfate reduces, according to the deposition reaction. Production of thiosulfate in the electroless bath affects the reduction voltammogram of gold thiosulfate. A higher thiosulfate concentration causes the gold thiosulfate reduction voltammogram to shift to more negative potentials. The gold thiosulfate reduction voltammograms were obtained at a stationary gold electrode with a potential sweep rate of 100 mV/sec, pH=6.4 and 30°C. The mixed potential shift in Fig. 19 is explained by the Nernstian response of the gold thiosulfate reduction voltammogram to the increasing thiosulfate concentration. The mixed potential moves to more negative potentials as the

potential difference between the gold thiosulfate reduction and the ascorbic acid oxidation decreases. According to the mixed potential theory, a decrease in potential difference between the oxidant and reductant is expected to result in lower deposition rates in the electroless bath. Electroless baths with varying initial excess thiosulfate concentrations have confirmed that thiosulfate is responsible for lowering the deposition rates. The initial deposition rates, averaged over the first thirty minutes, of three 0.05 M ascorbic acid/0.03 M gold thiosulfate electroless baths (pH=6.4, 30°C) are listed in Table 3. As the excess thiosulfate concentration increased, the initial deposition rate decreased.

Table 3:   Electroless Bath Initial Deposition Rates.

Thiosulfate Concentration (mol/l)	Initial Deposition Rates (μm/hr) ($\pm 2\,\sigma$)
0	0.89 ± 0.10
0.0001	0.74 ± 0.09
0.001	0.67 ± 0.21
0.005	0.61± 0.08

The consumption of gold thiosulfate in the deposition reaction explains the observed decrease in gold thiosulfate concentration in the electroless bath. However, the reduction rate of gold thiosulfate varied with time. Voltammograms of the electroless bath monitored the partial redox reactions and confirmed shifts in the electroless bath mixed potential with time. The production of thiosulfate in the deposition reaction, and subsequent accumulation of thiosulfate in the electroless bath explains this mixed potential shift. The mixed potential shift is the Nernstian response of the gold thiosulfate reduction voltammogram to increasing thiosulfate concentration. Gold thiosulfate reduction voltammograms, with excess thiosulfate, corroborate this effect of thiosulfate on the gold thiosulfate reduction potential.

Electroless bath results demonstrate that only small amounts of thiosulfate are necessary to significantly decrease deposition rates. The depletion of ascorbic acid in the homogeneous oxidation reaction cannot account for the low deposition rates over the first thirty minutes. Yet, the mixed potential shift, in response to the addition of thiosulfate, does explain the decline of bath activity in the first thirty minutes. Oxidation voltammograms of ascorbic acid give no evidence of interaction or reaction between ascorbic acid and thiosulfate. Therefore, the addition of thiosulfate to the electroless bath affects the gold thiosulfate reduction reaction only.

Cyclic voltammograms of the electroless bath monitored and confirmed decreases in reactant concentration with time. A decrease in reactant concentration was expected, taking into account the reactant consumption in the deposition reaction. However, the decrease in ascorbic acid concentration was too high to be explained by its consumption in the deposition reaction.

The consumption rate of ascorbic acid in homogeneous oxidation reactions was investigated in a citrate buffer solution (pH=6.4). The ascorbic acid concentration was monitored with time by using cyclic voltammetry. The ascorbic acid oxidation limiting current density varied linearly with concentration. An empirical relationship was used to calculate ascorbic acid concentration given a limiting current density.

The homogeneous oxidation of ascorbic acid was studied with: no catalyst, a gold substrate as a heterogeneous catalyst, gold thiosulfate as a homogeneous catalyst, and hydrogen peroxide as a co-oxidant. The homogeneous oxidation of ascorbic acid was assumed to be pseudo-first order, based on past investigations. All citrate buffer solutions (pH=6.4) were exposed to air for at least one day prior to experimentation. Mild agitation of the prepared solutions was controlled, either by a magnetic stir bar or a rotating electrode. The dissolved oxygen concentration was assumed to be constant.

All experiments were performed at 30°C, the electroless bath operating temperature. The rotating gold electrode was immersed into the solution approximately 20 seconds prior to the onset of the electro-oxidation and removed immediately after obtaining the voltammogram. The initial 20 seconds was necessary for reaching equilibrium at the solution/electrode

interface before the electrochemical experiment. Total immersion time of the gold electrode was less than 90 seconds. Oxidation voltammograms of ascorbic acid were obtained intermittently at a gold electrode with a potential sweep rate of 100 mV/sec.

Results from the homogeneous oxidation of ascorbic acid by dissolved oxygen confirm a pseudo-first order rate equation. The natural logarithm of ascorbic acid concentration varies linearly with time, see Fig. 20. Experiments were done with several initial ascorbic acid concentrations. The slope of the data set was used to calculate a first order rate constant of 0.00175 min^{-1} with a standard error of 7.96 x 10^{-5} min^{-1}. This kinetic rate constant corresponds to an 19 ± 0.5% decrease in ascorbic acid concentration in two hours. The reaction of ascorbic acid and dissolved oxygen is, therefore, responsible for a significant depletion of ascorbic acid. The addition of a gold substrate did not significantly increase the consumption rate of ascorbic acid, see Fig. 20. The consumption rate of ascorbic acid in the hydrogen peroxidation reaction in air did not occur significantly faster than in the oxidation reaction with dissolved oxygen, see Fig. 20.

The presence of gold thiosulfate in solution significantly increased the homogeneous oxidation rate of ascorbic acid. The consumption of ascorbic acid in a reaction with dissolved oxygen in the presence of gold thiosulfate was investigated at pH=6.4, 30°C. Results from the homogeneous oxidation of ascorbic acid in solution with gold thiosulfate showed first order rate dependence on ascorbic acid concentration. The natural logarithm of ascorbic acid concentration varies linearly with time, see Fig. 21. Experiments were done with initial ascorbic acid concentrations of 0.01 M, 0.08 M, 0.05 M and 0.04 M. The calculated first order rate constant is 0.0203 min^{-1} with a standard error of 3.42 x 10^{-4} min^{-1}. This kinetic rate constant corresponds to 32% decrease in ascorbic acid concentration in twenty minutes. Thus, the ascorbic acid reaction with dissolved oxygen in the presence of gold thiosulfate significantly depletes the solution of ascorbic acid.

The homogeneous oxidation of ascorbic acid behaves as a zero-order reaction with respect to the gold thiosulfate concentration. Results show no appreciable difference in the oxidation rate if the gold thiosulfate concentration is increased above 0.005 M. Zero-order reactions typically

Fig. 20:   Ascorbic Acid Concentration Data. Consumption of Ascorbic Acid in the Homogeneous Oxidation Reaction. pH = 6.4, 30°C.
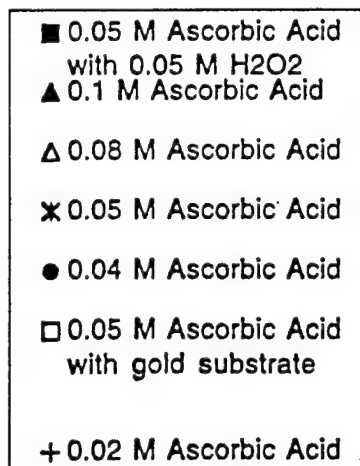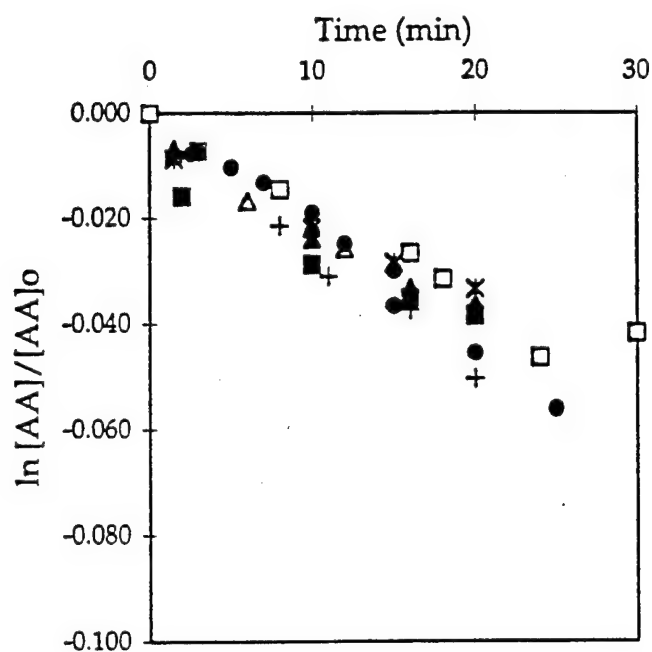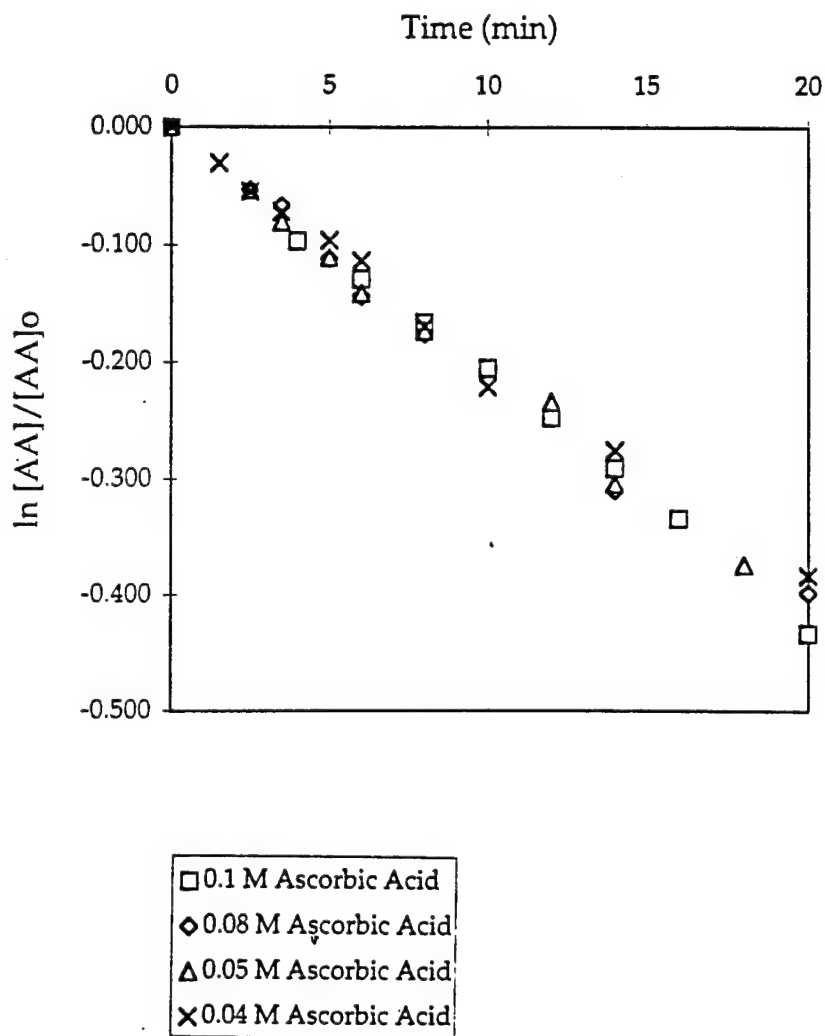

162

Fig. 21:   Ascorbic Acid Concentration Data. Consumption of Ascorbic Acid in the Homogeneous Oxidation Reaction in the Presence of Gold (I) Thiosulfate. pH = 6.4, 30°C.

increase in rate order if the reactant concentration is lowered enough. The above pseudo-first order rate constant is therefore, reported for gold thiosulfate concentrations above 0.005 M only. Determination of the true rate equation for all gold thiosulfate concentrations was unnecessary for this investigation. A gold thiosulfate concentration of less than 0.005 M in the electroless bath would make the bath very inefficient if effective at all.

The presence of gold thiosulfate in solution greatly enhanced the homogeneous oxidation rate of ascorbic acid at pH=6.4, 30°C, as in many other cases reported in literature. Metal ions and metal complexes have been found to have similar effects on the homogenous oxidation of ascorbic acid, according to literature. Therefore, it is reasonable that the homogeneous oxidation of ascorbic acid in the presence of gold thiosulfate consumed ascorbic acid at a fast rate.

The homogeneous oxidation of ascorbic acid in the presence of gold thiosulfate occurred as a first order reaction with respect to ascorbic acid concentration and a zero order reaction with respect to gold thiosulfate concentration. The consumption of ascorbic acid with gold thiosulfate present had a high rate constant of 0.0203 min^{-1}. The fast homogeneous oxidation rate of ascorbic acid in the presence of gold thiosulfate is distinguishably greater than the homogeneous oxidation rate of ascorbic acid in the absence of gold thiosulfate. The decrease in ascorbic acid concentration due solely to the reaction with dissolved oxygen in the presence of gold thiosulfate occurred at a rate high enough to explain the decrease the deposition rates observed in the electroless bath.

Although the deposition reaction results in the desired heterogeneous deposition of a gold film on a gold surface, the deposition reaction is responsible for increasing the thiosulfate concentration and decreasing the gold thiosulfate concentration. The thermodynamic reaction of thiosulfate and gold thiosulfate in the electroless bath immediately responds to variations in the equilibrium concentrations of thiosulfate and gold thiosulfate. As a result, the loss of bath activity with time is inevitable if the thiosulfate concentration is permitted to increase in the 0.05 M ascorbic acid/0.03 M gold thiosulfate electroless bath (pH=6.4, 30°C). The decrease in ascorbic acid concentration, in the homogeneous oxidation with gold

thiosulfate present, reduces the bath activity even further. This reactant depletion may be neutralized with ascorbic acid replenishment. In summary, the observed decrease in deposition rates with time is attributed to the consumption of ascorbic acid in the homogeneous oxidation reaction in the presence of gold thiosulfate and to the gold thiosulfate reduction potential shift accompanying the thiosulfate accumulation in the electroless bath.

Improving Electroless Bath Performance

Effect of Excess Complexing Agent Addition

The reduction voltammograms of 0.03 M gold thiosulfate were investigated with excess thiosulfate at a potential sweep rate of 100 mV/sec at a stationary gold electrode. The effect of excess thiosulfate on gold thiosulfate reduction potential is seen in Fig. 22. Table 4 lists the experimental and predicted reduction potentials at 1.5 mA/cm^2 as a function of excess thiosulfate concentration. The addition of excess thiosulfate shifts the experimental reduction potential of gold thiosulfate in the negative direction. For example, a tenfold increase in thiosulfate (from 0.005 M to 0.05 M) results in a 100 mV experimental reduction potential shift in the negative direction. The Butler-Volmer equation (8-4) calculates a predicted reduction potential based on reactant concentration. The predicted reduction potentials agree well with experimental data. The Butler-Volmer equation confirms that the experimental shift observed is related to the excess thiosulfate concentration.

Initial deposition rates of electroless baths with excess thiosulfate were averaged over the first thirty minutes in 0.05 M ascorbic acid/0.03 M gold thiosulfate electroless bath (pH=6.4, 30°C). The initial deposition rates decrease significantly with increasing thiosulfate concentration, see Table 5. All bath activity was lost with 0.05 M thiosulfate added in excess. The bath lifetime increased from approximately 3.5 hours for the standard bath (with zero excess thiosulfate) to approximately 4.5 hours with 0.005 M excess thiosulfate added, to approximately 5 hours with 0.01 M excess thiosulfate added. The bath temperature of the 0.05 M excess thiosulfate electroless bath was increased to 50°C in an attempt to restore bath activity. Initial deposition rates were increased to only 0.14 ± 0.08 μm/hr.

Fig. 22: Reduction of 0.03 M Gold (I) Thiosulfate. Current Density-Potential Variation with Excess Thiosulfate Addition. 100 mV/sec, 0 RPM, pH=6.4, 30°C.
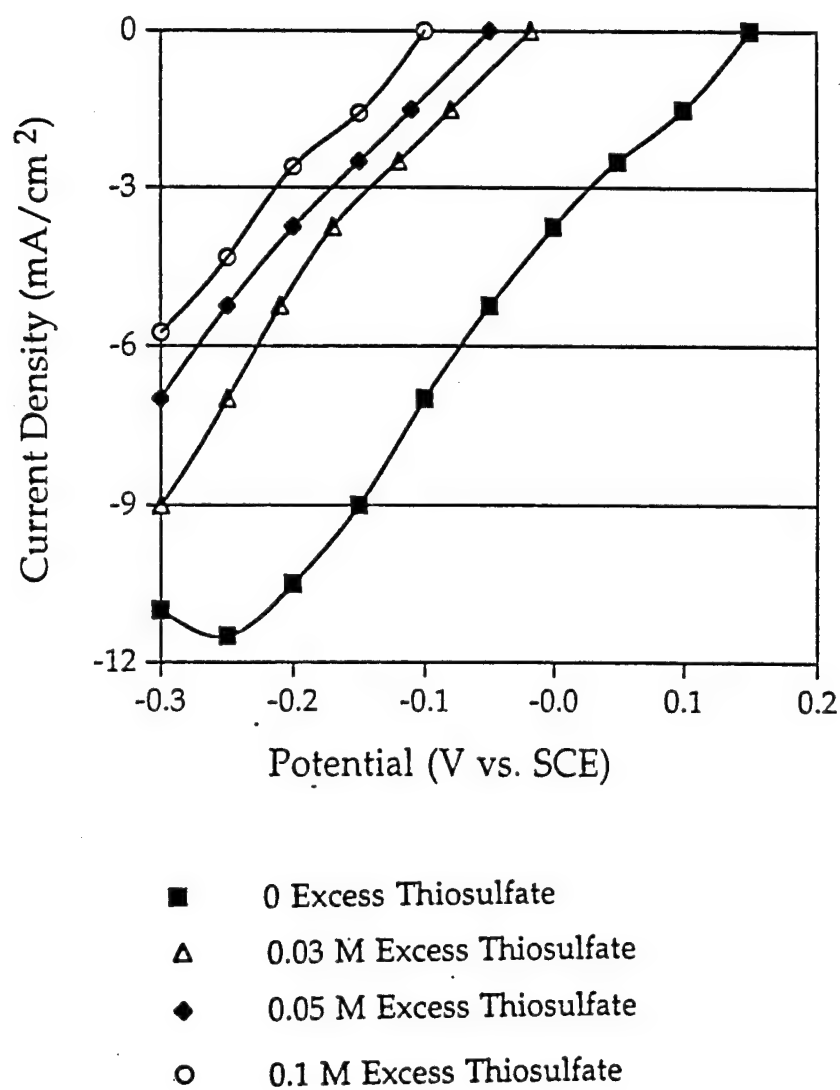

■	0 Excess Thiosulfate
△	0.03 M Excess Thiosulfate
◆	0.05 M Excess Thiosulfate
○	0.1 M Excess Thiosulfate

Table 4: Reduction Potentials of 0.03 M Gold Thiosulfate at 1.5 mA/cm^2.

Excess Thiosulfate Concentration (mol/l)	Experimental Reduction Potential at 1.5 mA/cm^2 (V vs. SCE) ($\pm 2\sigma$)	Predicted Reduction Potentials at 1.5 mA/cm^2 (V vs. SCE) ($\pm 2\sigma$)
0	0.090 ± 0.005	0.100 ± 0.005
0.005	-0.020 ± 0.005	-0.070 ± 0.005
0.02	-0.105 ± 0.005	-0.107 ± 0.005
0.03	-0.110 ± 0.005	-0.117 ± 0.005
0.05	-0.120 ± 0.005	-0.130 ± 0.005

Table 5:   Initial Deposition Rates for Varying Thiosulfate and Sulfite Initial Concentrations with Temperature.

Additive	Concentration (mol/l)	Bath Temperature (°C)	Initial Deposition Rates (μm/hr) (± 2 σ)
-	-	30	0.89 ± 0.10
Thiosulfate	0.005	30	0.61± 0.08
Thiosulfate	0.01	30	0.51± 0.10
Thiosulfate	0.03	30	0.27± 0.09
Thiosulfate		30	0 ± 0.04
Thiosulfate	0.05	50	0.14 ± 0.08
Sulfite	0.03	30	0.31 ± 0.08
Sulfite	0.05	50	1.52 ± 0.10

Free gold (I) ions complex with sulfite ions to form gold (I) sulfite with a low stability constant of 10^{10} (8, 10-12):

$$Au(SO_3)_2^{3-} = Au^+ + 2\ SO_3^{2-} \tag{10}$$

Existing literature reports no evidence of a reaction between sulfite and ascorbic acid. Oxidation voltammograms of ascorbic acid with and without added sulfite were obtained at electroless bath conditions with a potential sweep rate of 100 mV/sec at a stationary gold electrode (pH=6.4, 30°C). The addition of sulfite seems to have no effect on the ascorbic acid oxidation reaction. The oxidation of ascorbic acid with 0.01 M sulfite appears as the sum of the ascorbic acid oxidation voltammogram and the sulfite oxidation voltammogram, see Fig. 23.

The addition of sulfite as a complexing agent was studied in a gold thiosulfate solution (pH=6.4). Reduction voltammograms of 0.03 M gold thiosulfate with varying excess sulfite concentration were obtained at a stationary gold electrode with a potential sweep rate of 100 mV/sec, see Fig. 24. The reduction potential of gold thiosulfate shifts in the negative direction as the sulfite concentration increases. For example, the experimental

Fig. 23:   Oxidation of Ascorbic Acid.   Current Density-Potential Variation with Sulfite Addition.   100 mV/sec, 0 RPM, pH=6.4, 30°C on Gold Disk.

□   0.05 M Ascorbic Acid

◇   0.05 M Ascorbic Acid
        + 0.025 M Sulfite

Fig. 24: Reduction of 0.03 M Gold (I) Thiosulfate. Current Density-Potential Variation with Sulfite Addition. 100 mV/sec, 0 RPM, pH=6.4, 30°C on Gold Disk.
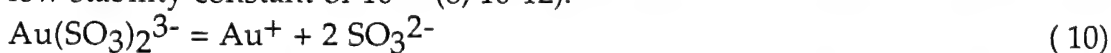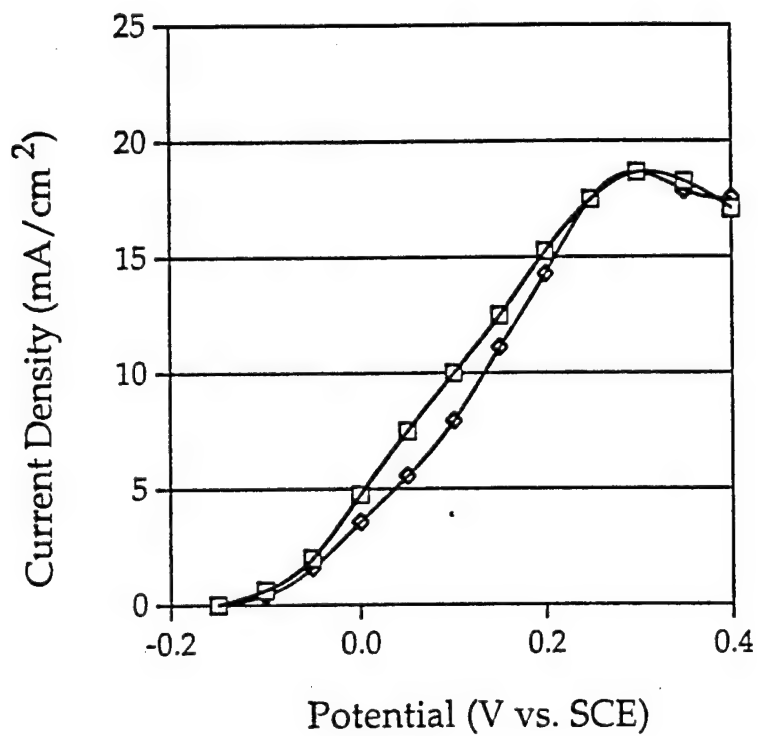

□	0 Excess Sulfite
◆	0.005 M Excess Sulfite
○	0.01 M Excess Sulfite
▲	0.05 M Excess Sulfite

reduction potential of 0.03 M gold thiosulfate solution, with no excess complexing agents, shifts approximately 100 mV in the negative direction with the addition of 0.05 M sulfite. Even though gold sulfite has a lower stability constant than gold thiosulfate, the addition of sulfite causes the reduction of gold thiosulfate to shift to more negative potentials. Similar potential shifts with the addition of sulfite were reported for gold chloride solutions with excess thiosulfate (11). Kato does not attempt to explain this effect of sulfite on the gold reduction voltammograms (11). An asymmetric complex may have formed between gold ions, thiosulfate and sulfite. Sulfite may adsorb onto the gold substrate, shifting the reduction voltammogram to more negative potentials. The exact mechanism by which sulfite affects the electroreduction of gold thiosulfate remains unclear.

The effect of adding excess sulfite to the 0.05 M ascorbic acid/0.03 M gold thiosulfate electroless bath (pH=6.4, 30°C) is similar to the effect of adding excess thiosulfate. The initial deposition rates decrease from 0.89 µm/hr ± 0.10 µm/hr to 0.31 ± 0.08 µm/hr with the addition of 0.03 M sulfite, see Table 5. The initial deposition rate of 0.31 ± 0.08 µm/hr in the 0.03 M excess sulfite bath is slightly higher than the initial deposition rate of 0.27 ± 0.09 µm/hr in the 0.03 M thiosulfate excess bath. The deposition rate of this bath slowly decreases over time from 0.31 ± 0.08 µm/hr to 0.25 ± 0.06 µm/hr in two hours to 0.20 ± 0.07 µm/hr in four hours. The lifetime of this bath, defined by the loss of bath activity, is approximately six hours.

An increase in bath temperature has a more dramatic effect on deposition rates of the sulfite bath than for the deposition rates of the thiosulfate bath, see Table 5. The initial deposition rate of the 0.05 M ascorbic acid/0.03 M gold thiosulfate electroless bath (pH=6.4, 30°C) with 0.05 M excess sulfite at 50°C was averaged over the first thirty minutes. The initial deposition rate of the sulfite bath at 50°C is 1.52 ± 0.10 µm/hr, a fivefold increase from the initial deposition rate at 30°C. However, the precipitation of gold occurs in less than two hours. Therefore, raising the temperature is not a practical solution for increasing bath deposition rates.

The slow decline in deposition rates of the sulfite bath at 30°C may be due to the slow accumulation of thiosulfate in the electroless bath. The production of thiosulfate in the electroless bath may result in a thiosulfate
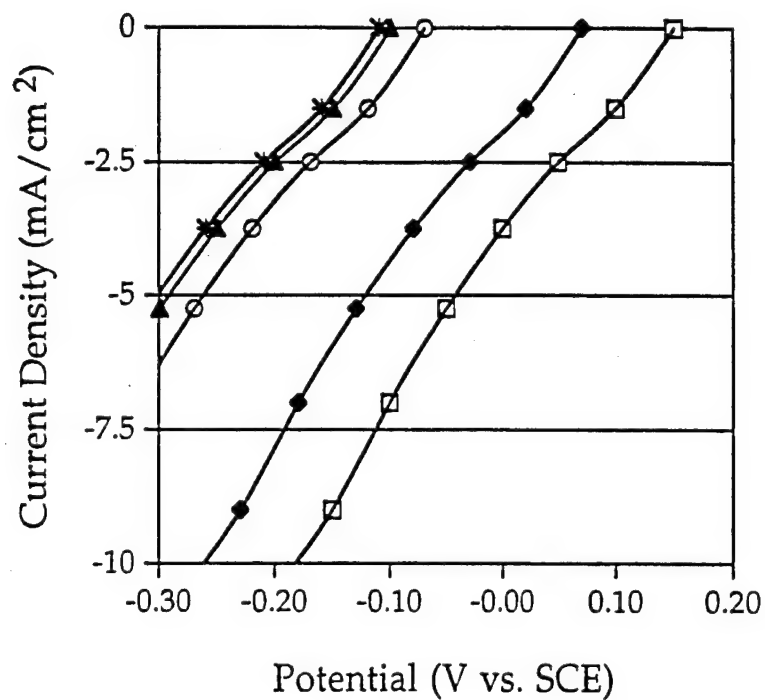
concentration on the order of 3 mM (5% of gold thiosulfate is consumed) to 60 mM (all gold thiosulfate is consumed). The effect of excess thiosulfate concentration on the partial electrochemical reduction reaction in the presence of sulfite was evaluated to determine the consequence of adding two complexing agents to a gold thiosulfate solution.

The reduction of 0.03 M gold thiosulfate with 0.05 M excess sulfite was investigated in a citrate buffer (pH=6.4). Gold thiosulfate reduction voltammograms were obtained at a stationary gold electrode with a potential sweep rate of 100 mV/sec. The experimental reduction potential of the 0.03 M gold thiosulfate solution shifts to more negative potentials with the addition of sulfite alone. The gold thiosulfate reduction voltammogram (0.03 M gold thiosulfate with 0.05 M sulfite) shifts to more negative potentials as the thiosulfate concentration increases, see Fig. 25. Therefore, excess sulfite does not prevent the potential shift associated with increasing thiosulfate concentration.

Another method of restoring bath activity to an electroless bath with an appreciable thiosulfate concentration is to increase the operating temperature of the bath. This method is often used in developing electroless baths, and is generally limited by the homogeneous production of gold. However, increasing the temperature of this 0.05 M thiosulfate electroless bath to 50°C resulted in a very slight improvement in bath performance. The deposition rates were raised to only 0.14 μm/hr. Apparently, the complexation strength of thiosulfate limits the free thiosulfate ion concentration in the bath, even at higher temperatures. In addition, the production of thiosulfate ions in the gold thiosulfate reduction reaction results in further decreasing deposition rates over time. Clearly, increasing the amount of thiosulfate present in the electroless bath is the demise of the bath.

The addition of sulfite to the 0.05 M ascorbic acid/0.03 M gold thiosulfate electroless bath (pH=6.4, 30°C) was considered as a possible means of increasing bath lifetime without decreasing deposition rates. The extent of complexation between sulfite and gold ions was expected to be low, provide a little more stability to the bath and not significantly affect the gold thiosulfate reduction rate. Closer analysis of the effect of sulfite on the reduction of gold thiosulfate negates the above assumption. If gold sulfite is

172

Fig. 25:   Reduction   of   0.03   M   Gold   (I)   Thiosulfate.   Current
Density-Potential Variation with Excess Thiosulfate and Sulfite.   100 mV/sec,
0 RPM, pH=6.4, 30°C on Gold Disk.

□	0 Excess Sulfite and 0 Excess Thiosulfate
◆	0.05 M Excess Sulfite with 0 Excess Thiosulfate
○	0.05 M Excess Sulfite and 0.01 M Excess Thiosulfate
▲	0.05 M Excess Sulfite and 0.03 M Excess Thiosulfate
✳	0.05 M Excess Sulfite and 0.05 M Excess Thiosulftate

formed by adding sulfite to the gold thiosulfate solution, the concentration of gold sulfite never reaches an appreciable amount for detection in the reduction voltammograms. Yet, the addition of sulfite has an unexpected effect on the gold thiosulfate reduction voltammogram. The gold thiosulfate reduction voltammogram shifts in potential in the negative direction as sulfite concentration increases in solution. A gold thiosulfate reduction potential shift with added sulfite (pH=6, 60°C), reported in literature, supports the results in this investigation (11). It is interesting to note that although sulfite forms only a weak complex with gold ions, the addition of sulfite causes a significant shift in the gold thiosulfate reduction potential. This effect of sulfite on the reduction potential cannot be satisfactorily explained by the complexation of gold ions with sulfite. The high stability of gold thiosulfate limits the gold ions available for complexation with sulfite. And, the stability constant of gold sulfite is not high enough to instigate the disproportionation of gold thiosulfate. An asymmetric gold thiosulfate-sulfite complex may form and have a higher stability constant than gold thiosulfate. Mixed halide complexes have been found to have higher stability constants than complexes with singular ligands. The existence of a gold complex with thiosulfate and sulfite ligands has been proposed by Inoue (10). Inoue states that the mixed gold complex has a stability constant higher than either gold sulfite or gold thiosulfate (10). Further evidence is necessary to substantiate the existence of the thiosulfate-sulfite complex with gold. Another explanation of the effect of sulfite on the gold thiosulfate reduction voltammogram may be that sulfite adsorbs onto the gold substrate, increasing the overpotential for the gold thiosulfate reduction reaction. In any case, the addition of sulfite has a negative effect on the gold thiosulfate reduction potential.

Removal of Thiosulfate Through Hydrogen Peroxidation

Initial addition of complexing agents, thiosulfate or sulfite, have been shown to increase bath lifetime and significantly decrease deposition rates. The lifetime of the bath is defined as the approximate time when the accumulated thiosulfate has shifted the gold thiosulfate reduction to a potential more negative than the ascorbic acid oxidation potential range. Gold thiosulfate is not reduced by ascorbic acid if ascorbic acid oxidizes at

potentials more positive than the gold thiosulfate reduction potential. The bath lifetime is, therefore, clearly limited by the thiosulfate concentration in the bath. Elimination of this bath lifetime limitation requires removal, complexation, or decomposition of thiosulfate.

One method of neutralizing the thiosulfate accumulation is to react the thiosulfate with an oxidizer and preferably, produce inert sulfur species, i.e. a solution species that does not complex with gold ions or passivates gold surfaces. The goal is to find an oxidizer that acts as an accelerator by controlling the thiosulfate concentration without compromising bath performance. The method of consuming thiosulfate by adding hydrogen peroxide was investigated as a potential means of restoring bath activity and maintaining high constant deposition rates. Thiosulfate reacts with hydrogen peroxide as follows ([28 - 293031323334]):

$$S_2O_3^{2-} + H_2O_2 --> S_4O_6^{2-} + 2OH^-$$ (11)

Previous investigations of this reaction at different conditions concluded that the reaction is not empirical (33-39).

Gold thiosulfate and ascorbic acid have been determined to be relatively inert to hydrogen peroxide. Tetrathionate, $S_4O_6^{2-}$, has not been cited as a complexing agent for gold and has shown no evidence of passivating gold surfaces (8, 9). A potential problem may be in maintaining pH, if a sufficient amount of hydroxide ions are produced.

The reaction between thiosulfate and hydrogen peroxide was studied at electroless bath conditions (pH=6.4, 30°C). Oxidation voltammograms of thiosulfate were used to monitor thiosulfate concentration with time for different initial reactant compositions. Initial rate data was used to find the reaction order and rate constant, see Table 6. The experimental rate expression is:

$$-d[S_2O_3^{2-}]/dt = k[S_2O_3^{2-}]^a[H_2O_2]^b$$ (12)

where the experimental rate constant, k, is 6.17×10^{-2} $((mol/l \ min)^{-1}$ with a standard error of 1.2×10^{-3} $((mol/l \ min)^{-1}$, and a is 1.455 and b is 2 with standard errors of 0.05. The experimental exponents in the rate equation, as expected, do not relate stoichiometrically to the reaction. Rather, they represent a fit of the data to the above equation (8-7). The rate constants corresponds to a 10% reduction in thiosulfate concentration in 10 minutes if

the initial concentrations of thiosulfate and hydrogen peroxide are 0.05 M and 0.5 M, respectively.

The effect of hydrogen peroxide on the deposition rates was investigated in several electroless baths. The initial deposition rates of the 0.05 M ascorbic acid/0.03 M gold thiosulfate electroless baths with varying initial concentrations of hydrogen peroxide are averaged over the first thirty minutes and listed in Table 7. The deposition rates increased with increasing hydrogen peroxide concentration. The hydrogen peroxide consumed thiosulfate as it was produced in the deposition reaction. The consumption of thiosulfate was to such an extent, that the bath activity increased within the first thirty minutes.

Table 6: Initial Rate Data for the Hydrogen Peroxidation of Thiosulfate at pH=6.4 and 30°C.

Initial [Hydrogen Peroxide] (mol/l)	Initial [Thiosulfate]/[Hydrogen Peroxide]	Initial Rate of Thiosulfate Consumption or $-d[S_2O_3^{2-}]/dt$ (mol/l min)
2.00	0.027	1.2×10^{-3}
1.00	0.053	8.88×10^{-4}
0.50	0.098	5.23×10^{-4}
0.20	0.247	3.10×10^{-4}
0.05	0.996	1.58×10^{-4}

Table 7:   Initial Deposition Rates for Varying Hydrogen Peroxide Initial Concentrations.

Initial [Hydrogen Peroxide] (mol/l)	Initial Deposition Rates (μm/hr) (±2σ)
0	0.89 ± 0.10
0.005	1.02 ± 0.15
0.01	1.52 ± 0.18

The deposition rates, averaged over thirty minutes intervals, varied with time in the hydrogen peroxide electroless baths. The time variations in deposition rates were measured for three electroless baths: the standard bath (0.05 M ascorbic acid/0.03 M gold thiosulfate at pH=6.4, 30°C) with no hydrogen peroxide addition, the standard bath with an initial addition of 0.005 M hydrogen peroxide and the standard bath with an initial and subsequent additions of 0.005 M hydrogen peroxide every fifteen minutes, see Fig. 26. The deposition rates increased with the addition of 0.005 M hydrogen peroxide and remained high for the first hour. When the hydrogen peroxide had been consumed, the accumulation rate of thiosulfate increased. The decrease in deposition rates may be explained by an increase in thiosulfate concentration during the second hour. The higher deposition rates also correspond to a faster depletion rate of the electroless bath reactants, another explanation for decreasing deposition rates in the second hour. The bath with a periodic addition of 0.005 M hydrogen peroxide had the highest deposition rates, yet still decreased with time. The production rate of thiosulfate exceeded the rate of the hydrogen peroxidation of thiosulfate. The subsequent increase in thiosulfate concentration and the inevitable decrease in reactant concentration explain the decreasing deposition rates in the third bath.

The Mathematical Model of the Reaction Mechanism

Information regarding necessary bath composition for constant gold deposition was obtained by modeling the consumption of electroless bath
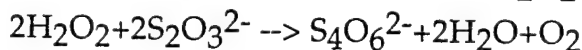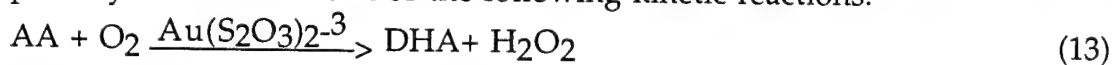
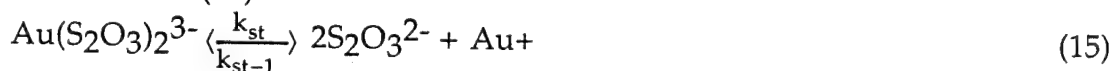Fig. 26:   Electroless Bath Deposition Rates. 0.05 M Ascorbic Acid/0.03 M Gold Thiosulfate pH=6.4, 30°C.

□   with no H_2O_2 addition

◇   with an initial addition of 0.005 M H_2O_2

○   with an initial and 15 minute periodic addition of 0.005 M H_2O_2

reactants and additives, as well as the formation of products. Results of this investigation have shown four reactions to be significant in the electroless bath: 1) the autocatalytic reduction of gold thiosulfate by ascorbic acid, 2) the equilibrium reaction between gold thiosulfate, thiosulfate and gold (I) ions, 3) the homogeneous oxidation of ascorbic acid by dissolved oxygen in the presence of gold thiosulfate and 4) the hydrogen peroxidation of thiosulfate.
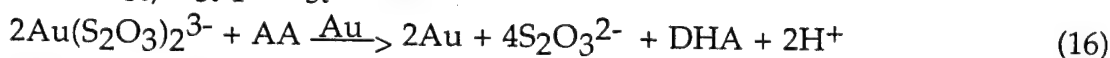
A mathematical model of the reaction mechanism in the electroless bath was developed to understand the relationship between initial reactant and additive concentrations and electroless deposition rates. Empirical rate constants and literature values of equilibrium constants were used to calculate the number of moles of gold produced over time, given initial bath composition. The mechanism incorporated four ordinary differential equations describing the unsteady state mole balance equations for the four primary bath reactants. For the following kinetic reactions:

$$AA + O_2 \xrightarrow{Au(S_2O_3)_2^{-3}} DHA + H_2O_2 \tag{13}$$

$$2H_2O_2 + 2S_2O_3^{2-} \dashrightarrow S_4O_6^{2-} + 2H_2O + O_2 \tag{14}$$

$$Au(S_2O_3)_2^{3-} \langle \xrightarrow[k_{st-1}]{k_{st}} \rangle 2S_2O_3^{2-} + Au^+ \tag{15}$$

where $k_{st}/k_{st-1} = K_{st} = 10^{28}$

$$2Au(S_2O_3)_2^{3-} + AA \xrightarrow{Au} 2Au + 4S_2O_3^{2-} + DHA + 2H^+ \tag{16}$$

the coupled four ODEs are:

$$\frac{d[AA]}{dt} = -k_1[AA] - k_3[AA]^5[Au(S_2O_3)_2^{3-}] \tag{17}$$

$$\frac{d[Au(S_2O_3)_2^{3-}]}{dt} = -k_3[AA]^5[Au(S_2O_3)_2^{3-}] - k_{st+1}[Au(S_2O_3)_2^{3-}]$$

$$+k_{st-1}[S_2O_3^{2-}]^2[Au^+] \tag{18}$$

$$\frac{d[H_2O_2]}{dt} = k_1[AA] - k_2[S_2O_3^{2-}]^a[H_2O_2]^b \tag{19}$$

$$\frac{d[S_2O_3^{2-}]}{dt} = 4k_3[AA]^5[Au(S_2O_3)_2^{3-}] + 2k_{st+1}[Au(S_2O_3)_2^{3-}]$$

$$-k_{st-1}[S_2O_3^{2-}]^2[Au^+] - k_2[S_2O_3^{2-}]^a[H_2O_2]^b \tag{20}$$

where $[AA]$, $[Au(S_2O_3)_2^{3-}]$, $[S_2O_3^{2-}]$, $[H_2O_2]$ are concentrations in mol/l of ascorbic acid, gold thiosulfate, thiosulfate and hydrogen peroxide, respectively. The reactant concentrations are interdependent, so the ordinary differential equations are coupled. The bath is assumed to be isothermal,

179

with a constant convection flow rate. Empirical rate constants were determined in systems with similar convection and diffusion flow rate patterns.

Deposition rates for different bath compositions can be predicted by using the numerical model of the electroless bath. The advantage of this numerical model is that the interactions between reactants, or the coupling effect, can be included in the calculation of concentrations over time. The disadvantage is that the kinetic model does not account for fluctuations in pH. Previous results have shown that an increase in pH may lead to homogeneous production of gold and that a decrease in pH may cause a decrease in deposition rates. The hydrogen peroxidation of thiosulfate may produce hydroxide ions. This production of hydroxide ions and the subsequent effect on ascorbic acid or other electroless bath reactants, is not included in the model. It was assumed that a citrate buffer maintained the pH in the electroless bath.

A 5th order Runge-Kutta method with adaptive stepsize was chosen as the numerical method of solving the four coupled ODEs. The stepsize is adjusted to limit the relative change in concentrations with time. Before proceeding to a new step in time, the relative change in concentration is calculated and compared to a maximum change, specified by the user. If the maximum change in concentrations is exceeded, the program returns to the previous step with a smaller stepsize. An iteration process is used to find an appropriate step size. The program is permitted to proceed to the next time increment, once the stepsize has been adjusted to a suitable value. A minimum stepsize is also specified by the user. The program alerts the user and stops, if solution of the equations requires a stepsize below the minimum. This adaptive stepsize minimizes the truncation error in the integration process.

The concentration time profiles for these reactants were solved as an initial value problem and stored. Interpolation of concentration values at specific times (30, 60 and 90 minutes) is necessary because the model finds the numerical solution at varying time steps and the solution to the four ODEs at specific times is not guaranteed. A cubic spline subroutine is used to

interpolate ascorbic acid and gold thiosulfate concentrations at 30, 60 and 90 minutes.

Deposition Rates with Periodic Addition of Ascorbic Acid and Hydrogen Peroxide

The fifth order Runge-Kutta subroutine with adaptive stepsize control was adjusted to accommodate periodic additions of reactants (ascorbic acid, gold thiosulfate, thiosulfate or hydrogen peroxide). Interactive input of additions to the system allowed user flexibility in designing a replenishment schedule. The amount and frequency of additions were chosen so that deposition rates were maintained at high constant values.

This program helped formulate two baths with constant deposition rates over two hours: a) 0.05 M ascorbic acid/0.03 M gold thiosulfate (pH=6.4, 30°C) with replenishment of ascorbic acid (every 20 minutes) and b) 0.05 M ascorbic acid/0.03 M gold thiosulfate (pH=6.4, 30°C) with initial and periodic addition (every 10 minutes) of 0.1 M hydrogen peroxide and replenishment of ascorbic acid (every 20 minutes). Predicted and experimental deposition rates are listed in Table 8. The deposition rates in Bath A remain relatively constant during the two hour experiment with an average deposition rate of 0.88 ± 0.09 ($\pm 2\sigma$) μm/hr. The deposition rates in Bath B remain consistent and are much higher than any other stable bath in this investigation. The average deposition rate in Bath B is 1.35 ± 0.19 ($\pm 2\sigma$) μm/hr. Thus, experimental results confirm that ascorbic acid replenishment with thiosulfate consumption leads to high, constant deposition rates. However, gold precipitate began to form shortly after the two hour experiment. There are two possible explanations for the shorter lifetime of Bath B. The production of hydroxide ions in the hydrogen peroxidation reaction with thiosulfate may have increased the pH. Previous results have shown that the gold thiosulfate reduction reaction occurs homogeneously in baths with pH greater than or equal to 7.2. The other explanation is that hydrogen peroxide, at very high concentrations, may react with gold thiosulfate to produce gold homogeneously. Previous results show that hydrogen peroxide does not react with gold thiosulfate if the hydrogen peroxide concentration is less than or equal to 2 M. It is unlikely that the hydrogen peroxide concentration exceeded 2 M in the electroless bath, considering that it is continuously being

consumed in the reaction with thiosulfate. Therefore, fluctuations in pH is a more plausible explanation for the shortened bath lifetime.

Table 8:   Predicted and Actual Deposition Rates for Improved Ascorbic Acid/Gold Thiosulfate Electroless Baths.

Time Interval (min)	Bath A (Ascorbic Acid Replenishment)		Bath B (H_2O_2 addition with Ascorbic Acid Replenishment)	
	Predicted Initial Dep. Rates ($\mu m/hr$)	Actual Initial Dep. Rates ($\pm 2\sigma$) ($\mu m/hr$)	Predicted Initial Dep. Rates ($\mu m/hr$)	Actual Initial Dep. Rates ($\pm 2\sigma$) ($\mu m/hr$)
0-30	0.93	0.88 ± 0.06	1.30	1.40 ± 0.10
30-60	0.88	0.90 ± 0.08	1.39	1.40 ± 0.10
60-90	0.93	0.88 ± 0.09	1.28	1.38 ± 0.09
90-120	0.93	0.86 ± 0.06	1.25	1.30 ± 0.10

Conclusions

A nonalkaline, nontoxic electroless gold plating bath, consisting of ascorbic acid and gold thiosulfate, was developed in this investigation. The electroless bath autocatalytically deposited conductive, adherent gold films on gold surfaces in the absence of homogeneous production of gold. Ascorbic acid autocatalytically reduced gold thiosulfate at deposition rates of approximately one $\mu m/hr$ in a cyanide-free solution at pH=6.4 and 30°C. The reaction sequence included various side reactions responsible for consuming reactants and lowering deposition rates. Electrochemical and kinetic studies were performed on all electroless bath reactions. Kinetic information and numerical models aided in identifying and neutralizing prime factors responsible for limiting bath performance.

Gold (I) thiosulfate and gold (I) cyanide were investigated as part of the selection process for a gold complex in the electroless bath. The

electroreduction of gold (I) thiosulfate was studied and compared to the electroreduction of gold (I) cyanide. The electroreduction of gold cyanide is pH dependent and occurs at potentials more negative than -0.08 V vs. SCE in a citrate buffer (pH=6.4, 25C). Gold thiosulfate reduces at potentials more positive than gold cyanide, near 0.15 V vs. SCE. The gold thiosulfate reduction reaction is an irreversible reaction. The gold thiosulfate reduction voltammogram responds to variations in gold thiosulfate concentration, thiosulfate concentration, potential sweep rate and electrode rotation rate. The gold thiosulfate reduction reaction has a low experimental, standard heterogeneous rate constant, 1.58×10^{-3} cm/sec, which is characteristic of a kinetically limited electrochemical reaction. The gold thiosulfate experimental, diffusion coefficient, 7.01×10^{-6} cm^2/sec , is lower than the reported diffusion coefficient of thiosulfate, 1.08×10^{-5} cm^2/sec.

The significant characteristic of the gold thiosulfate electroreduction reaction was the independence of the reduction potential and electroactive species concentrations to most variations in pH. Changes in solution pH shift the gold cyanide electroreduction potential as cyanide ions protonated. Hydrocyanic gas is formed by the protonation of cyanide ions ($pK_a = 9.14$) and is released into the atmosphere, depleting the solution of complexing agents. This undesirable depletion of complexing agents is avoided in most gold thiosulfate solutions. Thiosulfate does not protonate at pHs above 4 ($pK_{a2} = 1.69$).

Gold thiosulfate reduction products were confirmed in a collection experiment with a gold disk electrode and an amalgamated gold ring electrode. Determination of gold thiosulfate reduction products required experimental information about the suspected sulfur species. The oxidations of thiosulfate, sulfite and dithionite were investigated and electrochemical characteristics of the oxidation voltammograms were recorded. The ring collection oxidation voltammogram, obtained during the gold thiosulfate reduction at the disk, was identified as the oxidation of thiosulfate. Specifically, two moles of thiosulfate are produced in the reduction of one mole of gold thiosulfate.

Gold thiosulfate was chosen as the gold complex for the electroless bath for several reasons. Its high stability, solubility, availability and nontoxicity

make gold thiosulfate an attractive electroless bath reactant. More importantly, gold thiosulfate exhibits two characteristic improvements over gold cyanide: gold thiosulfate is independent of pH (pH>4) and is easier to reduce than gold cyanide. Both traits facilitated the task of finding a reducing agent for gold thiosulfate. One recommendation for future work is to investigate the electroreduction of other gold complexes with stability constants above 10^{20}. For example, gold thiourea has a stability constant of 10^{25}, but may be toxic (8). Gold complexes with stability constants lower than 10^{20} may be easier to reduce, but disproportionate too readily in aqueous solutions.

Five reducing agents were investigated to determine their potential for reducing gold thiosulfate in nonalkaline media. Variations in pH changes the redox potentials of each reducing agent and the electroactive species concentration of borohydride. Results confirmed the instability of the borohydride solution at pHs below 9. Electroactive borohydride species are quickly consumed in the hydrolysis reactions at these pHs. The hypophosphite electrochemical oxidation shows no evidence of electroactive species present at high pH.

The oxidation voltammograms of ascorbic acid, hydrazine and hydroxylamine shift in potential in the negative direction with increasing pH. The magnitude of the potential shift follows the Nernst equation, given the number of electrons transferred and the stoichiometric number of hydrogen ions reacting in the electro-oxidation reaction. The oxidation of ascorbic acid in pH=6.4 buffer solution occurs at potentials more negative than the oxidation of hydrazine, hydroxylamine and hypophosphite. The electro-oxidation of ascorbic acid is diffusion controlled, with an experimental diffusion coefficient of 6.46×10^{-6} cm^2/sec. The diffusion controlled C_rE_r mechanism characterizes the electrochemical oxidation of ascorbic acid with a preceding, reversible dissociation reaction. The electro-oxidation of ascorbic acid behaves as a reversible electrochemical reaction at slow rotation rates. It is recommended that other ene-diol lactones, similar to ascorbic acid, be considered as possible reducing agents. The ene-diol group in ascorbic acid is the oxidation site. Much information has been found on the oxidation of ascorbic acid, which may be due to its commonness. Other less known

organic molecules may have electrochemical characteristics similar to ascorbic acid. Finding a new reducing agent which is nontoxic and soluble in aqueous solutions, as well as having a higher diffusion coefficient or less pH dependency, would benefit the microelectronics industry.

The mixed potential theory assisted in selecting a reducing agent for gold thiosulfate. Mixed potential diagrams were used to evaluate the potential difference between the reductant oxidation and the gold thiosulfate reduction. The mixed potential theory assumes no interdependency between the metal complex reduction and the reducing agent oxidation and assumes the redox reactions in the electroless bath are identical to the partial electrochemical reactions studied at the working electrode. Therefore, the working electrode must be the same material as the electroless substrate, have the same catalytic properties as the electroless substrate and the electroless deposit. The electrochemical reduction and oxidation reactions used in the mixed potential analysis represent the initial electroless behavior. Changes in reactant concentration, for example, are inevitable in the electroless bath and result in a decrease in the exchange current at the mixed potential in the electroless system. A mixed potential diagram of the reactants at initial concentrations does not show this particular electroless behavior. Therefore, the mixed potential analysis is appropriate only for predicting initial electroless performance.

Mixed potential analysis and experimental electroless bath deposition rates confirmed that gold thiosulfate is reduced by ascorbic acid at higher rates than by hydrazine, hydroxylamine or hypophosphite. Furthermore, the ascorbic acid reduction of gold thiosulfate is limited to the gold surface, unlike the reduction of gold thiosulfate by borohydride or dithionite. Therefore, gold (I) thiosulfate and ascorbic acid were selected as the electroless bath reactants for this investigation.

The response of the initial time-averaged performance of the gold thiosulfate/ascorbic acid electroless bath to temperature, pH and reactant concentration variation was studied. Deposition rates increase with monoprotonated ascorbic acid concentration, gold thiosulfate concentration and temperature. The deposition rates of the stable baths are more sensitive to the ascorbic acid concentration than to the gold thiosulfate concentration.

The stability of the bath decreases with increasing pH, temperature and gold thiosulfate concentration. Stability and high initial deposition rates are observed in the 0.05 M ascorbic acid/0.03 M gold thiosulfate electroless bath at pH=6.4 and 30°C. Variations in pH, temperature and concentration result in either loss of bath stability or decrease in bath activity.

A detailed investigation of the 0.05 M ascorbic acid/0.03 M gold thiosulfate electroless bath (pH=6.4, 30°C) included characterization of the deposit, ascertainment of all significant reactions occurring in the bath, determination of kinetic parameters and an explanation of bath performance variations with time. Gold is autocatalytically deposited at a rate of 0.89 μm/hr during the first half hour. The electroless deposit is suited for some microelectronics applications. The electroless deposit has good conductivity, good adhesion and forms a uniform film on a gold substrate. Recommendations include studying the effect of stir rate on deposition rate and uniformity. Both gold thiosulfate and ascorbic acid have low diffusion coefficients, which may explain difficulties in depositing gold into small via holes. Designing the electroless bath reactor to have high, uniform convection, may increase deposition rates on substrates of small and large areas.

The performance of the 0.05 M ascorbic acid/0.03 M gold thiosulfate electroless bath (pH=6.4, 30C) changes significantly over time. Deposition rates decrease with time and bath activity ceases in 3.5 hours. The consumption of ascorbic acid in a side reaction and the accumulation of thiosulfate in the bath explain the decrease in deposition rate.

The reaction between ascorbic acid and dissolved oxygen significantly consumes ascorbic acid at electroless bath conditions. The presence of gold thiosulfate in solution significantly increases the homogeneous oxidation rate of ascorbic acid. This reaction was characterized as a pseudo-first order reaction with a rate constant of 0.0203 min^{-1}. Mixed potential analysis confirmed that the potential shift in the gold thiosulfate reduction reaction is due to the production and subsequent thiosulfate accumulation in the electroless bath. An increase in thiosulfate concentration causes a decrease in potential difference between the gold thiosulfate reduction and the ascorbic

acid oxidation. Electroless bath results verified that only small amounts of thiosulfate are necessary to significantly decrease deposition rates.

Numerous reactions were found to be less significant or nonexistent in the electroless baths. The reaction between ascorbic acid and hydrogen peroxide is insignificant at electroless bath conditions. No reaction was observed between gold thiosulfate and hydrogen peroxide, and between ascorbic acid and thiosulfate.

The addition of complexing agents was investigated as part of an effort to improve the performance of the 0.05 M ascorbic acid/0.03 M gold thiosulfate electroless bath. The addition of thiosulfate or sulfite results in a decrease in deposition rates. The bath lifetime is slightly increased by the addition of these complexing agents. Increasing the operating temperature increases deposition rates, but shortens the bath lifetime. A combination of excess complexing agents with higher temperatures, resulting in high, constant deposition rates, was not found in this investigation. However, the possibility exists that a practical electroless bath formulation with thiosulfate or sulfite can be developed, if both temperature and pH are increased. Supposedly, increasing the concentration of complexing agents will increase the bath lifetime and stability and decrease the potential difference between gold thiosulfate and ascorbic acid. Increasing the temperature will increase deposition rates in baths if the exchange currents at the mixed potential are small. The current densities of the partial electrochemical reactions increase with temperature. Increasing the pH will increase the deposition rates in baths limited by small potential differences between ascorbic acid and gold thiosulfate. The increase in pH would shift the ascorbic acid oxidation voltammogram to negative potentials, which may compensate for the gold thiosulfate reduction potential shift associated with the increased concentration of complexing agents. However, the homogeneous oxidation of ascorbic acid is expected to increase with pH. Therefore, the optimum conditions for the ascorbic acid/gold thiosulfate/thiosulfate electroless bath may be difficult to ascertain.

Another method of developing a gold thiosulfate/thiosulfate electroless bath with optimal bath performance is to select a reducing agent with a more negative redox potential. For example, borohydride may be a feasible

reductant for gold thiosulfate at pHs above 9 if excess thiosulfate is added as a stabilizer. However, borohydride is limited to high pHs, as mentioned earlier, and may not be a practical reductant for electroless baths used in microelectronic applications, where polymer films partially cover the substrate. One recommendation is to investigate uncommon reducing agents, such as thiourea or dithionite, or consider compounds with similar structure and oxidation mechanisms to known reducing agents.

Improvements in the ascorbic acid/gold thiosulfate electroless bath were attempted by neutralizing undesirable side reactions in the 0.05 M ascorbic acid/0.03 M gold thiosulfate electroless bath (pH=6.4, 30°C). The accumulation of thiosulfate and the consumption of ascorbic acid in side reactions were concluded to be responsible for the loss of bath activity in the standard bath. A numerical model of the kinetic reactions occurring in the electroless bath proved to be invaluable. Numerical model results aided in determining the extent of ascorbic acid depletion in the homogeneous oxidation of ascorbic acid with dissolved oxygen. The numerical model was used to formulate an ascorbic acid replenishment schedule and a hydrogen peroxide addition schedule. Bath performance is greatly enhanced by replenishing ascorbic acid and consuming thiosulfate in the hydrogen peroxidation reaction. The standard bath with ascorbic acid replenishment deposits gold at a constant rate of 0.9 μm/hr for two hours. The periodic addition of hydrogen peroxide to this bath increases these deposition rates and maintains them at approximately 1.35 μm/hr for two hours. Thus, bath degradation is neutralized by replenishing ascorbic acid and adding hydrogen peroxide.

The mixed potential theory can be used to determine the feasibility of increasing electroless deposition rates tenfold. The mixed potential theory defines an exchange current at the mixed potential of the electroless system. Theoretically, the exchange current is directly proportional to concentration. The concentrations of ascorbic acid and gold thiosulfate would have to increase tenfold (to 0.5 M and 0.3 M, respectively) in order to achieve deposition rates above 10 μm/hr at the same mixed potential, at pH=6.4 and 30°C. Experimental results have shown that increasing ascorbic acid and gold thiosulfate concentrations increases the rate of two undesirable reactions: the

homogeneous production of gold and the homogeneous oxidation of ascorbic acid.

The mixed potential theory predicts deposition rates above 10 μm/hr if the gold thiosulfate reduction current at the mixed potential is greater than 8 mA/cm^2. The mixed potential must also be more positive than the half peak potential for the electroreduction of gold thiosulfate. The quality of gold deposited at potentials more negative than the half peak potential is unacceptable for microelectronic applications. In order to fulfill the above criteria, the gold thiosulfate concentration must be greater than 0.12 M and the reductant oxidation voltammogram must intersect the gold thiosulfate reduction voltammogram near -0.15 V vs. SCE.

Ascorbic acid could be used as the reductant only if the anodic current density at the mixed potential can be increased to 8 mA/cm^2 and the ascorbic acid oxidation voltammogram can be shifted to more negative potentials. Increasing the pH to 9.2 shifts the potential of the 0.05 M ascorbic acid oxidation voltammogram in the negative direction, approximately 120 mV. The primary objective of this investigation, which is to develop a nonalkaline, gold electroless bath compatible with polymeric materials, prohibits further increases in the pH. The anodic current at -0.15 V vs. SCE (in the oxidation voltammogram of 0.05 M ascorbic acid at pH=9.2) is very small. Having an anodic current density of 8 mA/cm^2 would necessitate increasing the ascorbic acid concentration to an unacceptably high concentration of 2.0 M. Therefore, 10 μm/hr gold deposition rates would require 0.5 M ascorbic acid (or greater)/0.3 M gold thiosulfate (or greater) concentrations at pH=6.4 or 2.0 M ascorbic acid (or greater)/0.12 M gold thiosulfate (or greater) concentrations at pH=9.2.

An alternate method of increasing the deposition rates tenfold is to use a different reducing agent with an appropriate redox potential. The gold thiosulfate concentration must still be 0.12 M or greater, in order to deposit gold at 10 μm/hr. The redox potential of the reducing agent would preferably be near -0.4 V vs. SCE, if the standard heterogeneous rate constant of the reductant is similar to the gold thiosulfate standard heterogeneous rate constant. Excess thiosulfate should be added to increase the stability of the 0.12 M gold thiosulfate electroless bath. The addition of thiosulfate will shift

the mixed potential of the electroless bath as much as 200 mV in the negative direction. Therefore, the ideal reductant should have an onset potential near -0.6 V vs. SCE and a standard heterogeneous rate constant approximately 10^{-3} cm/sec. In addition, the homogeneous production of gold must not occur with 0.12 M concentrations of both gold thiosulfate and the reducing agent. Preferably, the reducing agent would be nontoxic and would not be consumed in any undesirable reactions. According to data reviewed by Koura, formaldehyde might have a suitable redox potential at $pH \geq 9$ (25). However, the formaldehyde oxidation potential region is nearing the hydrogen evolution potential region. Another disadvantage to using formaldehyde is that harmful vapors are released in electrodeposition processes (20, 21, 22). Clearly, finding an appropriate reducing agent, which reduces gold thiosulfate at 10 μm/hr in a nonalkaline, nontoxic electroless gold plating bath, is a challenging task. However, it is recommended that the search be continued for a reducing agent, which is capable of autocatalytically reducing gold thiosulfate in a nonalkaline, excess thiosulfate solution.

The focus of this investigation was on strengthening the performance of the ascorbic acid/gold thiosulfate electroless bath (pH=6.4, 30°C). Improvements in the 0.05 M ascorbic acid/0.03 M gold thiosulfate electroless bath (pH=6.4, 30°C) are attributed to meticulous evaluation of all significant reactions occurring in the electroless bath and the development of a kinetic model of the electroless bath reactions. The numerical model is limited in application and accuracy because the model relies on empirical data, uses assumption in the derivation of the kinetic equations and is only applicable to electroless baths at pH=6.4 and 30°C. In addition, the rate constants determined in the minimization program are not guaranteed to be absolute. However, the numerical model takes into account the interaction between reactants and allows for intermittent addition of reactants during the electroless deposition.

Having a clear understanding of the electroless gold deposition and accompanying electroless reaction proved to be immensely important. The electrochemical and kinetic results of the electroless bath reactions relate directly to deposition rate and bath lifetime. Further studies of the effect of

pH and temperature on the homogeneous gold production reactions would complete the ascorbic acid/gold thiosulfate precis. The design of practical, nontoxic, electroless gold plating bath with high deposition rates and moderate stability was achieved by studying of the effect of pH, temperature, additives and reactant concentrations on the electroless bath performance. This investigation represents a comprehensive analysis of the autocatalytic gold deposition in a nonalkaline, gold thiosulfate/ascorbic acid electroless bath (pH=6.4, 30°C).

REFERENCES

. Y.Okinaka, 'Electroless Plating of Gold and Gold Alloys' in *Electroless Plating: Fundamentals and Applications*, G. O. Mallory and J. B. Hajdu, Editors, Chapter 15, AESF, Orlando, Florida (1990).

1. C. D. Iacovangelo, *J. Electrochem. Soc.*, **138**, 976 (1991).

2. C. D. Iacovangelo and K. P. Zarnoch, *J. Electrochem. Soc.*, **138**, 983 (1991).

3. M. Matsuaoko, S. Imanishi, M. Sahara and T. Hayashi, *Plat. and Sur. Fin.*, **42**, 102 (1988).

4. Y. Okinaka, *J. Electrochem. Soc.*, **120**, 739 (1973).

5. Y. Okinaka, *Plating*, **57**, 914 (1970).

6. G. Stremsdoerfer, H. Perrot, J. R. Martin and P. Clechet, *J. Electrochem. Soc.*, **135**, 2881 (1988).

7. R. Puddephatt, 'Gold' in *Comprehensive Inorganic Chemistry*, J. C. Bailar Jr., H. J. Emeleus, Sir R. Nyholm and A. F. Trotman-Dickenson, Editors, **4**, Chapter 55, Pergamon Press, Elmsford, NY (1973).

8. G. M. Schmid and M. E. Curley-Fiorino, 'Gold' in *Encylopedia of Electrochemistry of the Elements*, A. J. Bard and H. Lund, Editors, **4**, Chapter 3, Marcel Dekker, Inc., NY (1978).

9. T. Inoue, S. Ando, H. Okudaira, J. Ushio, A. Tomizawa, H. Takehara, T. Shimazaki, H. Yamamoto and H. Yokono, 45th Electronic Components & Technology Conference, *IEEE*, 1059 (1995).

10. M. Kato, K. Nikura, S. Hoshino and I. Ohno, *J. Surf. Finish. Soc., Japan*, **42**, 69 (1991).

11. Y. Okinaka and T. Osaka, 'Electroless Gold' in *Advances in Electrochemical Science and Engineering*, J. Gerischer and C. Tobias, Editors, **3**, VCH (1994).

12. D. Lamouche, P. Clechet and J. R. Martin, *J. Electrochem. Soc.*, **134**, 692 (1987).

13. R. Sard, Y. Okinaka and H. A. Waggener, *J. Electrochem. Soc.*, **121**, 62 (1974).

14. Y. Okinaka, R. Sard, C. Wolowodiuk, W. H. Craft and T. F. Retajczyk, *J. Electrochem. Soc.*, **121**, 56 (1974).

15. L. A. D'Asaro, S. Nakahara and Y. Okinaka, *J. Electrochem. Soc.*, **127**, 1935 (1980).

16. C. D. Iacovangelo, U.S. Pat 4979988 (1990).

17. C. D. Iacovangelo, U.S. Pat 4863766 (1989).

18. Z. Mathe, *Metal Finishing*, 33 (1992).

19. A. Hung and K. Chen, *J. Electrochem. Soc.*, **136**, 72 (1989).

20. A. Hung and I. Ohno, *J. Electrochem. Soc.*, **137**, 918 (1990).

21. A. Hung, *Plat. and Surf. Fin.*, **75**, 74 (1988).

22. C. H. Ting and M. Paunovic, *J. Electrochem. Soc.*, **136**, 456 (1989).

23. C. H. Ting, M. Paunovic, P. L. Pai and G. Chiu, *J. Electrochem. Soc.*, **136**, 462 (1989).

24. N. Koura, 'Electroless Plating of Silver' in *Electroless Plating: Fundamentals and Applications*, G. O. Mallory and J. B. Hajdu, Editors, Chapter 17, AESF, Orlando, Florida (1990).

25. F. Vratny, U.S. Pat. 4154877 (1979).

26. E. L. Gostin, U.S. Pat 3032436 (1962).

27. J. Pouradier and M. Gadet, *Journal de Chimie Physique*, **66**, pt 1, 109 (1969).

28. M. Benedetti and J. Boulegue, *Geochimica et Cosmochimica Acta*, **55**, No. 2, 1539 (1991).

29. R. J. Tykodi, *Journal of Chemical Education*, **67**, 147 (1990).

30. K. G. Tan and E. Rolia, *Canadian Metallurgical Quarterly*, **24**, No. 4, 303 (1985).

31. S. A. Vejtasa and R. A. Schmitz, *AIChE Journal*, **16**, No. 3, 410 (1970).

32. V. A. Lunenok-Burmakina and A. N. Gerasenkova, *Russ. J. Inorg Chem.*, **9**, No. 2, 149 (1964).

33. K. F. Lin and L. L. Wu, *Chem. Eng. Sci.*, **36**, 415 (1981).

34. M. P. Brungs, B. G. Madden and P. L. Seage, *Chem. Eng. Sci.*, **43**, No. 9, 2451 (1988).

CHAPTER 8

Research Associates and Postdoctorial Fellows

Professor Gilherme Arroz

        Sabatical from the Technical University of Portugal, Fall 1992 to Fall 1993, Testing and Fabrication of electronic materials.

Dr. Stephen Ernst

        Fall 1991 to September 1995, Design and processing of semiconductor test structures.

Dr. Frank Stepniak

        August 1994 to August 1995, High Conductivity Metals for Electronic Packaging.

Graduate Students and Tasks

Anne Sullivan

        Advising Began: Winter 1990
        Graduation Date: Spring 1995
        Thesis Title: The Auto-catlaytic Deposition of Gold

Thomas Hodge

        Advising Began: Winter 1990
        Graduation Date: Spring 1995
        Thesis Title: Microstructures for Measuring Mechanical and Thermal Properties of Thin Polymer Structures.

Martin Ceiler

        Advising Began: Fall 1991
        Graduation Date: Fall 1993
        Thesis Title: Inorganic Dielectrics for GHz Multi-Chip Modules

Bilal Sinno

        Advising Began: Fall 1991
        Graduation Date: Fall 1993
        Thesis Title: Properties of Polyquinoline Interlevel Dielectrics

Kirk Laursen

        Advising Began: Fall 1991
        Graduation Date: Fall 1996
        Thesis Title: High FrequencyProperties of Low Dielectric Constant Insulators

Guerry Taylor

        Advising Began: Fall 1993
        Graduation Date: Fall 1996
        Thesis Title: Materials at Low Temperature

Nicole Grove

        Advising Began: Fall 1993
        Graduation Date: Spring 1998
        Thesis Title: Polyolefins for Use as Interlevel Dielectrics.

Undergraduate Students

Joel Edwards, Winter 1991 - Winter 1992, "DC Magnetron Sputtering"

Michael Houston, Winter 1991 - Spring 1993, "Photolithography and electron microscopy"

Mahesh Thadhani, Winter 1991 - Winter 1992, "Electrodeposition of Gold"

Gareth Sampson, Winter 1991 - Spring 1992, "Reactive Ion Etching"

Todd Cloud, Spring 1991 - 1994, " Photosensitive Polyimides"

Ralph Redd, Fall 1991 - Spring 1993, "Semiconductor Metallization"

Cassondra Farmer, 1992 -1993, "Wafer Coating Using MTI Flexifab"

Barry Coe, Summer 1992 - Fall 1992, "Electroplating of Gold"

Guerry Taylor, Summer 1992 - 1993, "Reactive Ion Etching"

Christine Roberts, Fall 1992 to Winter 1994 , "Chemical Etching"

Carnley Norman, Winter 1993 to Summer 1994, "Reactive Ion Etching"

George Obath, Winter 1993 to Spring 1994, "Electroplating"

Clifford Henderson, Spring 1993 to Summer 1994, "Rapid Processing of Materials"

Tim Huskey, Fall 1992 to Winter 1994, "Electroless Plating of Gold"

Joseph Ngo, Fall 1993 to Spring 1994, "Production of Gold Thiosulfate"

Michelle McClain, Fall 1993-present, "Photolithography"

Thuy Nguyen, Fall 1993 to Winter 1994, "Low Temperature Properties of Polymers"

Brian Carter, Summer 1994, "Moisture Measurements"

Jason Pickering, Fall 1994-1995, "Stress Measurements"

Steven Richter, Winter 1994-1995, "Moisture Measurements"

CHAPTER 9

Publications

Vogt, K., Kohl, P.A., Bell, R., Bottomley, L.A., and Carter, B., "Characterization of Thin Titanium Oxide Adhesion Layers on Gold: Resistivity, Morphology, and Composition.", Surface Science, 301, 203-213 (1994).

Cloud, T., Houston, M., Kohl, P.A., and Bidstrup, S.A., "High Performance Noble Metal MCMs" IEEE CHMT, 16, 724-730 (1993).

Hodge, T.C., Landmann, B., Kohl, P.A., and Bidstrup, S.A., "Rapid Thermal Curing of Polymer Interlayer Dielectrics" International Journal of Microcircuits & Electronic Packaging, 17, 10 (1994).

S. Han, M. Ceiler, S. Bidtrup, P. Kohl, and G. May, "Modeling the Properties of PECVD Silicon Dioxide Films Using Optimized Back-Propagation Neural Networks," IEEE Transactions on Components, Hybrids, and Manufacturing Technology, 17, 174-82 (1994).

Sullivan, A., and Kohl, P.A., "Electroless Deposition of Gold From a Non-Cyanide, Gold Thiosulfate Bath", Journal of the Electrochemical Society, 142, 2272 (1995).

Ceiler, M., Kohl, P., and Bidstrup, S.A., "PECVD Silicon Dioxide Deposited at Low Temperatures", Journal of the Electrochemical Society, 142, 2067-71 (1995).

Lee, J.B., Allen, M.A., Hodge, T.C., Bidstrup, S.A., and Kohl, P.A., "Modeling of Substrate-Induced Anisotropy in Through-Plane Behavior of Polymeric Thin Films", Submitted Journal of Polymer Science, Part B, Polymer Physics, submitted.

Laursen, K., Hertling, D., Berry, N., Bidstrup, S.A., Kohl, P., and Arroz, A., "Measurement of the Electrical Properties of High Performance Dielectric Materials for Multichip Modules", Hybrid Circuits, 34, 11 (1994).

Kohl P.A., "Processing and Yield Considerations in Multi-Chip Modules", Hybrid Circuit Technology, 45, May (1991).

Hodge, T.C., Bidstrup, S.A., Kohl, P.A., Lee, J.B., and Allen, M.A., "An in-situ Measurement Technique for Through-plane Thermal Properties of Thin Film Dielectric Films", SPIE 2256, 344-9 (1994).

Technical Presentations

Hodge, T., Ceiler, M., Sinno, B., Kohl, P.A., Bidstrup, S.A., Hertling, D.R., "Materials and Processes for High Performance MCMs" IEPC, September 1993.

Hertling, D.R., Laursen, K., Bidstrup, S.A., Kohl, P.A., Arroz, G.S.., "Measurement of the Electrical Properties of High Performance , Low Cost Dielectric Materials for Multichip Modules." IEPC, September 1993.

Hodge, T., Bidstrup, S.A., and Kohl, P.A., "The Effect of Moisture and Temperature on the Dielectric Properties of Polyimides", The Electrochemical Society, October, 1992.

Frye, D.C., Harris, R.H., Heistrand, R.H., Moyer, E.S., Rutter, E.W., Garrou, P., Berry, M.J., Rogers, B., Turlik, I., Bidstrup, S.A., Hodge, T., Kohl, P.A., Taylor, G., Berry, K., David, F., and Lanka, M., "Via Generation in Cytclotene", VLSI Packaging, Kyoto, Japan December 2, 1992.

Han, S.S., Ceiler, M., Bidstrup, S.A., Kohl, P.A., and May, G., "Neural Network-Based Modeling of the Plasma-Enhanced Chemical Vapor Deposition of Silicon Dioxide", 15th IEEE/CHMT Internation Electronics Manufacturing Technology Symposium, pp. 458-463, July 1993.

Sinno, B., Bidstrup, S.A., and Kohl, P.A., "Effect of Cure Schedule on Stress in Polyquinoline Films", Society of Plastic Engineers, New Orleans, LA, Vol. 39, 1922-4, November, 1992.

Gerhardt, R.A., Kokan, J.R. and Kohl, P.A., "Low Permittivity Porous Silica Thin Films for MCM-C/D Applications", NATO conference and Volume: "Advances in Ceramics Multi-Chip Module and High Performance Electronic Materials, ed. W.K. Jones, Kluwer Academic Publishers, 1994.

Laursen, K.G., Hertling, D., Hodge, T.C., Bidstrup, S.A., and Kohl, P.A., "Examination of High Frequency Dielectric Properties of Thin Film Polymers Using an In-situ Resonant Technique", IEEE Conference on MCMs, Santa Cruz, CA, February, 1995.

Hodge, T., Bidstrup, S.A., Kohl, P.A., Lee, J.B., and Allen, M.A., "In-situ Thermal Expansion Measurements of Interlevel Dielectrics", Fifth International Conference on Polyimide Films, Ellenville, NY, November 3, 1994.

Lee, J.B., Allen, M.A., Hodge, T., Bidstrup, S.A., and Kohl, P.A., "Modeling of Substrate Induced Anisotropy on Through Plane Coefficient of Thermal Expansion of Thin Films", Transducers '95.

Hertling, D.R., Laursen, K., Bidstrup, S.A., Kohl, P.A., Arroz, G.S.., "Measurement of the Electrical Properties of High Performance , Low Cost Dielectric Materials for Multichip Modules." IEPC, San Diego, CA, September 1993.

Houston, M., Cloud, T., Redd, R., Taylor, G., Kohl, P.A., and Bidstrup, S.A., "Evaluation of the Processing and Performance of Noble Metal MCMs", ISHM, Denver CA, April, 1993.

Kohl, P.A., Ceiler, M.F., Bidstrup, S.A., and May, G., "The Effect of Deposition Conditions on the Properties of PECVD Silicon Dioxide Films", The Electrochemical Society, vol. 93-12, 265-6, Honolulu, HI, May 1993.

Hodge, T.C., Bidstrup, S.A., Kohl, P.A., CLee, J.B., and Allen, M.A., "An In-Situ Measurement Technique for Through-Plane Thermal Properties of Thin Dielecric Films", ISHM, Denver, CO, April 13-15, 1994.

Kohl, P.A., "Sol-Gel Processing of Porous Silica Thin Films for Interlayer Dielectrics in Integrated Circuits", ECTC, Washington, D.C., May, 1994.

Bidstrup, S. A., Hodge, T.C., Lin, L., Kohl, P.A., Lee, J. B., and Allen M. G., "Anisotropy in Thermal, Electrical and Mechanical Properties of Spin-Coated Polymer Dielectrics", Materials Research Society, San Francisco, CA, April 8, 1994.

Hodge, T.C., Kohl, P.A., Bidstrup, S.A., lee, J.B., and Allen, M.G., "Mechanical Anisotropy in Interlevel Polymer Dielectric Films", AICHE, November, 1994.

Stepniak, F., Kohl, P.A., and Bidstrup, "Silver Metallization for Advanced Electronic Interconnections", SUR/FIN 95, American Electroplating Society, June 26, 1995.

Stepniak, F., Kohl, P.A., and Bidstrup, "Silver Metallization for Advanced Metallization", ISHM, Denver, CO, April 1995.

Hodge, T., Kohl, P.A., Bidstrup, S.A., Lee, J.B., and Allen, M.A., First International Symposium on Advanced Packaging Materials, Atlanta, GA February 9, 1995.

Bidstrup, S.A., Hodge, T., Lee, J.B., Kohl, P.A., and Allen, M.A., "Anisotropy in Thermal, Electrical and Mechanical Properties of Spin-Coated Polymer Dielectrics", Materials Research Society, Fan Francisco, CA April 4, 1994.

Sinno, B. Bidstrup, S.A., and Kohl, P.A., "Characterization of Polymer Dielectrics for Use in Low Temperature Electronic Applications", Materials Research Society, Palo Alto, CA, Spring 1993.

Hodge, T., Bidstrup, S.A., and Kohl, P.A., "The Effect of Moisture and Temperature on the Dielectric Properties of Polyimides", The Electrochemical Society, vol. 93-12, 451-2, St. Louis, MO, October 1992.

Hodge, T.C., Kohl, P.A., Bidstrup, S.A., Lee, J.B., Allen, M.G., "An In-Situ Measurement Technique for Through-Plane Thermal Properties of Thin Films", AICHE, St. Louis, MO, November 11, 1993.

Sullivan, A., Patel, A.J., and Kohl, P.A. "Low pH Electroless Gold", Plating and Surface Finishing, April 1994.

Sullivan, A., Patel, A.J., and Kohl, P.A. "Low pH Electroless Gold Deposition from gold thiosulphate", Electrochemical Society, San Francisco, CA, May 1994.

Kokan, J.R., Tadayon, F., Gerhardt, R., and Kohl, P.A. "Sol-Gel Processing of Porous Silica Thin Films", 98th Meeting of the American Cermic Society, Indianapolis, Indiana, 1994.